PREPARATION AND PROPERTIES OF RARE-EARTH COMPOUNDS

Annual Technical Report
(4 June 1970 to 4 Jun. 1971)

June 30, 1971

by

V. E. Wood, K. C. Brog, A. E. Austin, J. F. Miller,
W. H. Jones, Jr., C. M. Verber, E. W. Collings, R. D. Baxter

Sponsored By

Advanced Research Projects Agency

Under

ARPA Order No. 1588
PRON: W2-0-UX190-01-D1-DZ
Contract No. DAAH01-70-C-1076

(Project Technical Director: V. E. Wood)

BATTELLE
Columbus Laboratories
505 King Avenue
Columbus, Ohio 43201

UNCLASSIFIED

Security Classification

DOCUMENT CONTROL DATA - R & D

(Security classification of title, body of abstract and indexing annotation must be entered when the overall report is classified)

1. ORIGINATING ACTIVITY (Corporate author)

Battelle, Columbus Laboratories
505 King Avenue
Columbus, Ohio 43201

2a. REPORT SECURITY CLASSIFICATION

UNCLASSIFIED

2b. GROUP

3. REPORT TITLE

PREPARATION AND PROPERTIES OF RARE-EARTH COMPOUNDS

4. DESCRIPTIVE NOTES (Type of report and inclusive dates)

Annual Technical Report (4 June 1970 to 3 June 1971)

5. AUTHOR(S) (First name, middle initial, last name)

Van E. Wood, Kenneth C. Brog, Alfred E. Austin, James F. Miller, William H. Jones, Jr., Carl M. Verber, Edward W. Collings, and Ronald D. Baxter.

6. REPORT DATE	7a. TOTAL NO. OF PAGES	7b. NO. OF REFS
June 30, 1971	112	64

8a. CONTRACT OR GRANT NO.	9a. ORIGINATOR'S REPORT NUMBER(S)
DAAH01-70-C-1076	Battelle Project G-0550
b. PROJECT NO.	
c.	9b. OTHER REPORT NO(S) (Any other numbers that may be assigned this report)
d.	

10. DISTRIBUTION STATEMENT

Distribution of this document is unlimited.

11. SUPPLEMENTARY NOTES	12. SPONSORING MILITARY ACTIVITY
	Advanced Research Projects Agency Arlington, Virginia 22209

13. ABSTRACT

Research on preparation of, characterization of, and physical-property measurements on rare-earth compounds of technological potential is described. Work was in four areas: magnetoferroelectric materials, narrow-band narrow-gap semiconductors, rare-earth pnictides, and cooperative excitation of luminescence of rare-earth ions in insulators. In the first area, study of heavy rare-earth manganites and chromites and their solid solutions has been emphasized. Ranges of solid solution and weak ferromagnetism have been determined for Yb compounds. High pressure orthorhombic phases of Y, Ho and Yb manganites were shown to be antiferromagnetic. Work is in progress to determine the extent of ferroelectricity in all of the systems prepared. In narrow-band narrow-gap materials, it was attempted to determine the nature of a localized excited state in SmB_6 in order to understand the conductivity transition. However, work on very well characterized SmB_6 has thus far been inconclusive. Work on the pnictides was primarily on production of near-stoichiometric oxygen-free samples of DyN for magnetic resonance studies. Finally, studies on two-photon infrared-excited red fluorescence of Ho^{3+} ions in CaF_2 have established that at ion concentrations greater than about 0.5% the fluorescence arises from cooperative energy transfer between Ho^{3+} ions rather than from successive excitation of a single ion.

DD FORM 1 NOV 68 1473

UNCLASSIFIED

Security Classification

14. KEY WORDS	LINK A		LINK B		LINK C	
	ROLE	WT	ROLE	WT	ROLE	WT
Magnetoferroelectric Materials						
Semiconducting Compounds						
Semiconductor-to-metal transitions						
Rare-earth maganites						
Rare-earth chromites						
Rare-earth ferrites						
Rare-earth borides						
Rare-earth nitrides						
Cooperative luminescence						
$CaF_2:Ho^{3+}$						

PREPARATION AND PROPERTIES OF RARE-EARTH COMPOUNDS

Annual Technical Report
(4 June 1970 to 4 June 1971)

June 30, 1971

by

V. E. Wood, K. C. Brog, A. E. Austin, J. F. Miller,
W. H. Jones, Jr., C. M. Verber, E. W. Collings, R. D. Baxter

Sponsored By

Advanced Research Projects Agency

Under

ARPA Order No. 1588
PRON: W2-0-UX190-01-D1-DZ
Contract No. DAAH01-70-C-1076

(Project Technical Director: V. E. Wood)

BATTELLE
Columbus Laboratories
505 King Avenue
Columbus, Ohio 43201

SUMMARY

This report describes the first year of a research program on preparation, characterization, and measurement of relevant physical parameters of a number of rare-earth compounds of potential technological significance. The program includes work in four distinct, although not entirely unrelated, areas, which will be described in turn.

The first of these areas is what we have termed magnetoferroelectric materials. This has been the area of greatest effort - a little over half the total. The primary objective of this work is to develop a material that is both ferroelectric and at least weakly ferromagnetic (see Appendix A) in some useful temperature range. A number of possible devices using such materials are described at the end of Section IIA and in the references given there. The work during the first year has emphasized the heavy rare-earth manganites and chromites and their solid solutions with each other and with the rare-earth orthoferrites. The ranges of solid solution and of weak ferromagnetism have been largely determined for the ytterbium compounds, although a few questions remain about possible ferrimagnetic impurities. Work is now in progress on determining whether any of the weakly-ferromagnetic materials are ferroelectric, as the antiferromagnetic hexagonal forms of the heavy rare-earth manganites are known to be. The work is also being extended to holmium solid solutions; other cations may be considered later.

The second area is that of narrow-band, narrow-gap materials. While such materials have a number of interesting properties, the greatest attention during the past few years has been to those materials which undergo conductivity transitions - rapid changes from semiconducting to metallic behavior as temperature or some other external parameter is varied. For practical application,

those transitions which can be influenced by an applied electric field are most important, although no cases where this happens are known for certain. Among rare-earth compounds, those containing divalent samarium are of greatest interest because of the unique combination of low-lying excited states and narrow-band gaps. Our research has aimed principally at establishing conclusively the nature of the excited state in well-characterized samarium hexaboride, which undergoes a rather gradual conductivity transition at low temperature. Understanding this excited state should provide information about the nature of the transitions in other samarium compounds. We have not yet been able to prove the validity of present theories on the nature of the excited state, although we were able to characterize our samples quite thoroughly. Recently work has been extended to samarium sulfide-selenide solid solutions, but only preparative work has been done so far.

The third area is called rare-earth pnictides, although the experimental work has been limited to nitrides. There has long been controversy over whether the pure stoichiometric rare-earth mononitrides are semiconducting or metallic. If semiconducting, and if not too extraordinarily difficult to prepare, these materials should have useful optical and electronic properties. After following some relatively unprofitable trails, we concluded that the best test of the inherent nature of the material would be nuclear magnetic resonance measurements of hyperfine field (indicating conductivity character) and quadrupolar broadening (indicating relative stoichiometry) on powder materials as near stoichiometric as possible. Samples of DyN which appear to be close to stoichiometry and free of oxygen impurities have recently been prepared, but the NMR measurements have not yet been carried out.

Finally, a small part of the effort was directed toward study of the interaction of rare-earth ions (specifically Ho^{3+}) in CaF_2 and similar insulating crystals. It was shown that excitation of visible luminescence proceeds by a cooperative process involving two ions rather than by a sequential (two-step) process when the Ho^{3+} concentration is greater than 0.5%. Such effects may be important factors in limiting the performance of doped crystals as infrared-to-visible converters and similar optical devices.

TABLE OF CONTENTS

TABLE OF CONTENTS
(Continued)

Page

LIST OF FIGURES

TABLE OF CONTENTS
(Continued)

LIST OF TABLES


BLANK PAGE

I. GENERAL INTRODUCTION

This report describes the first year of a program of research on several classes of compounds containing rare earths:

1) Magnetoferroelectric materials

2) Narrow-band narrow-gap materials

3) Rare-earth pnictides

4) Fluorides containing dilute concentrations of rare-earth ions.

Although these are rather diverse areas, the electronic, optical, and magnetic properties resulting from the rare-earth 4f electrons are of primary importance in all of them. We proposed research in these areas because it appeared that they were all promising (and widely considered so) for applications within a few years, but that insufficient systematic work was being done to assess accurately their potentialities. The present work has therefore involved systematic exploration of some of the more promising groups of compounds, together with careful characterization of the materials synthesized, the principal objectives being i) to understand the factors affecting material parameters, ii) to attempt to develop better materials on the basis of this understanding, and iii) to develop some of these areas to the point that relatively specific application possibilities emerge. This is an ambitious undertaking, and has not, of course, been completed in one year; work is continuing under an extension of the program. Because of this, this report does not always present final conclusions, but does present in each section a discussion of present status, conclusions reached so far, and future plans.

The greatest part of the work (probably a little over half) has been in the first area listed, magnetoferroelectrics. In the second and third areas, the work has been primarily on methods of preparation and characterization, while in the last area, which represented only about 5% of the total effort, no preparative work was necessary, only measurements on commercially obtained samples. Well over a hundred separate preparative experiments have been carried out and the products characterized by X-ray diffraction and a variety of other means, principally optical emission spectroscopy, electron-probe microanalysis, nuclear magnetic resonance, and electron paramagnetic resonance. More than sixty substantially different samples (not just different pieces of material from the same preparation) have been used for one or more of the various physical measurements necessary to determine the parameters of interest.

The four areas of research are discussed in turn in this report, each in a relatively self-contained format. Certain detailed or background material has been relegated to several appendices. The references in the main text are numbered consecutively and listed together on pages 71 and 72. Each appendix, on the other hand, stands independently and has its own references, as well as its own table, figure, and equation numbers. Occasional reference is made to the Semiannual Report on this project. While nothing of major significance has been omitted from the present report, in a few cases it has not been thought worthwhile to repeat minor details from the Semiannual Report. A number of the results given in the Semiannual Report have been modified through measurements on better samples or more thorough analysis of data.

II. MAGNETOELECTRIC MATERIALS

IIA. INTRODUCTION

The term "magnetoelectric" encompasses more than one type of physical phenomenon; these phenomena and the types of materials which may be expected to exhibit them are discussed in Appendix A. The primary objective of the present work is the development of ferromagneto-ferroelectric materials - that is, materials which in some temperature range are ferroelectric and at least weakly ferromagnetic - containing rare earths and displaying magnetoferroelectricity at relatively high temperatures - at least liquid nitrogen temperature (77 K) and preferably room temperature. A secondary objective is determining whether the materials studied may have other magnetoelectric properties, and a tertiary objective is of course noting whether these materials have any other interesting or useful properties. There is no fundamental reason the development of magneto-ferroelectric materials should be limited to, or even concentrated on, compounds containing rare earths; but a previous theoretical study and review of known ferroelectrics indicated that the rare-earth manganites and molybdates and solid solutions based on them would be of interest; so they were selected for initial study. The work on the manganites was later extended to some rare-earth chromites and manganite-chromite and manganite-ferrite solid solutions.

The proposed applications of magnetoelectric phenomena are mainly based on the idea of electric field control or variation of the magnetization dependence of some property. Among the possibilities are electric field control of amplification of spin or magnetoelastic waves, electric field modulation of Faraday or other magnetooptical effects, simultaneous electric and magnetic storage in the same volume element (providing, with optical readout, what amounts to

a 3- or 4-position switch or ternary or quaternary memory element), and frequency doubling and other non-linear processes in the microwave region.[1-4]

IIB. MANGANITES AND CHROMITES

The simplest manganites of the heavy rare earths (Ho through Lu and yttrium) have formula $(RE)MnO_3$, have a hexagonal crystal structure, and are ferroelectrics with very high transition temperatures, 600 - 700 C. They become antiferromagnetic at low temperatures and weakly ferromagnetic only in a few cases when the rare-earth ions order at temperatures below 10 K.[5,6] By contrast the light (Ce through Dy) rare-earth manganites are orthorhombic, not ferroelectric, and weakly ferromagnetic at low temperatures.[6] The hexagonal heavy-rare-earth manganites can be transformed under high pressure and temperature to an orthorhombic form;[7] no studies of physical properties of materials in this form had been undertaken prior to the present work. (By way of completeness, we mention at this point that the rare-earth ferrites of similar composition are all orthorhombic, not ferroelectric, and weakly ferromagnetic with high transition temperatures; while the chromites of composition $(RE)CrO_3$, are orthorhombic, weakly ferromagnetic at low temperatures, and are claimed in some cases to be ferroelectric.[8]) Our research on these materials has aimed at providing answers (at least partial ones) to the following questions:

1. What are the properties of the orthorhombic forms of heavy rare-earth manganites?
2. Can weak ferromagnetism (at higher temperatures) occur or be made to occur in hexagonal manganites?
3. Can weak ferromagnetism be produced (in conjunction with ferroelectricity) in solid solutions of manganites (ortho or hex) with chromites or ferrites?

4. Are rare-earth orthochromites actually ferroelectric?

A study of the symmetry properties of these materials enables one to determine what sort of electrical and magnetic properties may be expected. The normal-form manganites have either the hexagonal space group[9] $P6_3cm$ or the trigonal one P3c1. The latter structure is only a very slight distortion of the former, and one cannot distinguish between them by X-ray diffraction, although they are not Buerger groups of each other. There are differences in the allowed magnetic symmetry, though. The group $P6_3cm$ allows both the antiferromagnetic groups $P6_3'c'm$ and $P6_3'cm'$ and the ferromagnetic group $P6_3c'm'$, while the trigonal group allows only ferromagnetic P3c'1. The antiferromagnetic order observed by neutron diffraction has led to the belief that the former structure is correct. It should be noted that in either symmetry, any net magnetic moment is parallel to the c-axis, as is the polarization direction in the ferroelectric state. Although these structures permit magnetoferroelectricity, of more general device interest are ones having an orthogonal relationship between magnetization and polarization. This requires orthorhombic, monoclinic, or triclinic structures.

The orthorhombic high-pressure phases of the heavy rare-earth manganites have one of two possible space groups, centrosymmetric Pbnm or noncentrosymmetric $Pbn2_1$, the latter being necessary for ferroelectricity. These two groups are Buerger groups - that is, they cannot be distinguished by X-ray diffraction alone; and physical property tests for acentricity are required for each compound. This is also the case for the light-rare-earth manganites and for the RE orthochromites and orthoferrites of similar composition. Some of the rare-earth gallates, such as $NdGaO_3$, are known to have the acentric structure.[10] The possible magnetic structures for these two space groups differ; for Pbnm there are both antiferromagnetic and ferromagnetic groups, while for $Pbn2_1$, the groups

are all ferromagnetic. In the latter case, for two magnetic groups, $Pbn'2'_1$ and $Pb'n2'_1$, the net magnetic moment and electric polarization are orthogonal.

In the research performed this year, we prepared polycrystalline materials, and studied the properties of both forms of Y, Ho, and Yb manganites. The rare-earth cations were selected to provide a variety of atomic radii and magnetic moments. An investigation was started on the extent of solid solutions of $YbMnO_3$ with both $YbCrO_3$ and $YbFeO_3$. We also measured magnetic susceptibilities of the solid solutions and of $YbCrO_3$. Ytterbium was chosen as the cation in the initial solid-solution work on the basis of greatest compatibility of molecular volumes. It does tend to lead to somewhat low magnetic transition temperatures, though, and other cations will also be studied.

IIB1. Preparation and Characterization

The rare-earth manganites $YMnO_3$, $YbMnO_3$ and $HoMnO_3$ in powder form were prepared by solid-state reaction. Initially samples were made by the reaction of an intimate mixture of 99.9 percent pure rare-earth oxide and MnO_2 in platinum containers. The reaction conditions and phase analyses are given in Table I. These samples were used for establishing conditions for the high pressure transformations and for initial electric and magnetic property studies. It was found that at about 1300 C in oxygen there was some reduction of the manganese to form Mn_3O_4. The detection of Mn_3O_4 in $YMnO_3$ by magnetic susceptibility measurements indicated reduction even at the lower temperatures of 1250 to 1300 C. The rare-earth manganites $YbMnO_3$ and $HoMnO_3$ appear to be slightly more stable than $YMnO_3$.

The preparations of $YMnO_3$, $YbMnO_3$, and $HoMnO_3$ made by the sintering reaction of the oxides were checked for phase by X-ray diffraction. The materials had the hexagonal rare-earth manganite structure. The unit cell parameters and

TABLE I. Data on the preparation of rare-earth manganites from oxides.

Reactants	Reaction Conditions	Detected in Product by X-ray Diffraction Analysis
$Y_2O_3 + MnO_2$	1350 C in oxygen, 4 hrs.	$YMnO_3$ + minor Mn_3O_4 phase
(refired)	1275 C in oxygen, 6 hrs.	$YMnO_3$ only
$Y_2O_3 + MnO_2$	1250 to 1300 C in oxygen 3 hrs.	$YMnO_3$ *
$Ho_2O_3 + MnO_2$	1350 C in oxygen, 5 hrs.	$HoMnO_3$ + minor Ho_2O_3 phase
above + 1 wt% MnO_2	1280 C in oxygen, 5 hrs.	$HoMnO_3$ + trace Ho_2O_3 *
$Yb_2O_3 + MnO_2$	1350 C in oxygen, 5 hrs.	$YbMnO_3$ + minor Yb_2O_3 phase
above + 1 wt% MnO_2	1280 C in oxygen, 5 hrs.	$YbMnO_3$ + trace Yb_2O_3

*Sources of material used for initial high pressure transformation and for electric and magnetic measurements.

volume per molecule are given in Table II. The X-ray diffraction data are indexed for hexagonal space group $P6_3cm$. The heavy rare-earth manganites can be transformed under high pressure from the normal hexagonal phase into a more dense orthorhombic phase.[7] The conditions for the transformation of $YMnO_3$, $YbMnO_3$ and $HoMnO_3$ were investigated using both girdle and piston-cylinder high-pressure devices.[11] Powders of the compounds were sealed in platinum and heated to 1000 C for 2 hours at pressures from 35 to 60 kbar. The specimens were quenched from 1000 C while kept under high pressure. Hexagonal $YMnO_3$ and $HoMnO_3$ were transformed completely at pressures greater than 35 kbar, while hexagonal $YbMnO_3$ required pressure of 40 kbar at 1000 C for transformation. The specimens were produced in the form of sintered discs, 2-3 mm diameter. The hexagonal phase of $YbMnO_3$ was also compressed into sintered discs at 1000 C under 35 kbar pressure.

The X-ray diffraction data of the high-pressure phases are indexable on orthorhombic unit cells (Table II). The possible space groups are centrosymmetric Pbnm and noncentrosymmetric $Pbn2_1$. Thus the crystal structure is similar to that of the rare-earth orthoferrites, orthochromites and light rare-earth manganites, and the space group of each compound must be determined by physical property tests for acentricity. There is a volume decrease of about 9% in the transformation from the hexagonal to orthorhombic phase. This is in part due to the increase in cation-oxygen coordination, with that of manganese going from 5 to 6 oxygens and that of the rare earth going from 7 to 12.

To aid in interpretation of observed electrical and magnetic properties, several samples of $YMnO_3$ were analyzed by the optical-emission spectrographic method. Samples of Mn metal and Mn oxides also were analyzed to evaluate these materials for potential use in future preparative work. The results, which are given in Table III, show significant concentrations of several impurities in the

TABLE II. Crystal structure data on rare-earth manganites, chromites, and ferrites.

Unit cell parameters in angstroms* at 25C.

Compound	Hexagonal			Orthorhombic			
	a_o	c_o	Ω	a_o	b_o	c_o	Ω**
$YMnO_3$	6.12	11.39	61.6	5.24	5.84	7.36	56.3
$HoMnO_3$	6.13	11.43	62.0	5.26	5.84	7.35	56.48
$YbMnO_3$	6.05	11.36	60.04	5.22	5.81	7.30	55.34
$YbCrO_3$	-	-	-	5.19	5.50	7.48	53.46
$YbFeO_3$ (a)	-	-	-	5.233	5.557	7.57	55.02
$YbMn_{.95}Cr_{.05}O_3$	6.05	11.34	59.97	-	-	-	-
$YbMn_{.25}Cr_{.75}O_3$	-	-	-	5.19	5.55	7.46	53.72
$YbFe_{.5}Mn_{.5}O_3$	6.02	11.50	60.15	-	-	-	-
$YbFe_{.25}Mn_{.75}O_3$	6.024	11.43	59.87	-	-	-	-

* Error = 0.01 Å

** Volume per formula unit, $Å^3$

(a) Literature values.

TABLE III. Spectrographic analysis of manganites and chromites.

	Concentration of Impurity Elements, weight %*								
	Fe	Si	Mg	Mo	Al	Ca	Ti	V	Co
$YMnO_3$ (from Y_2O_3+MnO_2)	.03	.1	<.001		1.	.02			.01
MnO_2	.1	<.001	<.001		<.002	<.001			<.001
Mn metal	<.001	<.001	<.001		<.002				<.001
$YbMnO_3$	<.001	.02	.002	.05	.001	.02	<.003	<.001	<.003
$YbCrO_3$	<.001	.002	<.001	.003	.001	.005	<.003	<.001	<.003

	Ni	Cu	Cr	Mn
$YMnO_3$ (from Y_2O_3+MnO_2)	.005	.002	<.001	High
MnO_2	.003	<.001	.01	High
Mn metal	<.001	<.001	<.003	High
$YbMnO_3$	<.001	.0005	.001	High
$YbCrO_3$	<.001	<.0005	High	<.001

* Accuracy ± 50%.

manganite samples: Al, Si, Ca, Co and Fe. X-ray data indicate that these impurities may be present in minor phases (e.g., $YAlO_3$). The analytical results suggest that the high Al and Si concentrations did not originate in either the MnO_2 or the Y_2O_3. Contamination during processing was suspected, and all operations were monitored carefully in follow-up preparations. The analyses of sources of Mn indicate that the Mn metal is, from the standpoint of purity, to be preferred over available MnO; so this was used in subsequent preparations. (The success of these procedures in reducing impurities is indicated by the spectrographic data also given in Table III on a later preparation of $YbMnO_3$. This is discussed further below.)

Compositions across the $YbMnO_3$-$YbCrO_3$ and $YbMnO_3$-$YbFeO_3$ system were prepared. The method consisted of solid-state reaction of an intimate mixture prepared by evaporating to dryness a solution containing the reactants. High-purity manganese metal (99.97%) (see Table III), ammonium dichromate (reagent grade), and ferrous chloride (99.999 + %) converted to oxide were sources of the 3d elements, while 99.9% Yb_2O_3 was used. The solutions were mixtures of nitric and/or hydrochloric acid solutions of the separate constituents. The mixed oxides from the evaporation were calcined in platinum at increasing temperatures up to 1175 C in air. This temperature was chosen to avoid Mn_3O_4 formation. The $YbMnO_3$-$YbCrO_3$ mixtures were also subsequently fired to 1300 C in air. The $YbMnO_3$-$YbFeO_3$ mixtures were finally fired to 1300 C in one atmosphere of O_2. Table IV lists the reaction conditions and phase analysis by X-ray diffraction. Spectrographic analyses of the $YbMnO_3$ and $YbCrO_3$ preparations (Table III) show much lower impurity content compared to the initial preparation of $YMnO_3$ from MnO_2, particularly of the 3d elements which could substitute for Mn or Cr and affect electric conductivity.

TABLE IV. Reaction conditions and phase analysis of $YbMnO_3$ - $YbCrO_3$ and $YbMnO_3$ - $YbFeO_3$*

Composition	Temp. C	Time Hr.	Temp. C	Time Hr.	Phases** Produced
$YbMnO_3$	1100	15			hex $YbMnO_3$
	1250	2			"
	1175	15			"
$YbMn_{.95}Cr_{.05}O_3$	1175	21			hex $YbMnO_3$ + trace ortho $YbCrO_3$
$YbMn_{.90}Cr_{.10}O_3$	1175	21			hex $YbMnO_3$ + $YbCrO_3$
	1300	8			" " " + trace Yb_2O_3
$YbMn_{.75}Cr_{.25}O_3$	1175	110			hex $YbMnO_3$ + $YbCrO_3$
	1300	8			" " "
$YbMn_{.5}Cr_{.5}O_3$	1175	16			" " "
	1300	8			" " "
$YbMn_{.25}Cr_{.75}O_3$	1175	20			$YbCrO_3$ + hex $YbMnO_3$
	1300	8			" + trace $YbMnO_3$
$YbCrO_3$	1100	16			ortho $YbCrO_3$
	1300	17			"
			1300	17	"
$YbFeO_3$	1175	21			$YbFeO_3$ + trace Yb_2O_3
	1300	36			ortho $YbFeO_3$
$YbFe_{.25}Mn_{.75}O_3$	1175	16			hex $YbMnO_3$
			1300	16	
$YbFe_{.5}Mn_{.5}O_3$	1175	17			hex $YbMnO_3$
			1300	16	"
			1300	24	"
$YbFe_{.75}Mn_{.25}O_3$	1175	16			
			1300	16	$YbFeO_3$ + hex $YbMnO_3$
$YbFe_{.6}Mn_{.4}O_3$	1175	16			
			1300	16	hex $YbMnO_3$ + $YbFeO_3$

* From calcination of evaporated solutions.

** $YbMnO_3$ and $YbCrO_3$ denote type of phase.

$YMnO_3$ was also prepared from 99.99% Y_2O_3 and high-purity manganese metal by evaporation to dryness of a solution of the elements. The final calcination conditions were 1175 C in air for 21 hours and yielded single-phase hexagonal $YMnO_3$. This preparation was converted completely to the orthorhombic phase by treatment at 35 kbar and 1000 C for 2 hours.

The solid solution fields between hexagonal $YbMnO_3$ and orthorhombic $YbCrO_3$ were found to be quite restricted at 1175 C, the limits being less than 5 mol percent $YbCrO_3$ in hexagonal $YbMnO_3$ and 25 mol percent $YbMnO_3$ in $YbCrO_3$. At 1300 C the solid solution was extended slightly to approximately $YbCr_{.05}Mn_{.95}O_3$ for the hexagonal $YbMnO_3$ phase and $YbCr_{.75}Mn_{.25}O_3$ for the orthorhombic chromite phase. The unit cell constants and molar volumes of these phases are given in Table II. Chromium addition decreases the molar volume of the manganite phase while manganese substitution increases the molar volume of the chromite phase. In the latter case the shift in the unit cell parameters is not uniform, there being an increase in the b- and a decrease in the c-axis. This is in accord with the difference between the orthorhombic phase of $YbMnO_3$ and $YbCrO_3$.

In contrast, extensive solid solution was found of $YbFeO_3$ in hexagonal $YbMnO_3$, with the limit at about 50 mol percent $YbFeO_3$. The solid solution has a decrease in the a parameter and an increase in the c parameter with almost constant molar volume (Table II). This marked difference between Fe^{3+} and Cr^{3+} in substitution in $YbMnO_3$ must be dependent on the cation-oxygen bonds and not on ionic radii which are quite comparable: 0.61Å for Cr^{3+}, 0.63Å for Mn^{3+} and 0.64Å for Fe^{3+}. This is similar to the difference in site stabilization energy for octahedral versus tetrahedral coordination in spinels where Cr^{3+} has larger excess octahedral stabilization energy while that of Mn^{3+} and Fe^{3+} is zero. Thus the Cr^{3+} ion is much more stable for the octahedral coordination in the orthorhombic chromite than for the five-fold coordination in the hexagonal manganite.

Reactions under high pressure (up to 40 kbar) of the $YbMnO_3$-$YbCrO_3$ compositions were investigated to determine the range of solution between the orthorhombic $YbMnO_3$ phase and $YbCrO_3$. For these isomorphous structures, one should expect a region of complete solid solution. The powder samples were pressed and sealed in platinum tubing to form specimens about 3 mm diameter and 6 mm long. These were reacted under 40 kbar at temperatures from 1000 C to 1240 C for about 6 hours and were quenched while under high pressure. The specimens were sintered solid discs. Phase analysis was done by X-ray diffraction, $CrK\alpha$ radiation, of crushed powder. At 1000 C there was no appreciable increase in the solid solution range of $YbMnO_3$ in the orthorhombic $YbCrO_3$ beyond that for the prior reaction at 1300 C and one atmosphere. The hexagonal $YbMnO_3$ phase was transformed into a new phase which did not have the orthorhombic structure found previously in $YMnO_3$, $YbMnO_3$, and $HoMnO_3$. The new phase is termed $YbMnO_3$ III, since it was also found as a minor phase in experiments with just the $YbMnO_3$ at 35 to 40 kbar and 1000 to 1100 C. The stability field of the orthorhombic $YbMnO_3$ phase ranges from 1100 C at 30 kbar to 1000 C at 35 kbar with the hexagonal phase being stable at 30 kbar and 1000 C. The composition $YbMn_{.95}Cr_{.05}O_3$ at 1000 and 1240 C under 40 kbar was converted to the new $YbMnO_3$ III phase plus some of the orthorhombic $YbMnO_3$. The other $YbMnO_3$-$YbCrO_3$ compositions after reaction at 1000 C under 40 kbar were composed of $YbMnO_3$ III and orthochromite phases. The pure $YbCrO_3$ composition remained unchanged.

However, reaction at 1240 C under 40 kbars did extend the solid-solution field of the orthochromite phase to about $YbMn_{.5}Cr_{.5}O_3$. The manganese-rich compositions remained two-phase, the orthochromite phase and the new $YbMnO_3$ III. The composition of the latter phase did not extend beyond $YbMn_{.95}Cr_{.05}O_3$. Fig. 1 shows these phase fields for pressure versus composition at 1000 C and about

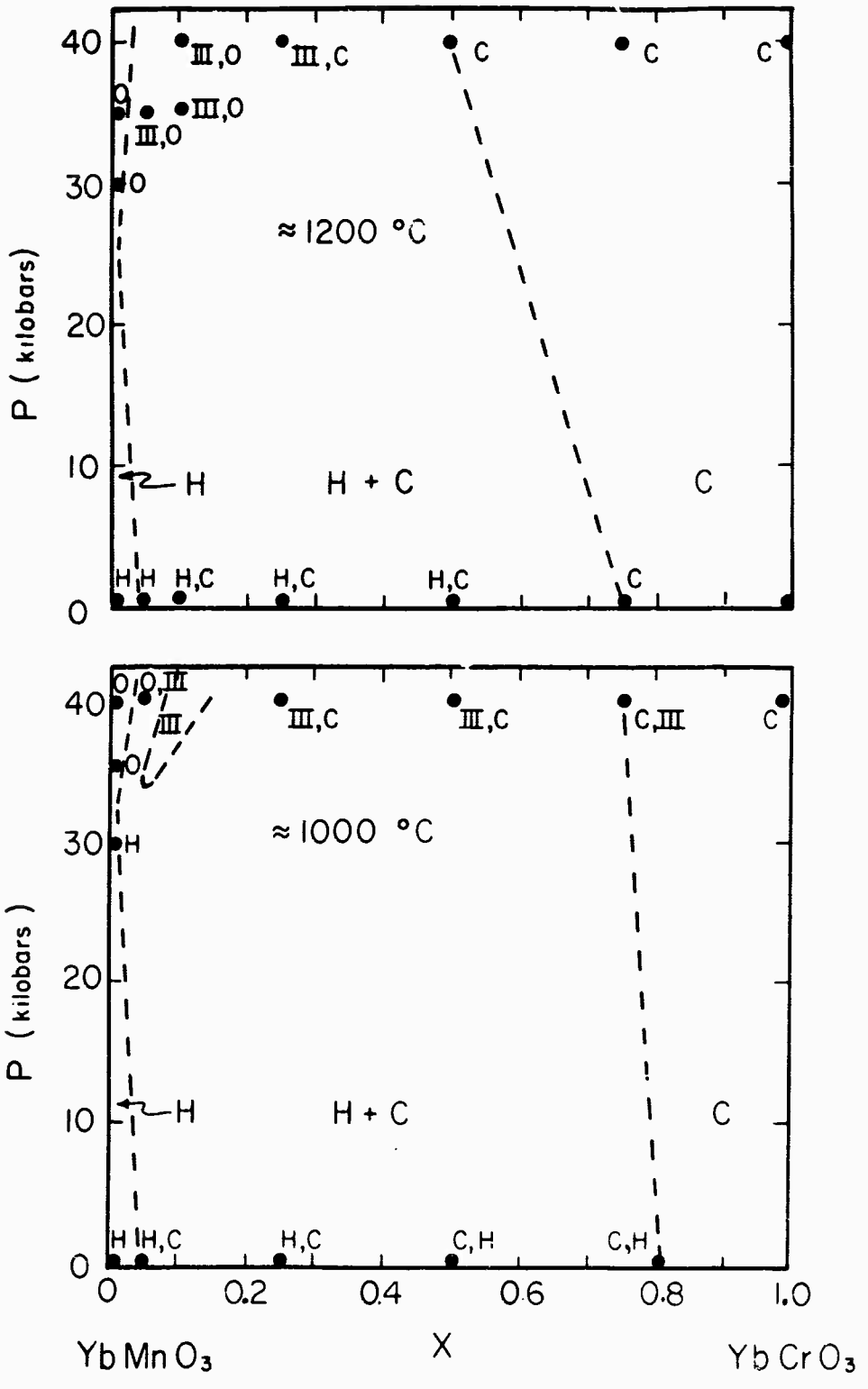

FIGURE 1. PHASES FORMED IN THE $YbMnO_3$-$YbCrO_3$ SYSTEM AT ABOUT 1000 AND 1200 C. H: HEXAGONAL $YbMnO_3$ PHASE; O: ORTHORHOMBIC $YbMnO_3$ PHASE; III: NEW ORTHORHOMBIC (PSEUDOTETRAGONAL) $YbMnO_3$ PHASE; C: ORTHORHOMBIC $YbCrO_3$ PHASE. DOTTED LINES MARKING LIMITING COMPOSITIONS ARE ONLY APPROXIMATE.

1200 C. The region of stability of the new phase $YbMnO_3$ III has not been well defined, though. Both hexagonal and orthorhombic $YbMnO_3$ phase fields have quite limited solid solution with $YbCrO_3$.

The homogeneity of the sintered solid specimens from the 40 kbar-1240 C reaction was investigated by electron probe microanalysis. Of the three apparently single-phase samples, only the $YbMn_{.75}Cr_{.25}O_3$ was uniform in composition from grain to grain. It did have a very small amount of Yb_2O_3 also. The $YbMn_{.5}Cr_{.5}O_3$ specimen had a variable ratio of Mn to Cr from grain to grain, and it apparently would require much longer reaction time than 6 hours of the present experiments. The $YbMn_{.95}Cr_{.05}O_3$ specimens had chromium concentration fluctuating from zero to 1.9 weight percent versus the nominal 0.9 weight percent. Nevertheless, the ytterbium concentration remained essentially constant and agreed with that of hexagonal $YbMnO_3$. Thus the new phase $YbMnO_3$ III has the same composition and is not a higher manganate.

The structure of the high pressure $YbMnO_3$ III phase has not been resolved. Powder X-ray diffraction data indicate probable orthorhombic symmetry with a unit cell which is almost tetragonal. Further experiments on $YbMn_{.95}Cr_{.05}O_3$ at 1100 C under 35 kbars show both high-pressure phases. Apparently there is a narrow temperature-pressure region for the new phase field.

For the study of electrical conductivity, solid sintered specimens of $YbMnO_3$ and $YbCrO_3$ were annealed at 1175 C in argon for 22 hours. The $YbCrO_3$ remained stable but the $YbMnO_3$ decomposed into Yb_2O_3 and MnO.

Chemical Vapor Deposition. Single crystals of $YMnO_3$-type compounds have been grown previously from molten fluxes of lead and bismuth oxides. In this method there is always some question of impurities in solid solution and of trapped inclusions. An alternative method of crystal growth was sought which

might also permit growth of oriented thin films suitable for optical transmission measurements. Chemical vapor deposition appeared to be suitable for growth of $YMnO_3$ crystals free of the impurities encountered in the flux method and also for deposition of thin films. The process is similar to that employed for growth of ferrites and garnets.[12]

Various vapor-phase reactions that could be used for growth of rare-earth manganites were evaluated thermodynamically. Favorable processes were:

1. Growth of rare-earth manganites by hydrolysis of the rare-earth and manganese chlorides in a continuous flow system.
2. Deposition of rare-earth manganite by decomposition and oxidation of the rare-earth and manganese acetylacetonates in a continuous flow system.
3. Regrowth of the rare-earth manganite by chloride vapor phase transport through a temperature gradient with a HCl atmosphere is a sealed tube.

Experiments on vapor transport through HCl were first tried with source material of $YMnO_3$ powder. Thermodynamic calculations for vapor transport[13] show that there is no dependence of the free energies of reaction on HCl pressure and that the hot and cold temperatures respectively should be above and below about 1000 C. Accordingly, experiments were tried using a source of $YMnO_3$ powder at 1025 C under 0.2 atmosphere HCl in a sealed silica tube. Crystals of Mn_3O_4 and possibly Y_2O_3 were deposited in the cold end at 810 C. However, there was also some silica reaction with the HCl and deposition of some silicate phases. Because of these side reactions in the closed system, the experiments were directed to the first reaction using an open tube continuous-flow system for oxidation of

YCl_3 and $MnCl_2$ vapors by H_2O. With this method, the corrosive HCl gas should be swept away by the carrier gas. The initial experiments yielded deposits of Y_2O_3 at 1000 to 1025 C. Increased temperature and oxygen pressure apparently are needed for reaction of the $MnCl_2$ vapor.

Further vapor deposition experiments on $YMnO_3$ were done with substrates of alumina and platinum separately heated at 1200 C in an ambient furnace temperature of 1000 C using injection of wet oxygen. In one experiment, $YMnO_3$ was formed as small particulate platelets on a platinum substrate but only Mn_3O_4 was deposited on an adjacent alumina substrate on top of the platinum. The $YMnO_3$ was identified by both X-ray diffraction and electron microprobe analysis. The difference was probably due to a lower temperature for the alumina substrate. Subsequent experiments had deposits of Mn_3O_4 with some silicon contamination. The latter appeared to result from reaction of hydrated YCl_3 with the silica tube. Therefore, the YCl_3 is being purified and addition of HCl vapor is planned to control the decomposition of the YCl_3.

IIB2. Magnetic Properties

A complete series of magnetic susceptibility measurements from 4.2 K to room temperature, and in a number of cases to several hundred degrees higher, was made on samples with the following nominal compositions and structures:

Hexagonal

$YMnO_3$	$Yb\ Mn_{.95}Cr_{.05}O_3$*
$HoMnO_3$	$Yb\ Mn_{.5}Fe_{.5}O_3$*
$YbMnO_3$	

Orthorhombic

$YMnO_3$*	Yb CrO_3
$HoMnO_3$*	Yb $Cr_{.75}Mn_{.25}O_3$*
$YbMnO_3$*	
$DyMnO_3$ (77 - 300K only)	

On the materials marked with asterisks, no previous measurements have been reported in the literature. For most of the other materials, we believe our measurements are on samples somewhat better than those used in previous work. Results on materials in the left-hand column were presented in the semiannual report, but in most cases new measurements have been made on higher-purity samples and it is those that are reported here. No measurements have yet been made on samples in which the new orthorhombic phase $YbMnO_3$-III (see Section IIB1) predominates. The primary purpose of these measurements is of course to determine the temperature and composition ranges over which ferrimagnetism exists in these compounds, in order to determine which might possibly be ferromagnetoferroelectric. In most cases magnetic measurements properly take precedence over those designed to reveal the presence of ferroelectricity, since the latter are more sensitive to the presence and nature of impurities and thus require more extensive preparation efforts.

In several specimens, the susceptibility results had to be corrected for the presence of small amounts of second-phase material which was often ferrimagnetic. The manner in which this is done is described for the most severe case, an impure sample of ortho-$YMnO_3$, in Appendix B. A discussion of the general problem of second-phase magnetic effects is given below in this section. One specimen, orthorhombic $HoMnO_3$, was found to be metamagnetic at low temperatures; a detailed data-analysis for such a case is described in Appendix C. The

low-temperature-data analysis of a typical weak-ferromagnet, $YbCrO_3$, is described in Appendix D. A discussion and justification of the method of treatment of high-temperature data for all materials, using $YbCrO_3$ as an example, is also to be found in Appendix D.

The principal results of the magnetic susceptibility measurements are as follows:

1. $YbCrO_3$ and $YbCr_{.75}Mn_{.25}O_3$ are weakly ferromagnetic below around 114 and 111 K respectively. The latter material appears to have a region around 70 K where the moment disappears. Hexagonal $YbMn_{.95}Cr_{.05}O_3$ may be weakly ferromagnetic below 70 K, but this must be regarded as not yet proven. The apparent zero-field magnetizations and high-field susceptibilities, as defined in Appendix D, are shown respectively in Figs. 2 and 3. To make the curves clearer, we do not show individual data points; the overall consistency of the data (apart from possible systematic errors) is, however, indicated, and individual points for the orthochromite are given in Appendix D.

2. Orthorhombic $YMnO_3$ is antiferromagnetic below 42 K.

3. All the other materials appear paramagnetic down to 10 K, although many of them are believed to have higher-temperature antiferromagnetic transitions which are not signalled by any noticeable changes in the susceptibility.

4. Orthorhombic $HoMnO_3$ becomes metamagnetic just below 10 K.

There are two factors complicating the interpretation of the low-temperature data:

1. The susceptibility varies rapidly with temperature at the lowest temperatures, and the temperature varies fairly rapidly with time as the system

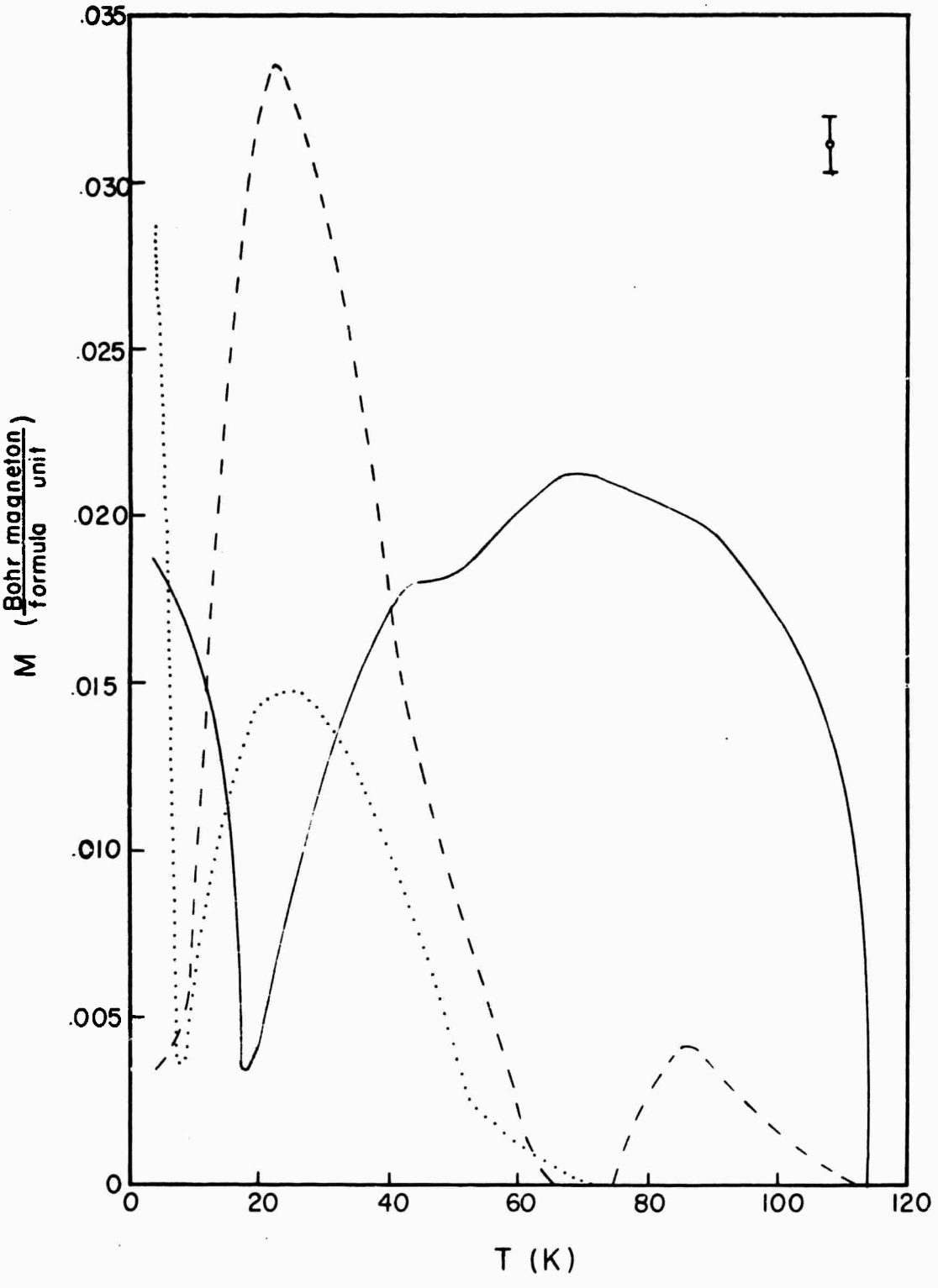

FIGURE 2. APPARENT EFFECTIVE ZERO-FIELD MAGNETIZATION OF Yb COMPOUNDS. SOLID LINE: $YbCrO_3$; DASHED LINE: $YbCr_{.75}Mn_{.25}O_3$; DOTTED LINE: $YbMn_{.95}Cr_{.05}O_3$. IN UPPER RIGHT CORNER: ESTIMATE OF LIMITS OF ACCURACY OF CURVES, BASED ON SCATTER OF DATA AND ESTIMATES OF POSSIBLE SYSTEMATIC ERRORS.

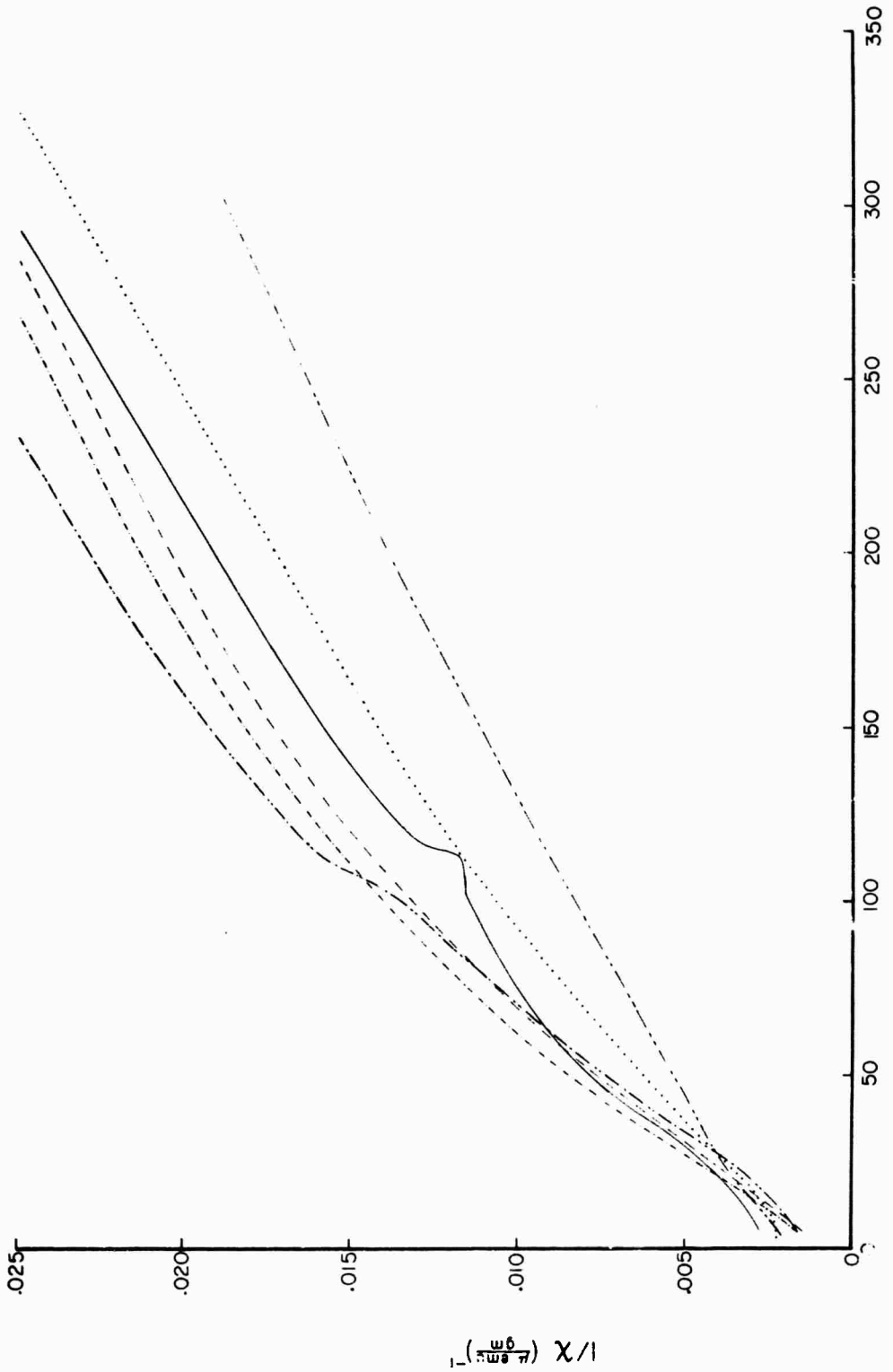

FIGURE 3. INVERSE SUSCEPTIBILITY OF SOME Yb COMPOUNDS.
———: $YbCrO_3$; .....: $YbCr_{.75}Mn_{.25}O_3$;
-.-.-.: HEXAGONAL $YbMnO_3$; — — —: ORTHORMBIC $YbMnO_3$;
- - - -: $YbMn_{.95}Cr_{.05}O_3$; -.-.-.-.-.: $YbFe_{.5}Fe_{.5}O_3$.

begins to warm up. This means that data points must be caught on the fly, leading to some scatter in the data and possible systematic temperature errors due to thermal lag of the thermometer. These effects might be amplified by the smoothing and extrapolation procedure used to analyze the data (Appendix D). On the other hand, a meaningful kink in the data might be interpreted as scatter and smoothed out of existence. All this is principally a problem below 10 or 12 K, which is hardly the region of greatest technological interest. More detailed measurements in this range might be helpful in separating out the effects of various possible minor second phases, as would neutron diffraction measurements, but we have not felt that the substantial expense involved was justified.

2. There are several possible compounds which may be present in one or another of the samples as second phases. Even below the 1% level, these materials may significantly affect the observed susceptibility and magnetization, since the effective moment per molecule in the ordered state of the weakly ferromagnetic materials is very small (Fig. 2). The principal such compounds are:

a) Mn_3O_4, hausmannite, a tetragonally-distorted spinel. This compound orders ferrimagnetically[14,15] at around 42-46 K, and was responsible for the belief held for several years that hexagonal $YMnO_3$ was weakly ferromagnetic below such temperatures. As discussed in Section IIB1, we have succeeded in substantially eliminating this material in certain cases, and could presumably do so in others if we felt that it was worthwhile.

b) $MnCr_2O_4$, a cubic spinel. This material has a Curie temperature and magnetization curve similar to Mn_3O_4, but the maximum moment developed is somewhat smaller.[16]

c) Mn_2CrO_4, a slightly tetragonal spinel. Very little seems to be known about this compound, but its Curie temperature is reported[15] to be 65 K.

d) $YbFeO_3$. Although this weakly ferromagnetic orthoferrite has a much smaller magnetic moment[17] than the ferrimagnetic spinels listed above, it has a high Curie temperature (around 625 K) and its effect is noticeable in the iron-containing solid solution.

The effective magnetic moments of these possible impurities, insofar as they are known, are shown as functions of temperature in Fig. 4. One might expect that second phases of importance would show up in some of the preparations in amounts sufficient to be detectable by X-ray analysis. The compounds $MnCr_2O_4$ and Mn_2CrO_4 have not been found by this means in any of our preparations; this is scarcely proof, however, that they are not there, particularly since when present as impurity phases, they may not show up in their pristine form but rather with dissolved rare-earth or other 3d ions.

The high-temperature (150-200 K to 300-400 K) magnetic properties of the samples measured are summarized in Table V. The effective high-temperature moment is in all cases close to the "theoretical" value obtained by assuming the spin-only moment for the 3d-ions and the strong LS coupling moment for the rare earths. The most obvious generalizations about the paramagnetic Curie temperatures (θ_p's) are

i) the θ_p's for the orthomanganites are smaller than those for the corresponding hexagonal manganites, and

ii) there seems to be the same general sort of dependence of θ_p on rare-earth ion found in the hexagonal manganites and the orthochromites.

We now proceed to give a few details on the measurements on each material.

1. Hexagonal $YMnO_3$ The susceptibility of a sample of hex-$YMnO_3$ nearly free of Mn_3O_4 is shown in Fig. 5. Within the accuracy of the data there is not

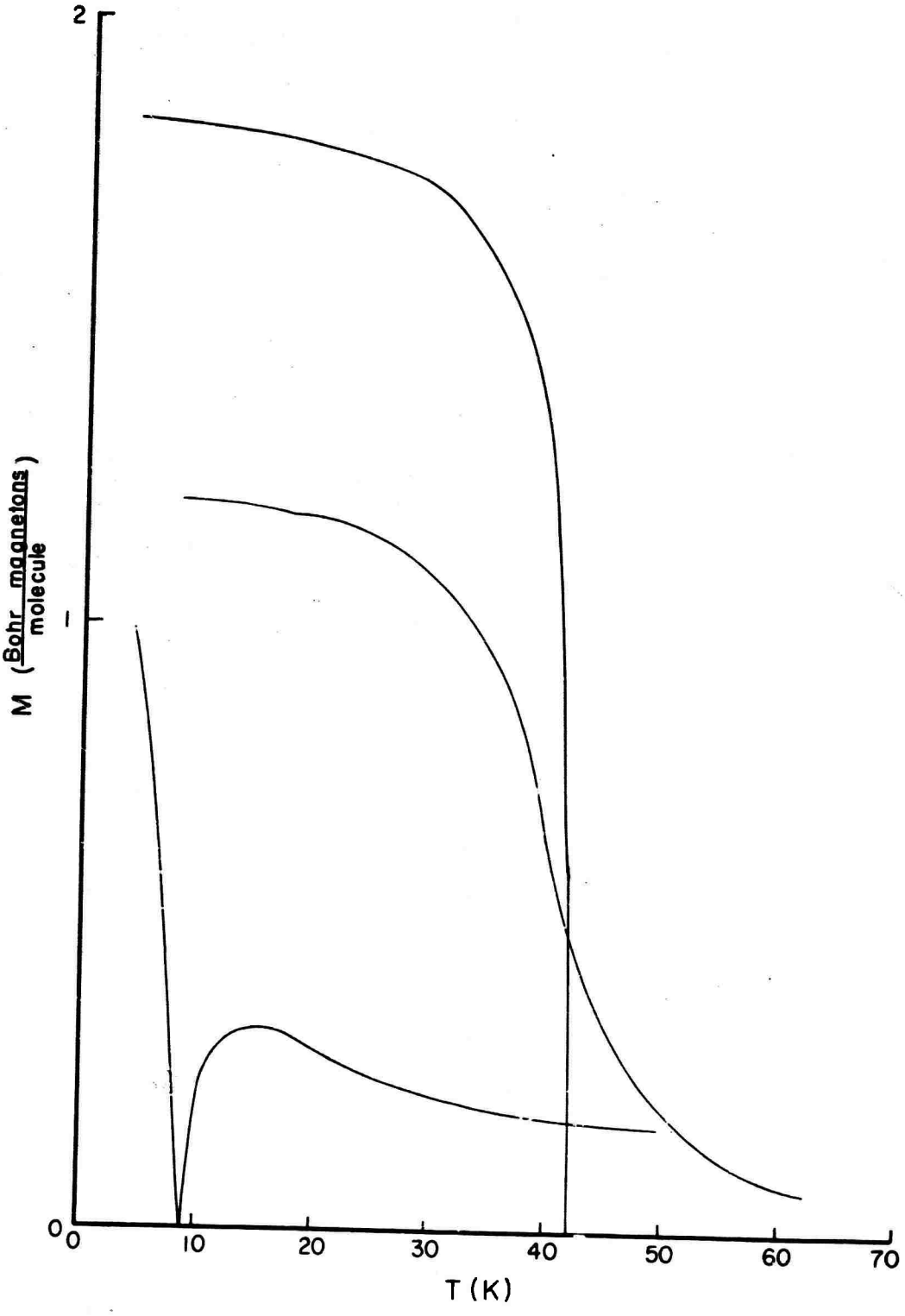

FIGURE 4. LOW-TEMPERATURE MAGNETIC MOMENTS OF POSSIBLE MINOR SECOND-PHASE MATERIALS (TAKEN FROM REFERENCES 14-17). TOP CURVE: Mn_3O_4; MIDDLE CURVE: $MnCr_2O_4$ (HIGH-FIELD MOMENT); BOTTOM CURVE: $YbFeO_3$.

TABLE V. High-temperature magnetic properties of rare-earth manganites and chromites and solid solutions based on them.

Material	Crystal System	Paramagnetic Curie Temp., θ_p (K)	Effective moment μ_{eff} Bohr magnetons	"Theoretical" moment μ_{th} Bohr magnetons
$YMnO_3$	hex	-550(-502[a])	5.37 (5.34[a])	4.90
$YMnO_3$	ortho	-67	4.98	4.90
$HoMnO_3$	hex	-23(-35[a])	11.1(11.4[a])	11.68
$HoMnO_3$	ortho	-23	11.3	11.68
$YbMnO_3$	hex	-200(-219[a])	6.43(6.74[a])	6.68
$YbMnO_3$	ortho	-83(-79[b])	6.72(6.70[b])	6.68
$YbCrO_3$	ortho	-102(-110[c])	5.87(6.05[c])	5.96
$YbMn_{.95}Cr_{.05}O_3$	hex	-166	6.31	6.64
$YbMn_{.25}Cr_{.75}O_3$	ortho	-83	5.99	6.15
$YbMn_{.5}Fe_{.5}O_3$	hex	-173	6.00	7.08

a. Results of Pauthenet and Veyret (Ref. 6).

b. Results on sample prepared with lower purity starting materials.

c. Results of Bertaut et al (Ref. 18).

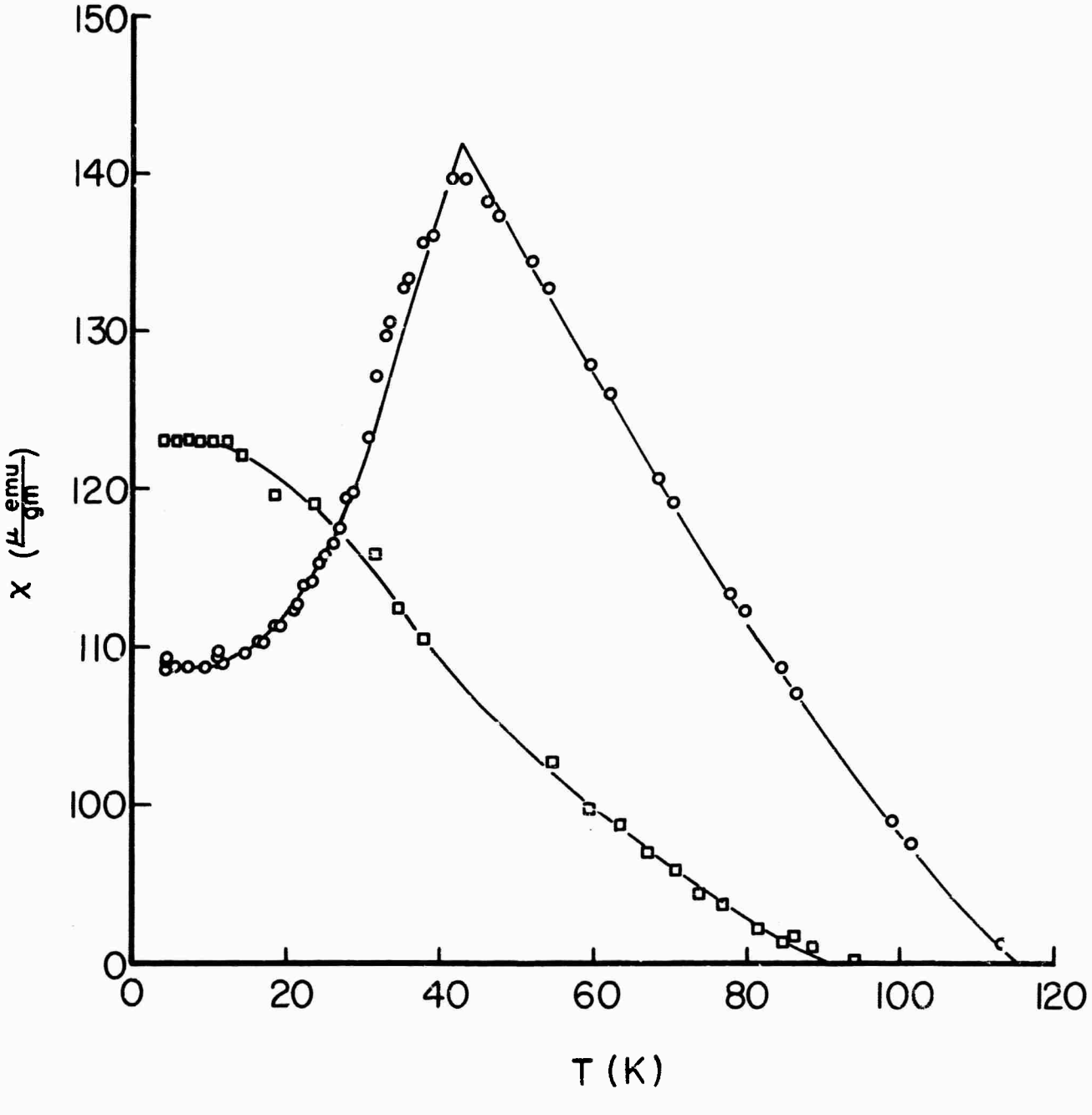

FIGURE 5. LOW-TEMPERATURE MAGNETIC SUSCEPTIBILITY OF $YMnO_3$. CIRCLES: ORTHORHOMBIC FORM; SQUARES: HEXAGONAL FOPM - MEASURED SUSCEPTIBILITY MULTIPLIED BY 3 TO FIT ON SAME AXES.

the slightest break at 80 K, which is known from neutron diffraction measurements[6] to be the Néel temperature. There is no noticeable break in the $1/\chi$ vs T curve either. The extent to which this behavior is related to the unusual spin ordering in the hexagonal compounds is an important unanswered question.

2. Hexagonal $HoMnO_3$ Above 77 K the susceptibility of this material is in close agreement with that found by Pauthenet.[6] Results of measurements down to 4.2 K have not yet been analyzed, but no unusual features were noted.

3. Hexagonal $YbMnO_3$ The inverse susceptibility of this material, corrected for the presence of around 0.6 weight percent Mn_3O_4, is shown in Fig. 3. No ordering above 4.2 K is apparent; Pauthenet (private communication) stated that in his material the Yb spins ordered at 3.8 K, the Mn at 86 K. It is to be noted that the deviation from simple Curie-Weiss behavior occurs well above the Mn ordering temperature.

4. Ortho-$YMnO_3$ The susceptibility of a Mn_3O_4-free sample is shown in Fig. 5. Data at both 5.7 and 9.9 kOe are included. The sharp Néel transition at 42 K is particularly striking since it is the only case we have found in these systems where a purely antiferromagnetic ordering of the 3d-ions shows up in the susceptibility. The reason for this is completely unknown. This system is simple enough crystallographically and magnetically that one can make a guess at the magnetic ordering using molecular-field theory. Following the work of Bertaut[18] on the orthochromites, one finds that "G"-type ordering (Fig. 6) is strongly favored and that second-nearest-neighbor interactions are relatively weak. The absence of weak ferromagnetism requires that the spins lie along the crystallographic "b"-axis.

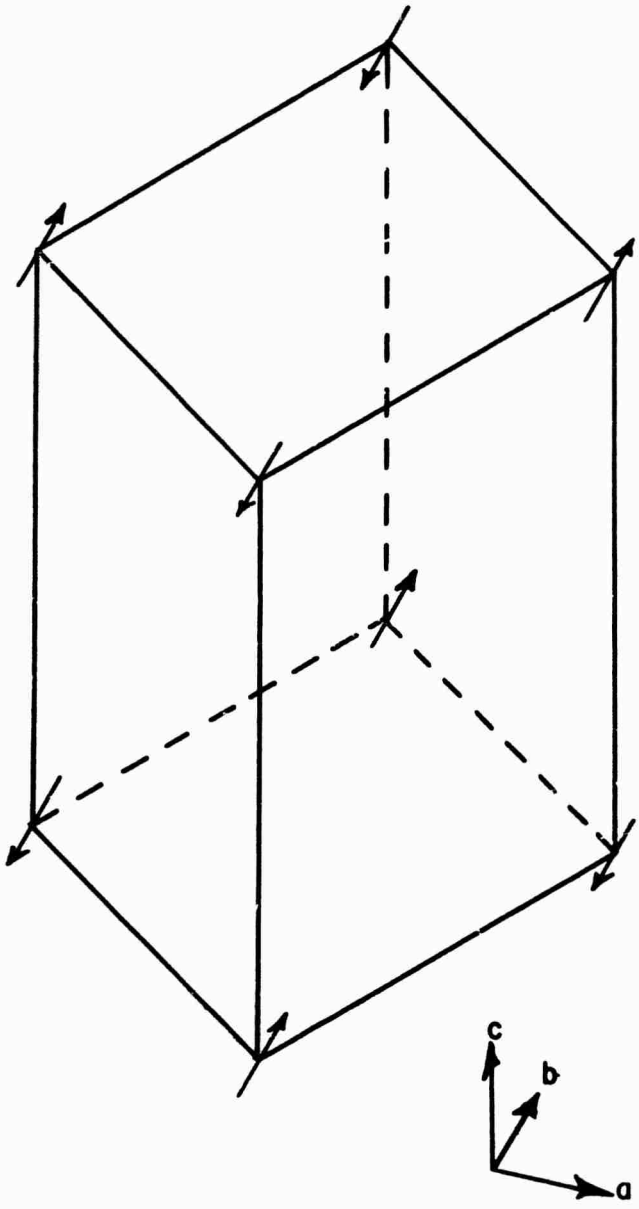

FIGURE 6. "G"-TYPE ANTIFERROMAGNETIC ORDER AS IT IS PRESUMED TO OCCUR IN ORTHORHOMBIC $YMnO_3$

5. Ortho-$HoMnO_3$ This material is metamagnetic below 10 K. It is discussed in detail in Appendix C.

6. Ortho-$YbMnO_3$ Like the hexagonal form, orthorhombic $YbMnO_3$ shows no magnetic transitions above 4.2 K. It shows slight deviations from Curie-Weiss behavior below about 200 K (Fig. 3). The data have been corrected for the presence of a very small amount of some unknown ferromagnetic compound.

7. Ortho-$DyMnO_3$ Measurements above 77 K on this normal form of $DyMnO_3$ agreed very well with those of Pauthenet[6] and served to provide a check between our data and his on an essentially paramagnetic material of the same general type as the others investigated. (The data are not plotted.)

8. Hexagonal $YbMn_{.95}Cr_{.05}O_3$ Data on this solid solution are shown in Figs. 2 and 3. We believe the apparent dip in the magnetization around 8 K is specious; there is a great deal of scatter in the data in this region. It is possible the low temperature rise in the magnetization indicates an incipent ordering of the Yb ion; on the other hand, it may be specious too, since except for these lowest temperatures the susceptibility is very similar to that of hexagonal $YbMnO_3$. The question immediately arises whether the observed magnetization below around 70 K is a property of the material itself or whether it is due to some impurity phase such as Mn_2CrO_4, which as mentioned above is supposed to have a Curie point of 65 K. We hope to resolve this point in the future through work with nearby compositions. It will also be interesting and helpful to compare this data with measurements on the $YbMnO_3$ III phase material.

9. Hexagonal $YbMn_{.5}Fe_{.5}O_3$ This material appeared slightly ferromagnetic at all temperatures between 4.2 and 300 K. Analysis of the apparent

moment showed that it was very similar in temperature variation to that of $YbFeO_3$, which is known from X-ray work to be present in small amounts in the sample. This seems to account adequately for all the observed moment, and the high-field susceptibility (Fig. 3) is again quite similar to $YbMnO_3$. It is somewhat surprising that the introduction of such a large amount of iron makes such a small change in the magnetic properties, but perhaps not as surprising as the fact that the iron enters the lattice in the first place.

10. Orthorhombic $YbCrO_3$ This compound is weakly ferromagnetic below 114 K. Its properties are discussed in detail in Appendix D.

11. Orthorhombic $YbCr_{.75}Mn_{.25}O_3$ This solid solution has the most unusual magnetic properties of any we have studied so far (Figs. 2 and 3). A small magnetization sets in at about 111 K, which we have chosen to call the Curie point, although, given the shape of the magnetization curve, the actual Curie temperature might be somewhat lower. There appears to be some further change at about 108 K in the original data, but this does not show up in Figs. 2 or 3. As the temperature is reduced, a small moment builds up, and then, surprisingly, falls to zero or a very small value in the range 65 - 75 K. One is tempted to believe that there is some structural change at 75 K. Before this is looked for, further checking of the magnetic data will be required, although it must be said that data from low-temperature (4.2 - 140 K) and high-temperature (77 - 300 K) runs match well in the region of overlap. Below 65 K, the magnetization again increases, and then decreases sharply below 23 K. The possibility that much of this low-temperature moment is due to ferrimagnetic impurities is not great, since the small magnitude of the moment at 4.2 K is quite certain. Through all these changes, the high-field susceptibility varies very smoothly. If these

magnetic properties are confirmed, preparation of compact samples, preferably films, should be undertaken in order to observe the domain structure.

IIB3. Electrical Properties

In the investigation of magnetoelectric materials the most important electrical property is the electric polarization, which may be induced by a magnetic field or, in the case of ferroelectrics, may exist spontaneously. Generally, the electrical resistivity and other transport properties are of secondary importance. However, all of the manganites and chromites examined to date are low-activation-energy semiconductors which at room temperature have sufficiently high conductivities that the standard techniques for detecting electric polarizations are not reliable. Thus electrical resistivity measurements become more important, especially since some authors claim that such measurements may be used to infer the existence of ferroelectricity.[8] We first discuss the problem of electric polarization measurements in these types of materials and then give a detailed description of the electrical resistivity of several manganite and chromite specimens.

A standard method for measuring the electric polarization, and thereby detecting ferroelectricity, is to study in detail the temperature dependence of the dielectric constant using capacitance measurements. Most ferroelectric materials are characterized by very large dielectric constants in the ordered state and much smaller values in the paraelectric state so that it is not necessary to vary the temperature continuously, or even in small steps, to infer the existence of ferroelectricity below a certain temperature. But in some materials the dielectric constant in the ferroelectric state is comparable to that in the paraelectric state and the transition can only be detected by an increase in the

dielectric constant very near the Curie point. An example of this is $Gd_2(MoO_4)_3$ in which the dielectric constant has almost identical values in the two states and increases by only 30 percent over a few degree temperature range around the Curie point of 159 C (as reported in the semiannual report this material was used to test our apparatus). This small effect is readily observed in $Gd_2(MoO_4)_3$ because it is an insulator. The difficulties encountered in applying the same capacitance techniques to low-activation-energy semiconductors may be seen by considering our results for orthorhombic $YMnO_3$. A very large room temperature dielectric constant, of order 1000, was measured with a fixed-frequency capacitance bridge operating at 1600 Hz. This result suggested the existence of ferroelectricity in ortho-$YMnO_3$ at 300 K. Subsequent measurements with a variable frequency capacitance bridge showed a pronounced frequency dependence in the apparent dielectric constant. Since capacitance and resistance effects at the surface of the sample could produce this result, we were led to suspect that the large dielectric constant observed at 1600 Hz was due to contact problems. This suspicion was confirmed by DC and pulse conductivity measurements which yielded the typical current-voltage relationship, $i = i_o(e^{eV/kT} - 1)$, of a Schottky barrier. It was concluded that the low-frequency capacitance studies actually measured the capacitance of the fired silver-paste contact to the specimen. By extending the frequency range to 100 MHz it was determined that the dielectric constant of orthorhombic $YMnO_3$ at 300 K is less than 3 indicating either that this material is not ferroelectric at room temperature or that the dielectric constant in the ordered state is comparable to that expected in the paraelectric state. In either case the existence of ferroelectricity in orthorhombic $YMnO_3$, or any other low-activation-energy semiconductor, can be established in this way only by using high frequency capacitance measurements. When there is little

difference between the ferroelectric and paraelectric dielectric constants, these measurements must be made at closely-spaced temperature intervals. The extreme difficulty of performing such measurements in a reliable manner on small, polycrystalline specimens has led us to seek other methods to infer the existence of ferroelectricity and to indicate the Curie point.

One general method is to determine whether the crystal structure is centrosymmetric or acentric since the latter is required for ferroelectric ordering. In Appendix E we discuss four techniques for detecting acentricity. Three of these, X-ray diffraction, pyroelectricity and piezoelectricity, have been applied unsuccessfully to all the manganites and chromites mentioned in the previous section. The X-ray technique fails because the crystal space groups are Buerger groups. The pyroelectric technique and a very sensitive piezoelectric resonance technique (see Appendix E) are believed to have failed because any induced polarization of the lattice was screened out by the free carriers. Such an effect is known to occur when measurements are made at frequencies below the free carrier relaxation frequency, $f = \sigma/2\pi\epsilon$. The fourth method discussed in Appendix E is to establish acentricity by the observation of second-harmonic generation. Since such experiments involve optical or infrared frequencies, free carrier effects are a problem only in metallic samples. The necessary apparatus to perform second harmonic generation experiments is currently being assembled.

Recently it has been reported that electrical resistivity measurements can be used to infer the existence of ferroelectricity in semiconducting materials. In these experiments ferroelectric-to-paraelectric transitions are correlated with subtle changes in the temperature dependence of the electrical resistivity.[8] Before attempting to use this method for the investigation of ferroelectricity in the high-pressure orthorhombic phases of $YMnO_3$ and $YbMnO_3$,

measurements were made on hexagonal $YbMnO_3$ and orthorhombic $YbCrO_3$ to test the reliability of the technique. The former compound is known to be ferroelectric with a Curie temperature of 993 K,[5] while in the latter case the existence of ferroelectricity is the subject of controversy. Other reasons for performing resistivity measurements were to obtain data necessary to estimate the free-carrier relaxation frequency of each of these compounds (as discussed above and in Appendix E this quantity determines the degree to which piezoelectric resonances may be observed at a given frequency), and to provide general knowledge about the conduction mechanisms in this important class of materials.

All data were obtained by the Van der Pauw method[19] applied to pressed and sintered discs having a nominal diameter of 3 mm and thicknesses in the range of 0.3 to 1.0 mm. Initial measurements were made using four fired-silver (Dupont 7713) electrodes arranged in a symmetric pattern on the perimeter of the discs. These electrodes were found to be unsatisfactory at temperatures above 900 K, however, and were replaced by four stainless-steel knife-edge contacts. In general, it was found that the room temperature resistivities were controlled by impurity and/or defect levels, while at higher temperatures, up to 1070 K, the conduction process seemed to be dominated by levels which are believed to be characteristic of the materials. Below we discuss the results for each compound.

The variation in resistivity with inverse temperature for two different specimens of hexagonal $YbMnO_3$ is shown in Fig. 7. The data points represented by solid circles were obtained with fired-silver contacts on the sample prepared under 36 kbar pressure and 1000 C using the lower purity starting materials (see Section IIB1). At temperatures above 400 K the resistivity may be represented by the familiar expression $\rho = \rho_o e^{\sigma/kT}$ where σ is the activation energy, k is Boltzmann's constant and T is the temperature in degrees Kelvin. From the obvious

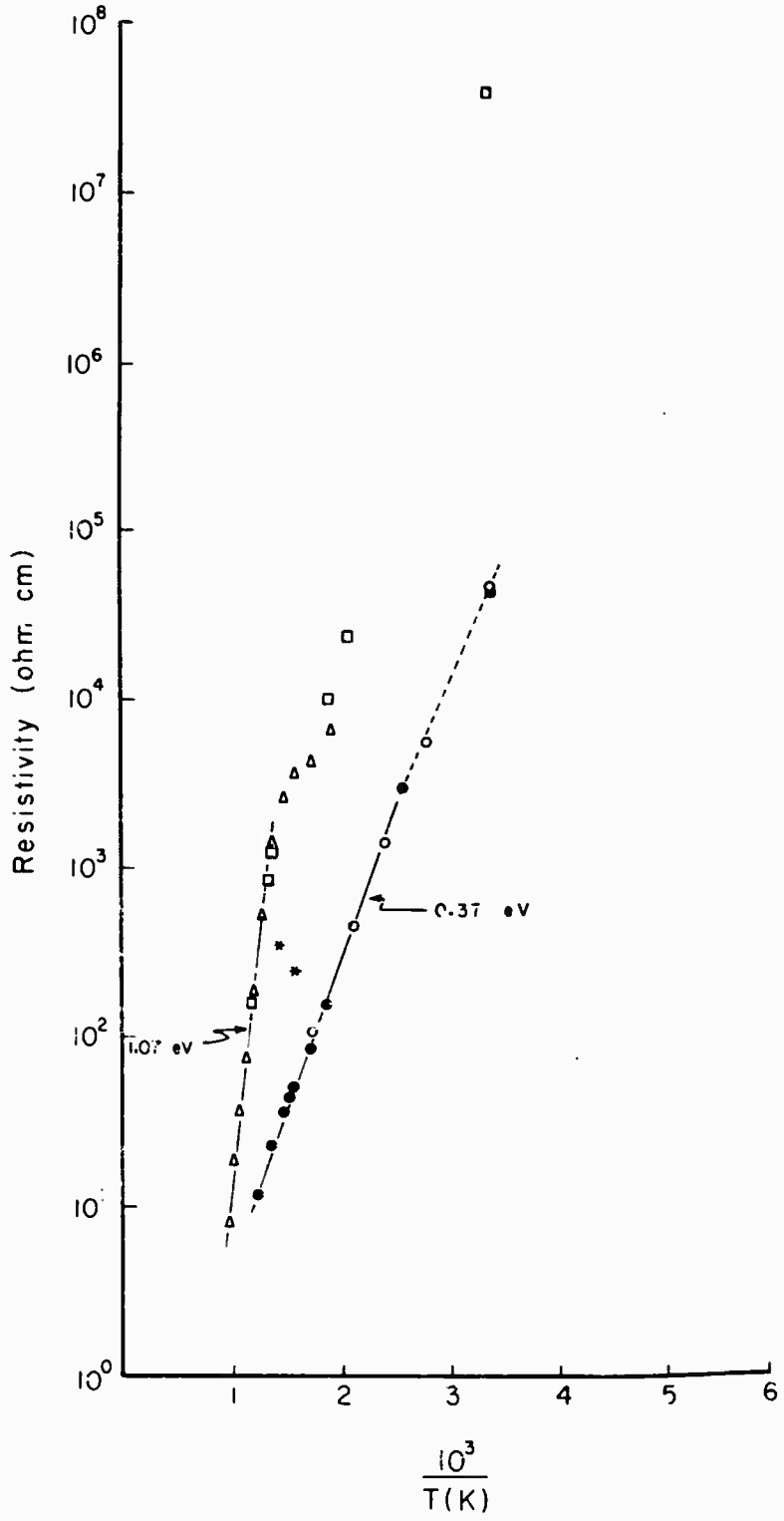

FIGURE 7. ELECTRICAL RESISTIVITY AS A FUNCTION OF INVERSE TEMPERATURE FOR HEXAGONAL $YbMnO_3$. SYMBOLS ARE DISCUSSED IN THE TEXT.

straight line fit the activation energy is found to be 0.37 eV. Below 400 K (dotted line) the limited number of data points suggest a slightly smaller activation energy. The results for this sample are in disagreement with those reported by Rao et al.[8] for hexagonal $YbMnO_3$. The activation energies are much smaller than theirs (0.99 eV and 0.73 eV), the resistivities are lower, and the slight break in the log ρ vs 1/T curve occurs near 400 K as opposed to 973 K reported by them. Since these results suggested the presence of additional impurities in our samples, similar experiments were performed on specimens prepared from higher-purity starting materials. In addition, the stainless-steel knife-edge contacts were used to allow measurements above 900 K. Starting at room temperature and proceeding to 580 K the data, represented by the open circles in Fig. 7, conformed exactly to that observed in the previous case. Above this temperature, however, the resistivity was found to be unstable, showing a monotonic increase with time as the temperature was held fixed. This effect is indicated by the two non-equilibrium data points (*) lying above and to the left of the curve described previously. It is likely due to oxidation of an initially reduced surface. After holding the temperature at about 700 K for several minutes the specimen was cooled to room temperature and examined for any obvious degradation. Showing no signs of such degradation the specimen was remounted, again using pressure contacts. Subsequent measurements yielded much higher resistivity values and, more significantly, showed no further changes upon cycling the temperature over the entire range of 300 to 1070 K. These results are shown by the triangles (increasing temperature) and the squares (decreasing temperature) in Fig. 7. These resistivity values are similar to those reported in Ref. 8. Above 740 K the activation energy is found to be 1.07 eV, in very good agreement with the value 0.99 eV determined by Rao et al. In their case the 0.99 eV value

was observed only above 970 K. Below this temperature they found an activation energy of 0.73 eV, and they attributed the break in the log ρ vs 1/T curve to the known ferroelectric transition in hexagonal $YbMnO_3$. It is obvious that no such break occurs near this temperature in our sample. At this point, it can only be speculated that the level which yields an activation energy of 1.07 eV in our sample is the same as that which gives an activation energy of 0.99 eV in their sample. In any case, our results show that, apart from the remote possibility that our sample has a very low Curie temperature, the ferroelectric-to-paraelectric transition in hexagonal $YbMnO_3$ does not necessarily cause an anomaly in the temperature dependence of the electrical resistivity. This conclusion is reinforced by similar results obtained on orthorhombic $YbCrO_3$.

The electrical resistivity of two $YbCrO_3$ specimens is shown as a function of inverse temperature in Fig. 8. The lower resistivity values at each temperature (open circles) show the behavior of the specimen which was prepared by reacting the starting materials in air (see Section IIB1). Again using an equation of the form $\rho = \rho_o e^{\sigma/kT}$, the high temperature activation energy is found to be 0.26 eV in excellent agreement with the value of 0.24 eV reported by Rao et al. But just as in the case of hexagonal $YbMnO_3$, there is a problem in equating these activation levels because the onset of such behavior occurs at very different temperatures; Rao et al. reported 760 K for this temperature, whereas the results on this specimen yield a value of about 590 K and show no evidence of a break at 760 K. Equally significant is the fact that our low temperature activation energy, 0.55 eV, is much higher than Rao's value of 0.37 eV. This suggests that the low-temperature resistivity of their specimen was controlled by additional impurities despite the fact that they found, in general, lower resistivity values. Support for this idea is found from the data (solid circles)

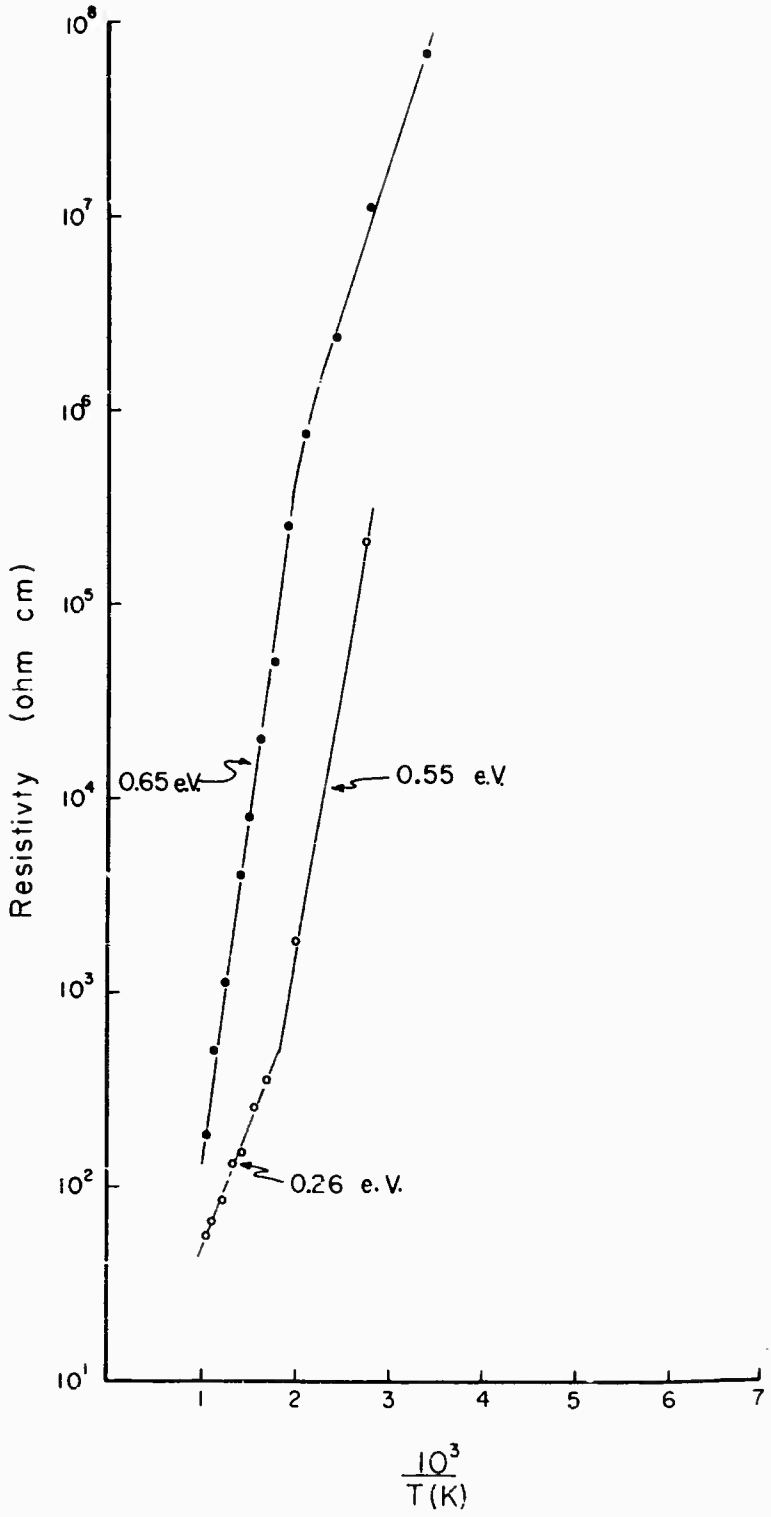

FIGURE 8. ELECTRICAL RESISTIVITY AS A FUNCTION OF INVERSE TEMPERATURE FOR ORTHORHOMBIC $YbCrO_3$. SYMBOLS ARE DISCUSSED IN THE TEXT.

obtained on the sample which was prepared by further reaction of the same preparation in one atmosphere of oxygen at 1300 C. As discussed in Section IIB1, this procedure was used to improve stoichiometry by enhancing the ratio of Cr^{3+} to Cr^{2+} oxidation states. The resulting powder was pressed and sintered at 40 kbars and 1200 C. It is seen in Fig. 8 that over the entire temperature range studied both the resistivity and the activation energy are much larger than in the case of the air-fired sample which is believed to contain an appreciable number of divalent chromium ions. Likewise these quantities are much larger than the corresponding ones found by Rao et al. Even this sample showed no evidence for a break in the log ρ vs 1/T curve at 760 K. Thus either $YbCrO_3$ does not undergo a ferroelectric-to-paraelectric transition near 760 K or such a transition is not reflected in the temperature dependence of the resistivity. Since Rao et al. do not show their data for the reported ferroelectric hysteresis-loop measurements or pyroelectric measurements and since our resistivity results are in disagreement with theirs, the existence of ferroelectricity in orthorhombic $YbCrO_3$ remains an open question.

These results for hexagonal $YbMnO_3$ and orthorhombic $YbCrO_3$ raise serious doubts about the use of electrical resistivity measurements to infer the existence of ferroelectricity in the orthorhombic phases of $YMnO_3$ and $YbMnO_3$. Nevertheless such measurements were made on these materials in order to estimate the free carrier relaxation frequencies. In Figs. 9 and 10 the variation of resistivity with inverse temperature is shown for ortho-$YMnO_3$ and ortho-$YbMnO_3$ respectively. The most striking feature about the two curves which have been drawn to fit the data is that they are remarkably similar in all respects. In particular, both curves exhibit the same transition temperature between regimes having different activation energies and in each temperature regime the activation

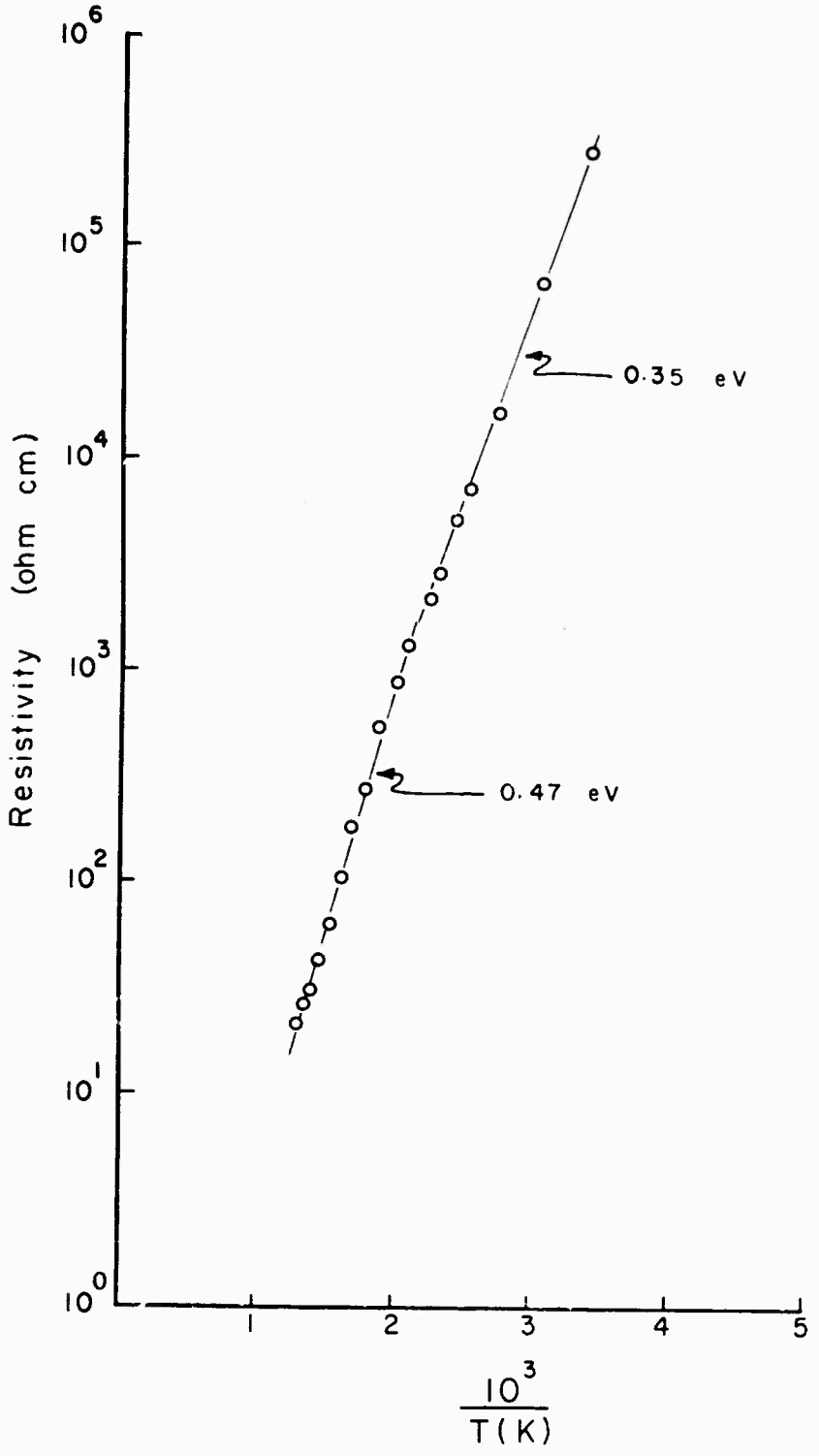

FIGURE 9. ELECTRICAL RESISTIVITY AS A FUNCTION OF INVERSE TEMPERATURE FOR ORTHORHOMBIC $YMnO_3$.

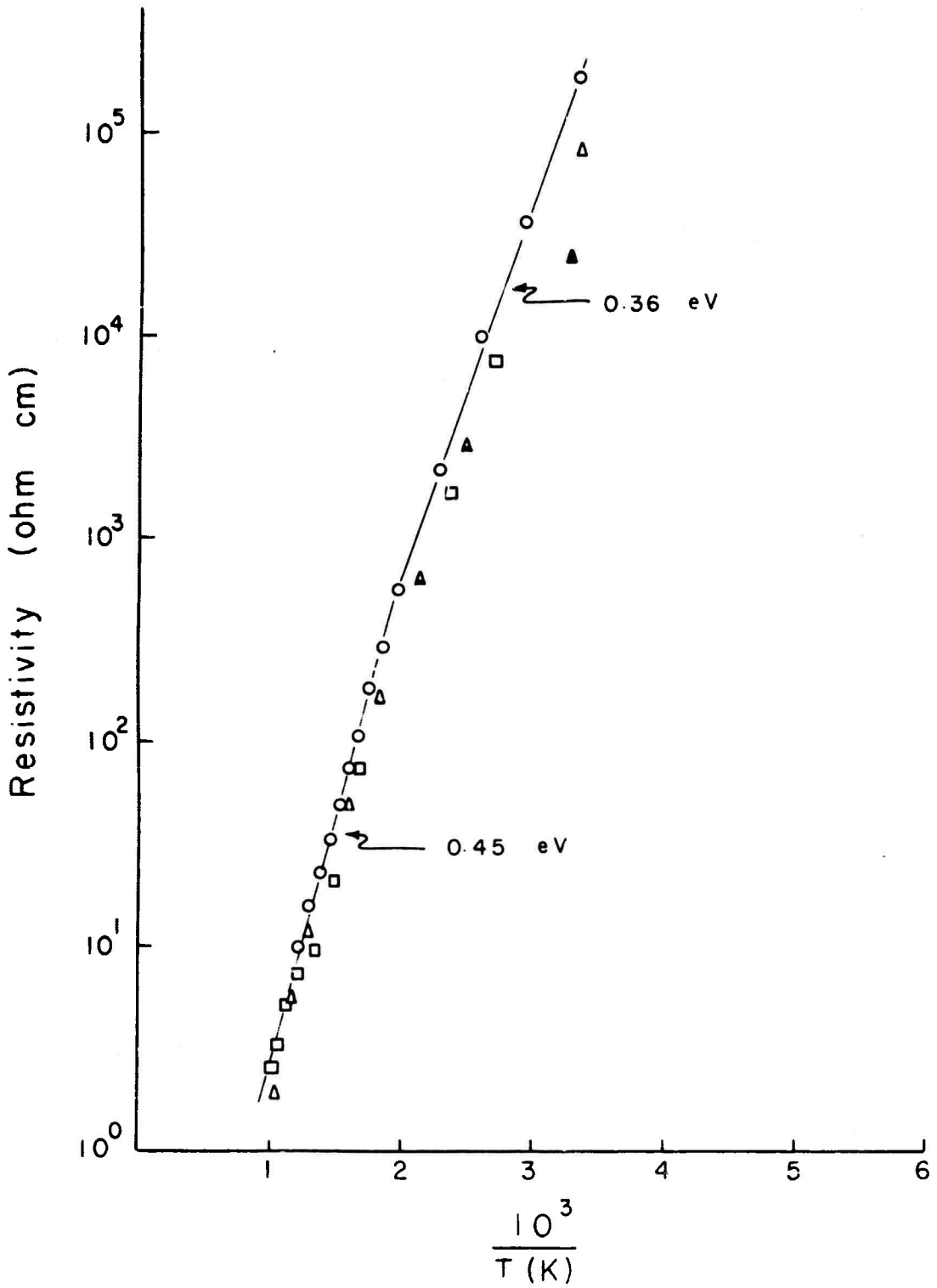

FIGURE 10. ELECTRICAL RESISTIVITY AS A FUNCTION OF INVERSE TEMPERATURE FOR ORTHORHOMBIC $YbMnO_3$. CIRCLES: FIRED SILVER CONTACTS, FIRST RUN; TRIANGLES: FIRED SILVER CONTACTS, SECOND RUN; SQUARES: PRESSURE CONTACTS, THIRD RUN; SOLID TRIANGLE: ROOM TEMPERATURE VALUE AFTER LAST RUN.

energies of the two samples are identical within experimental error. Even the magnitudes of the resistivities are nearly the same. Since the van der Pauw method employed in these measurements is not affected by contact resistance, the observed resistivities are believed to be characteristic of these specimens. The fact that two different compounds show the same results suggests that the activation levels are produced by the same kind of impurity and/or defect. In this regard, it is interesting to note that in the range of 530 to 770 K, Rao, et al. found an activation energy of 0.41 eV for hexagonal $YMnO_3$. It is possible that the impurity and/or defect which causes this activation level is the same as that which produces the 0.32 eV activation energy in our orthorhombic materials. In any case, the fact that both materials show a break point in the log ρ vs 1/T curve is not regarded as definitive evidence for ferroelectric transitions even though the break points are almost identical and the two materials, if ferroelectric, might be expected to show similar Curie temperatures.

IIB4. Prospects

The development of rare-earth magnetoferroelectrics has been approached by introducing ferrimagnetism in known ferroelectrics and also by seeking ferroelectric properties in magnetic compounds where crystalline symmetry and chemical similarity to known ferroelectrics make the occurrence of such properties relatively likely. The initial classes of compounds studied were ferroelectric rare-earth molybdates and hexagonal manganites. Neither of these classes was found to exhibit magnetoferroelectricity above about 10 K. However, the heavy rare-earth manganites remain promising because of the extensive solid solution of other 3d cations, particularly Fe^{3+}, which may develop ferrimagnetism. Here studies of the field dependence of magnetic susceptibility will be needed on the solid solutions in the hexagonal phase. Also solid solutions between the manganites and ferrites of other heavy rare earths besides ytterbium need investigation.

There remains the question of possible ferroelectricity in the high-pressure orthorhombic phases of the heavy rare-earth manganites and also in the rare-earth orthochromites. As previously mentioned, the recent report of non-centrosymmetric space group $Pbn2_1$ for the isomorphous compound $NdGaO_3$[10] confirms the need for separate examination of each compound. The observed weak ferromagnetism of $YbCrO_3$ below 114 K accentuates the need for clarification of whether it is also ferroelectric. Here study of single crystals grown from alkaline borate flux is needed. Probably other rare-earth chromite single crystals should also be studied. The rather extensive solid solution of $YbMnO_3$ in orthorhombic $YbCrO_3$ may lead to further control of the magnetic properties. Also we expect there will be solid solutions between the high-pressure phase of $YbMnO_3$ and $YbFeO_3$.

The present results indicate the need for further study of the effects of partial substitution of a second 3d cation in both the hexagonal heavy rare-earth manganites and in the orthorhombic phases.

The solid solutions between bismuth ferrite, $BiFeO_3$, and rare-earth orthoferrites appear similarly to offer regions with possible magnetoferroelectric properties. Here $BiFeO_3$ is a ferroelectric antiferromagnet while $(RE)FeO_3$ compounds are weak ferromagnets. Recently, a study of the $BiFeO_3$-$PrFeO_3$ system[20] has indicated the presence of both ferroelectricity and weak ferromagnetism at room temperature in a phase of 20 to 25 mole percent $PrFeO_3$. This system and those with other rare-earth ferrites should be investigated further with emphasis first on obtaining single-phase solid solutions for study of magnetic and electric properties.

IIC MOLYBDATES

In the β-phase, the rare-earth molybdates of formula $(RE)_2 (MoO_4)_3$ are ferroelectric[21] below about 430 K. Although this phase is nominally metastable, it is stable for all practical purposes. One might not anticipate these compounds would order magnetically at very high temperatures, but at least one molybdenum compound, MoF_3, orders antiferromagnetically[22] at 185 K; and in view of the interesting elastic properties[23] and good optical characteristics[24] of the molybdates, they seemed to warrant at least preliminary investigation.

Accordingly, powder samples of gadolinium, terbium, and europium molybdates were prepared by direct reaction of the oxides. Single crystals of $Gd_2(MoO_4)_3$ and $Tb_2(MoO_4)_3$ were then grown by the Czochralski method. While the achievement of outstanding optical quality was not a major goal, it was found that transparent material could best be grown by melting pre-reacted molybdate powder and by using low growth rates. The reported ferroelectric transitions were verified dielectrically and, in the case of $Gd_2(MoO_4)_3$, optically. The existence of piezoelectricity and pyroelectricity at room temperature was also verified. The magnetic susceptibility of $Gd_2(MoO_4)_3$ was measured from 77 K to above the ferroelectric Curie point; no anomaly at the transition was noted. At about this time, we received a preprint of the work of Keve et al.,[25] in which it was stated that no magnetic transitions were found in gadolinium or terbium molybdates down to 1.6 K. Their high-temperature data for $Gd_2(MoO_4)_3$ agreed well with ours. In view of these results, and since we could not think of a reasonable way to induce a transition by adding other ions, we decided these materials were not of sufficient magnetoferroelectric interest to justify further investigation. These materials have been most useful in testing and calibrating the piezoelectric resonance spectrometer described in Appendix E, and they appear to have some

possible applications which are being actively pursued by other workers. Some further details concerning our work in this area can be found in the Semiannual Technical Report.

III NARROW-GAP AND NARROW-BAND COMPOUNDS

IIIA INTRODUCTION

There is great current interest in materials which undergo transitions from a semiconducting or insulating state to a metallic one. Such transitions occur with changes in temperature or pressure, and also possibly with applied electric field, although this has never been unambiguously confirmed. Such an electric-field-induced transition might be of great practical value. While the understanding of these transitions as a general phenomenon is at best rudimentary, the difficulties, both experimental and theoretical, being formidable, it appears that many transitions involve the formation, from what were localized states, of some sort of narrow conduction band. Certain samarium compounds, where low-lying excited states may be just localized, are among the most interesting materials having such transitions.[26] Of particular importance for initial studies because of the gradual low-activation-energy transition it shows at low temperature is samarium hexaboride,[27] SmB_6. It was at first thought that the transition in this material simply reflected a gradual valence change of Sm^{2+} to Sm^{3+} with increasing temperature. Subsequently, Mossbauer measurements[28] were interpreted as showing that both divalent and trivalent ions were present in a proportion independent of the temperature. More recently, a model of activation of localized excited states has been proposed to explain the electric and magnetic properties of SmB_6.[29] Simply stated, this model assumes that the electrical properties may be accounted for by the promotion of a 4f electron of the divalent Sm ion ($4f^6$ configuration) to the 6s conduction state, but that this excited electron is sufficiently well localized that the magnetic properties may be described by applying Hund's rules to the pseudo-ion $4f^5$-$6s^1$ (in Section IIIB2 the magnetic properties of this pseudo-ion are discussed in detail). It is important to

establish the degree of validity of such a model for SmB_6 so that extensions can be made to the samarium monochalcogenides, which are technologically more interesting because they undergo pressure-induced insulator-to-metal transitions at room temperature. It seemed to us that the situation in SmB_6 could be clarified by i) electron spin resonance studied to establish the existence of the $4f^5$-$6s^1$ pseudo-ion, or alternatively to determine the valence state of the Sm ion, and ii) resistivity measurements on single crystals, rather than the powders previously used. Also it seems that SmB_6 might be a good material in which to look for an electric-field-induced transition.

In the following section we describe in detail the preparation and characterization of SmB_6 specimens and then discuss the results of electron spin resonance, nuclear magnetic resonance and electrical resistivity measurements on these samples. In Section IIIC we describe preliminary work on the preparation of samarium monochalcogenides and some solid solution alloys which might have similar electronic properties.

IIIB SAMARIUM HEXABORIDE

IIIB1 Preparation and Characterization

SmB_6 was prepared in powder form by reacting an intimate mixture of Sm_2O_3 and B_4C powders. The reaction was accomplished by raising the temperature of the mixture of 1500 C in a rf-heated tantalum susceptor-container in vacuo and holding at that temperature for several hours. The reaction is presumed to be[30]

$$Sm_2O_3 + 3B_4C \rightarrow 2SmB_6 + 3CO \quad .$$

Following these steps the material was ground and re-mixed, and the reaction procedure was repeated to ensure completeness. Initial preparations were made with 99.9% Sm_2O_3, while subsequent preparations were made with 99.99+% Sm_2O_3. The boron carbide was nominally 98+% pure, with a measured boron content of 76 wt% versus 78 wt% theoretical.

The SmB_6 powder was hydrostatically pressed at 6 kilobars into ~ 1/4-inch diameter rodlike slugs which were used as starting material for the preparation of dense, bulk specimens.

Three methods were used to prepare the bulk specimens: sintering, rf melting, and arc melting. Sintering was accomplished by rf heating at 1500 C - 1900 C for 0.5 to 2 hours in a tantalum susceptor-container in an atmosphere of pure helium. The sintered slugs were still porous, with porosity estimated at about 10% in the better cases.

For the rf melting and crystal growth, the pressed slugs were placed in a water-cooled copper boat in vacuo or in a hydrogen or helium atmosphere and were melted by use of a 4 MHz rf field. The melting temperature, determined by uncorrected optical pyrometry, was about 2300 C. In the course of melting, some material vaporized from the melt and deposited on adjacent cooler portions of the system. In vacuo, this rate of vaporization was found to be unacceptably high, thus forcing use of atmospheric pressure. Material melted in hydrogen was found to contain numerous bubble-like voids, presumably due to the dissolution of hydrogen in the molten material and its exsolution as freezing occurs. Material melted in helium, however, was virtually void-free. Although melting in a water-cooled copper boat yielded the first sizable fused pieces of SmB_6, the portions of the charge in contact with the copper were held at low temperature, and it was not possible to fuse the material completely. In an attempt to improve the technique, with the aim of preparing larger sound specimens and single crystal

specimens, pyrolytic boron nitride was utilized as a container material. Following a run, X-ray diffraction analysis of material from the interface region showed only BN and SmB_6 to be present. This suggests that there was no reaction between the BN container and the molten boride, and that pyrolytic BN is a suitable container for the fusion and growth of crystals of rare-earth borides and possibly other refractory rare-earth compounds of this type.

"Buttons" of dense material were prepared by arc-melting the pressed slugs on a water-cooled copper hearth in a pure helium atmosphere using a tungsten electrode. These buttons contained some voids and fracture lines, presumably because of the intensely localized heating and the severe thermal gradients imposed in the process. The best SmB_6 melt-growth results were obtained by rf melting. Sizable, sound pieces of SmB_6 were prepared with dimensions up to 1 cm. These contained relatively large crystals with faces up to 4 mm^2, revealed by cleavage. Further development of the method to yield large single crystals should be possible.

SmB_6 powder, prepared from stoichiometric quantities of Sm_2O_3 and B_4C, was found by X-ray diffraction analysis to contain SmB_4 as a second phase. It was possible to eliminate this second phase and to get roentgenographically single-phase powder by adding a calculated excess of B_4C. However, the observed loss of material by vaporization during melt growth suggested the possibility of a shift in composition in the course of this processing step.

Material vaporized from the melt during growth runs could not easily be identified by X-ray diffraction analysis since it was amorphous, but emission spectrography showed that the vaporized material contained major concentrations of both samarium and boron. When one specimen that contained a minor phase of SmB_4 was melted, X-ray diffraction analysis revealed that the SmB_4 concentration

was decreased appreciably in the process. In the course of arc melting, also, samarium was lost preferentially from the melt; when the starting material was stoichiometric, the arc-melted material was found by electron microprobe analysis to contain boron intergranular phase. By starting with excess Sm, material was prepared which did not contain this boron phase after remelting. This was shown both metallographically and by electron probe microanalysis.

The above discussion on the characterization of the SmB_6 specimens can only be made complete by reference to some particular results of the ESR and NMR experiments described in the following two sections. Among other things, both resonanance techniques clearly showed the presence of remnant B_4C and/or amorphous boron even in those specimens which were shown to be substantially single phase by X-ray diffraction. In fact, it was this result which suggested the use of emission spectroscopy and electron-microprobe analysis discussed earlier. For example, we consider the powder sample which was prepared with an excess of B_4C. The B^{11} NMR studies showed two types of resonances, one being characteristic of SmB_6, as described in Section IIIB3, and the other characteristic of B_4C as determined by comparison with NMR measurements on this compound alone. Relative intensity measurements on this "SmB_6" sample suggested that only about 80% of the boron nuclei were contained in the SmB_6 compound. Assuming the remainder were contained in B_4C, the calculated weight percent of carbon would be about 2 percent. Subsequent micro-combustion analysis revealed a carbon content of about 1 weight percent. A sample of remelted SmB_6 (not however, prepared with excess B_4C) was also analyzed for carbon content and was found to contain only 0.01 weight percent carbon. This is not surprising since B_4C has a considerably higher melting point and lower density than SmB_6 so that any unreacted excess will tend to float out on remelting. This was confirmed metallographically. NMR measurements on the low-carbon-content sample showed a much reduced intensity

for the unwanted resonance; however, these measurements were not commensurate with the extremely low value found by microcombustion. This led to the suspicion that the remaining unwanted signal was due to B^{11} nuclei in amorphous boron which would not be detected by X-ray or carbon content analysis.

Finally, it should be mentioned that B^{11} NMR resonances were never observed in powder samples of SmB_6 prepared from 99.9% pure Sm_2O_3 while intense resonances were seen in those powders prepared with the higher purity starting material. The signal intensity observed in the latter case indicated that most of the boron nuclei contributed to the pattern. This observation is the best available evidence that the SmB_6 portions of the samples are quite homogeneous, since random deviations from crystallinity would cause a distribution of electric field gradients and, thus, broaden the resonance to such an extent that it would be difficult to see. It is unfortunate that such a good test of sample quality does not seem to have been made on SmB_6 samples investigated in other laboratories.

IIIB2 Electron Spin Resonance

As mentioned in Section IIIA, the conduction mechanism in SmB_6 is believed to involve the delocalization of a 4f electron of the divalent Sm ion ($4f^6$ configuration) by thermal excitation to the 5d or 6s conduction band. Indeed, Mossbauer experiments have been interpreted[28] in terms of the simultaneous existence of both $Sm^{2+}(4f^6)$ and $Sm^{3+}(4f^5)$ ions. However, no changes in the Mossbauer spectrum were observed as the temperature was varied through the region where the electrical conductivity[27] undergoes a transition. In addition, magnetic susceptibility measurements have been unsuccessful in detecting the expected paramagnetism of the Sm^{3+} ion. Thus, one of two points of view must be adopted;

either the Mossbauer observation of the $4f^5$ configuration is in error, or one must postulate a model whereby the paramagnetism of the $4f^5$ configuration is cancelled by a relatively localized 5d or 6s electron which is generated from a well-localized 4f electron of the Sm^{2+} ion. In the following we discuss separately these two possibilities.

The ground state of the Sm^{2+} ion has no net angular momentum and is thus nonmagnetic, while the Sm^{3+} ion has a J = 5/2 ground state which is highly paramagnetic. It therefore seemed reasonable to use ESR experiments to determine the valence state of the Sm ion in SmB_6. Operating at both X-band and K-band frequencies a very intense, extremely broad resonance was observed in the first prepared specimens. However, the effective gyromagnetic ratio was not commensurate with that expected for the Sm^{3+} ion in a crystal field appropriate to the SmB_6 lattice. Crystal field calculations did suggest that the observed properties could result from the first excited angular momentum state (J = 1) of the Sm^{2+} ion. This state, which we estimate to be about 380 K above the ground state, is expected to have a very short relaxation time leading to an extremely broad ESR signal in agreement with that observed. In addition, the signal intensity showed approximately the temperature dependence corresponding to the population predicted by the Boltzmann distribution for a state situated 380 K above the ground state. Since the ESR of such thermally excited multiplet states had never been observed it was felt that similar observations in other systems were necessary to establish the validity of the proposed explanation. Several unsuccessful attempts were made to detect the ESR of the first excited state of the Sm^{2+} ion in SmF_2, SmSe and Sm-doped CaF_2. It was concluded that the resonance observed in the initially prepared SmB_6 specimen was due to large scale impurity concentrations of unknown origin. Subsequent ESR studies on higher purity

specimens confirmed this by showing no evidence of the above-mentioned signal. Thus it is clear that although SmB_6 may contain a large number of Sm ions having five 4f electrons these ions do not correspond to the unperturbed Sm^{3+} valence state.

An alternative explanation for the lack of paramagnetism associated with Sm^{3+} ions is that the transition from $4f^6$ to $4f^5$-5d or 6s leaves the 5d or 6s electron sufficiently localized that its magnetic moment cancels that of the $4f^5$ configuration. One possibility is that the excited electron occupies the 6s state which has its spin angular momentum parallel to the net spin of the 4f electrons. Assuming the 6s electron is relatively localized and applying Hund's rules to this pseudo-ion yields the following total angular momentum vectors: S = 3, L = 5 and J = L - S = 2. The interesting aspect of such a state is that although the total angular momentum is finite the Landé g factor,

$$g_J = 1 + \frac{J(J+1) - L(L+1) + S(S+1)}{2\,J(J+1)} \quad ,$$

is zero resulting in a magnetic moment which is likewise zero. Subsequent to our recognition that the $4f^5$ - 6s|| "ion" is non-magnetic, it was shown[29] that such a model is consistent with all known properties of SmB_6. However, these results do not confirm the validity of the proposed model, and a direct test of the postulated state is needed, especially since the mechanisms involved are believed to be responsible for the semiconductor-to-metal transitions observed in a large number of Sm chalcogenides. One test of the above model is to detect the paramagnetism associated with the so-called antiparallel state, i.e., the state in which the spin of the 6s electron is opposite to the net spin of the five 4f electrons. This state, designated $4f^5$-6s#, must also be present if the $4f^5$-6s|| state exists, and it has been predicted[29] that it lies about 80 K above the ground state. The fact that this state is magnetic may be seen from Hund's

rule, which predicts S = 2, L = 5 and J = L - S =3, and the Landé g factor which for this case is $g_J = 0.5$. We have searched diligently for the ESR associated with this state. According to Cohen[28] about 70% of the SM ions in SmB_6 are in the $4f^5$-6s configuration. Assuming the value of 80 K for the $4f^5$-6s# state relative to the $4f^5$-6s|| ground state is correct, it is estimated that about 30% of the available ions are in the magnetic state at room temperature. Furthermore, crystal field calculations have been made to predict an effective g value for ESR of $g_{eff} = 3/2\ g_J = 3/4$. Resonances have not been observed at this position in any of the SmB_6 specimens, but because various broadening mechanisms could render such a resonance unobservable this negative result does not necessarily imply that the proposed model is not applicable to SmB_6.

IIIB3 B^{11} Nuclear Magnetic Resonance

Although the presence of small concentrations of unreacted B_4C and/or precipitated boron has complicated the study of the B^{11} NMR properties in SmB_6, it has not precluded a determination of the electric quadrupole coupling constant. Since this quantity is the product of the electric quadrupole moment of the B^{11} nucleus, the value of which is well known, and the electric field gradient at the boron site, information about the electron distribution in SmB_6 can be inferred. Using a standard continuous-wave, induction spectrometer similar to that manufactured by Varian Associates and conventional lock-in detection, a typical powder pattern spectrum of the central ($1/2 \rightleftarrows - 1/2$) transition and both satellite ($1/2 \rightleftarrows 3/2$; $- 1/2 \rightleftarrows - 3/2$) transitions has been observed over the frequency range of 4 to 24 MHz. The central transition is complicated by the fact that resonances from B_4C and/or free boron are superimposed on the quadrupole-broadened pattern. However, the satellites, being well removed, do not suffer from this difficulty and the satellite splitting yields a well-defined electric quadrupole

coupling constant of 0.58 MHz. Using this value it is possible to identify self-consistently those peaks which belong to the central transition and to correlate the extra peaks with B^{11} resonances from the unwanted contaminants. As discussed in the last two paragraphs of Section IIIB1, the latter resonances have been useful in characterizing the homogeneity of our specimens. Since the electric quadrupole moment of the B^{11} nucleus is quite large, the rather small value of the quadrupole coupling constant (0.58 MHz) indicates that the point symmetry at the boron site (tetragonal C_4) in SmB_6 is actually only a small distortion of the overall cubic (O_h) symmetry of the lattice.

Finally, it is noted that the B^{11} resonance in SmB_6 is easily saturated; this indicates that the sample does not contain an appreciable number of highly paramagnetic ions, such as Sm^{3+}, at room temperature. Thus in agreement with the fact that ESR signals associated with this state have not been found, it seems improbable that the high conductivity can be explained as a simple ionization of the divalent samarium ions to the trivalent state.

IIIB4 Electrical Properties

Two samples of SmB_6 were used for measurement of electrical transport properties. One was obtained from the initial pressed and sintered ingot and one from a fused ingot. As discussed in Section IIIB1 there were substantial differences in porosity, density, and hardness and rather smaller differences in composition between the two specimens. The sintered specimen was rather porous and soft, but was single phase. The fused specimen, on the other hand, was hard and dense but contained SmB_4 in trace amounts. Measurements have not yet been made on the newest arc-melted samples. These samples do not contain SmB_4 or free boron and are not porous, but they do have a small number of minor cracks and voids.

As a result of the high porosity in the one case, and the presence of SmB_4 in the other, neither sample was of the quality desired. Nonetheless, resistivity data were obtained on both specimens at 300 and 77 K. The results were:

Sample	Resistivity ρ, ohm-cm	Temperature, °K	ρ_{77}/ρ_{300}
Sintered	7.13×10^{-4}	300	1.20
	8.58×10^{-4}	77	
Fused	6.37×10^{-4}	300	1.42
	9.05×10^{-4}	77	

Both specimens appear to be semiconducting. The resistivity ratio is higher in the fused specimen and also appears a little higher than that reported by Menth, et al. It is not known at this time whether the difference between the samples is the result of voids, crystalline perfection, variation of composition, or impurities. However, the differences are small indicating intrinsic conductivity as expected.

In view of the fact that the activation energy in SmB_6 is intrinsic to the material, rather than being controlled by impurity levels as in Ge, we are considering the possibility of using SmB_6 as a low-temperature thermometer (in the range 4-40 K). The sensitivity is adequate, and the compound appears to have other desirable properties.

Work was undertaken to estimate the change in conductivity resulting from a rise in temperature when a narrow-gap semiconductor like SmB_6 is subjected to a short voltage pulse. Because of the non-linearity of the problem, and since not all the relevant thermal properties of the material are known accurately, a complete solution of the problem is rather difficult. But it appears that study of certain limiting cases should enable us to rather simply identify relevant combinations of parameters and to make reasonable estimates of conductivity changes.

The conductivity change in SmB_6 owing to a rise in temperature when the sample is subjected to a short voltage pulse was estimated for the conditions of

a) a sample thin in the direction of current flow, and

b) thermometric contacts (that is, no heat flow away from the contacting surfaces).

The temperature rise above the ambient for a very short pulse is given by

$$T = \frac{\mathcal{E}^2 \pi \sigma(T)}{\rho\, c(T)} \quad ,$$

where $\mathcal{E}$ is the applied field, π is the pulse length, σ the electrical conductivity, ρ the density, and c the specific heat. This is independent of the thermal conductivity since it is based on a diffusion approximation to a transport equation; in practice, this means there is some limitation on the sample thickness for which the temperature may be considered constant across the sample. Utilizing the recently published data of Nickerson, et al,[29] we find that at low temperatures the ratio $\sigma(T)/c(T)$ is almost temperature-independent (as is required for the above equation to hold). For a 20 ns pulse of strength 500 volts/cm, we obtain a temperature rise of only 18 degrees. Even with somewhat stronger pulses, there does not seem much likelihood of thermal breakdown as long as the pulse length is short. Also, the heat capacity of the contacts will doubtless reduce the temperature rise below that which we have calculated here. Whether fields of this order of magnitude are sufficient to induce some sort of breakdown effects remains to be determined experimentally; it should be noted that even for such a narrow-gap material as SmB_6, the Zener tunneling breakdown field should be about 1000 to 20,000 volts/cm (depending on approximations and values of parameters used in calculating it).

IIIC SAMARIUM CHALCOGENIDES

In Section IIIA it was emphasized that we regard our efforts to establish the validity of a simple model to describe the electrical properties of SmB_6 as prerequisite to understanding the condiction mechanisms in the samarium monochalcogenides. These interesting materials undergo pressure-induced semiconductor-to-metal transitions at room temperature; in the selenide and telluride the transition is continuous while in the sulfide a discontinuous transition occurs at 6.5 kilobars. These results suggest that solid solutions of SmS-SmSe and SmS-SmTe might have extremely interesting properties; for example, it may be possible to obtain discontinuous transitions in both pseudobinary systems and simultaneously to achieve semiconducting state resistivities which are much higher than that of SmS.

The samarium monochalcogenides have been prepared[31] by reacting samarium-metal filings or turnings with the Group VI element at moderate temperatures (400-850 C) in sealed silica ampoules. Subsequently the material was melted in a tantalum container in an inert atmosphere to form a polycrystalline-fused ingot. Usually the ingot contained large crystals from which single-crystal specimens could be cleared or cut.

Work has been started on the SmS-SmSe solid solution. Granular samples of $SmS_{.5}Se_{.5}$, $SmS_{.75}Se_{.25}$, and $SmS_{.9}Se_{.1}$ were prepared by direct reaction of the elements as described above. Melting these materials in an rf field and refreezing yielded single-phase crystalline material only for the composition $SmS_{.75}Se_{.25}$. This composition is estimated to be near the threshold of the discontinuous transition.

IV PNICTIDES

IVA INTRODUCTION

The rare-earth monopnictides are the compounds of formula (RE)(Pn) where Pn denotes one of the so-called pnigogens - N, P, As, Sb or Bi. Almost all of these compounds have the simple NaCl structure. The nature of these materials--whether they are semiconducting or metallic, or whether they are inherently non-stoichiometric--has been subject of investigation and controversy for at least ten years. In the past year or so, however, a good deal of experimental evidence has been presented[32] which is interpreted as showing that these materials are all metallic. The evidence is relatively clear in the phosphides, arsenides, antimonides and bismuthides, where there are fewer problems with stoichiometry and where there are (in the first three cases) recent nuclear magnetic resonance measurements[33] which indicate a hyperfine field more typical of a metal. The situation is not nearly so unambiguous in the nitrides, where stoichiometry is very difficult (perhaps impossible) to attain. The principal arguments one might advance that the rare-earth nitrides should be semiconductors are as follows:

1) Band calculations using neutral ion potentials indicate semiconductivity [34]
2) Optical absorption[35] shows evidence of something resembling an energy gap
3) Metallographic examination[36] of some nitrides shows a tendency for metal to concentrate at grain boundaries.

Likewise, the principal arguments[32] for metallic character of these compounds are:

1) Transport property measurements are generally typical of metals
2) Specific heat measurements can be interpreted as indicating a considerable density of electrons at the Fermi surface
3) Changes in magnetic properties on adding small amounts of oxygen or carbon are of the sort expected in a metal.

Objections can easily be raised to the arguments on both sides, but it is more profitable to ask what would be convincing experiments. When we undertook work to understand something of the nature of these materials, we considered transport measurements on compact, polycrystalline specimens (previous measurements having all been on pressed powders) of as near stoichiometric composition as possible. Reflection showed that this was not necessarily a good idea, since one has no way of knowing how near stoichiometry is near enough. What is more, it may well be that difficulty in obtaining sound samples is not independent of difficulties in achieving stoichiometry (such is the case in some III-V semiconductors), and to the extent that non-stoichiometry is intrinsic, compact homogeneous samples of reasonable size might prove extremely difficult to produce. In view of this, it seems more reasonable to undertake nuclear magnetic resonance measurements on samples prepared as nearly stoichiometric as possible. In addition to providing information about metallic character by virtue of the hyperfine field at the nitrogen site, NMR measurements may be used to reveal directly the degree to which the compound conforms to stoichiometry. Large deviations from stoichiometry will lead to distortions of the cubic symmetry of the lattice and thus to quadrupolar broadening due to a distribution of electric-field gradients. Some previous NMR measurements[37] on TbN and TmN indicate that the nitrogen resonance is observable.

As described in the following section, we have quite recently succeeded in preparing samples of DyN apparently near stoichiometry for NMR studies. These experiments have not been done yet, but should be completed soon. If we conclude the nitrides are metallic, or if the results are ambiguous, we plan to report our findings and dismiss the monopnictides from further consideration. If we find they are clearly semiconductors, and that they can be prepared near stoichiometry, we will consider possible further developments as part of a separate program.

IVB PREPARATION AND CHARACTERIZATION

In work by others, rare-earth nitrides have been prepared by arc melting[35] and by "flash" melting[38] in nitrogen atmospheres and by reaction between the rare-earth hydrides and ammonia.[36,39] In all cases for which analytical data have been presented, the material was found to be nitrogen deficient, with deficiencies ranging from a few tenths percent (concluded indirectly) to 10%. In one investigation,[35] films were formed by vacuum evaporation. However, the films were kept in high vacuum and no analysis or characterization was made of the film material other than that of optical transmission. In all other investigations for which material preparation has been described, powder material was pressed and sintered to obtain bulk specimens for study.

One objective of our synthesis work has been the development of techniques for the direct preparation of bulk specimens, thus circumventing the need for the pressing and sintering step and avoiding its deficiencies. A second objective has been the preparation of pure, stoichiometric nitride in powder form for use in NMR studies. In working toward this second objective, emphasis has been put on the use of low-reaction temperatures in order to minimize potential deviation from stoichiometry resulting from a tendency for thermal dissociation to occur in such compounds.

Three methods were explored for the preparation of the nitrides. They are reactions of:

1. chloride with ammonia,
2. metal with ammonia,
3. metal with nitrogen.

GdN was selected as the pilot material and initial work was concerned with its preparation. When it was noted in a recent RCA report[40] that GdN and LaN were observed to be the most unstable of the nitrides, our effort was shifted to the preparation of DyN.

Although thermodynamic analysis predicts that the reaction of rare-earth chloride with ammonia will not proceed, Dismukes and Yim[40] reported successful vapor-epitaxial preparation of scandium and rare-earth nitrides on sapphire substrates by use of this reaction. Therefore this reaction was investigated as a method for preparing rare-earth nitride for NMR studies.

To avoid the formation of dysprosium oxides which would interfere with NMR measurements, it was desirable to carry out the reaction in two steps, with the anhydrous chloride being prepared, then converted <u>in situ</u> to the nitride:

$$2\ Dy_2O_3 + 3CCl_4 \rightarrow 4\ DyCl_3 + 3\ CO_2$$

$$DyCl_3 + NH_3 \rightarrow DyN + 3HCl \quad .$$

The reaction system that was designed and assembled also made possible the synthesis of the product nitride in a silica tubing section that could be sealed off to form a silica ampoule suitable for direct use in the NMR studies. The ammonia employed was dried with sodium metal.

Several runs were made on the chloride-ammonia reaction. The first step for the preparation of $DyCl_3$ from Dy_2O_3 proceeded satisfactorily in each case in accord with our previous experience.[41] However, no evidence of reaction

between $DyCl_3$ and NH_3 was seen, even after prolonged periods at temperatures in the range 800 - 900 C. This lack of reaction is in accord with our estimates of the free-energy change of the reaction. Thus it is concluded that the nitride cannot be prepared in this way.

Dismukes and Yim[40] also reported the involvement of rare-earth metal vapor (e.g., Yb) in some of their "nitride-forming" reactions. The conclusion reached in other work in our laboratories,[42] which is supported by both thermodynamic and experimental results, is that rare-earth metal vapor will react with both Al_2O_3 (used as substrate material) and SiO_2 (reaction-tube material) to form complex oxides, including aluminates and silicates. Since the oxide formation is thermodynamically heavily favored, it is not clear how a pure nitride film can be formed on Al_2O_3 substrates under such conditions.

In synthesis involving direct nitriding of rare-earth metal, several types of reactions were investigated:

1. the reaction of metal in solid, bulk form with ammonia or nitrogen,
2. the reaction of metal in solution in tin or indium with ammonia,
3. the reaction of metal filings with ammonia or nitrogen.

The reactions are very sensitive to traces of moisture and/or oxygen, and if detectable traces of either are present the material produced generally will be predominantly oxide--with only minor amounts or thin layers of nitride present. Oxygen and water vapor can be introduced by diffusion through system parts--such as polymeric tubing and heated ceramic (e.g., mullite) tubing--and as impurities in reactant gases. Both of these were factors in early synthesis on this project which yielded mixed oxide-nitride material. Mixed nitride-oxide

compounds with a relatively large amount of oxygen, yet retaining the halite structure, are easily produced; we eventually found this out by electron microprobe analysis--the literature has little to say on this point. These compounds, which are almost surely metallic and of very little intrinsic interest, do have slightly reduced lattice parameters compared to supposed <u>echt</u> material (see below). The diffusion was eliminated or minimized by making all tubing of copper, stainless steel, or silica; and by utilizing fused silica reaction chambers with the chamber walls kept at low temperatures through use of rf induction heating of the reactants. The ammonia was dried (and deoxidized) by forming sodium-liquid ammonia solutions, then utilizing the dry ammonia that distilled from the solutions. Pure, dry nitrogen was obtained by using the gas that distilled from a 100-liter reservoir of liquid nitrogen; in other work at our laboratories it has been determined that this is a high grade of nitrogen.

Attempts to prepare bulk specimens of nitride by reacting nitrogen or ammonia with bulk, solid rare-earth metals were unsuccessful. Reactions attempted involved Gd, Dy, and Er and ammonia at temperatures in the range 1000 to 1200 C, and Gd and nitrogen at temperatures in the range of 1200 to 1530 C. If the rare-earth metal was heated gradually, only a thin skin or layer of nitride formed and this apparently retarded further reaction greatly. If the rare-earth metal was heated rapidly in nitrogen, a highly exothermic reaction was initiated and the heat generated melted the rare-earth metal. In such "runaway" reactions, small cubic crystals of GdN (< 1 mm on a side) were formed from solution in the molten Gd metal, and some GdN crystals formed on the surface of the Gd metal that remained solid. Lattice constants for this material ranged from $a_o = 4.985$Å to $a_o = 4.966$Å. Since these values are below that reported for pure GdN,[39] it is presumed that the nitride contains some oxygen[38] or is nitrogen deficient.

Attempts to grow bulk crystals of rare-earth nitride from solution in molten metal likewise were unsuccessful. A number of experiments were conducted which involved the reaction of Dy in solution in molten tin or indium at temperatures in the range 820 to 1500 C. No evidence of nitride formation was seen.

Samples of granular DyN for use in NMR studies were successfully prepared by reacting Dy metal filings with nitrogen. The filings were contained in a pyrolytic boron nitride container within a graphite susceptor. The nitrogen flowing through the system was that distilling from a liquid nitrogen reservoir (as discussed above). The Dy was heated slowly to the selected reaction temperatures which were 1625 C and 1800 C, respectively, for the two samples prepared for NMR studies. The temperature was held for 10 - 15 minutes, then was reduced gradually at a rate of about 100 C per hour to about 900 C. The main portion of the material was poured into the sample-tube section of the reaction system and sealed off. A small sample was retained and removed from the reactor in a dry atmosphere for X-ray diffraction analysis. Lattice constants for the two samples were $a_o = 4.9015 \pm 0.0005$Å and $a_o = 4.9060 \pm 0.0005$Å, respectively. These are close to the literature value[39] for pure DyN, $a_o = 4.905 \pm 0.005$Å. Since either oxygen impurity or deficiencies of either Dy or N would be expected to reduce the lattice constant, it is believed that these samples, particularly the one prepared at 1800 C, are of good quality.

Studies on powder samples prepared in the manner just described should help determine whether the rare-earth nitrides are semiconductors or are semimetallic. Further development of material preparation techniques appears feasible. Although efforts to produce bulk specimens directly have not so far been successful, only limited experimentation with appropriate combinations of pure reactants, reaction and heating conditions, and reaction temperatures has been possible.

V. RARE EARTH IONS IN INSULATORS

Our research concerning the optical properties of rare-earth-doped dielectric crystals generally has been confined to the effect of interactions among the rare-earth ions on their fluorescence properties. The fluorescence properties of the rare-earth ions present as dopants in dielectric crystals are relevant to the design and understanding of devices such as lasers and infrared-to-visible converters. Though the spectroscopic properties of isolated rare-earth ions in many host crystals have been studied extensively, until recently the effects of interactions among the ions have not received much attention. These interactions can have a profound influence on quantum efficiencies and decay times of particular fluorescence schemes and can also lead to new fluorescence excitation schemes. Hence, a series of experiments designed to increase our understanding of how interaction among rare-earth ions leads to cooperative excitation of fluorescence was undertaken. Specifically, we have studied the infrared excitation of red fluorescence in Ho^{3+}, present as a dopant in CaF_2.

In our initial experiments the steady-state red fluorescence output was measured as a function of infrared input. That the output depended on the square of the input intensity led to the conclusion that two infrared photons were involved in the excitation process. Additionally, the dependence of the steady-state red output on the Ho^{3+} ion concentration indicated that more than one ion was involved in each fluorescence event. Problems associated with the study of optically thick samples precluded the determination of the number of Ho^{3+} ions involved. Consequently, a dynamic theory applicable to pulsed excitation of the fluorescence and measurement of the lifetimes of the optical energy levels was developed. Comparison of this theory with the experiments using pulsed infrared excitation clearly showed that two Ho^{3+} ions were involved in each red fluorescence event.

The explanation of the process by which the fluorescence was excited is that two ions, each excited to the $^5I_6$ level, cooperate in the transfer of excitation from one ion to the other, with the result that one ion is further excited to the $^5F_5$ level and the other deexcited to the ground state. Examination of the energy level diagram (Fig.11) shows that the energy of the $^5F_5$ level is considerably less than twice that of the $^5I_6$ level. Furthermore there is no single-ion excited state with this energy. This means that there is an apparent lack of conservation of energy in this process which we felt had to indicate the emission of phonons into the crystal lattice. The probability of this type of event is a strong function of the number of phonons involved. The CaF_2 lattice will support relatively energetic phonons compared to LaF_3, which has a much lower Debye temperature. To verify the participation of the lattice in the cooperative event, the cooperative excitation experiment was attempted in LaF_3. No red output could be seen, thus confirming the notion that the lattice must participate in the cooperative excitation process. A paper describing this work will appear in the June 1971 issue of the Journal of Applied Physics.

More recently, our research has been directed to study of the role of lattice phonons in the energy balance of the cooperative process. If emission of phonons is involved in the decay from the postulated pair-state to the single-ion $^5F_5$ state, the transition probability (at least in a naive sense) will be proportional to $(n + 1)^r$. Here n is the temperature- and phonon-frequency-dependent number density of phonons given by

$$n = \left[\exp\,(h\nu/kT) + 1\right]^{-1} \quad ,$$

where ν is the phonon frequency and r is the number of phonons involved in the pair-state to $^5F_5$ transition. For energy conservation, r x $h\nu$ must be equal to the energy level spacing of 0.21 eV (leading to a value of r of 5 or 6 in CaF_2).

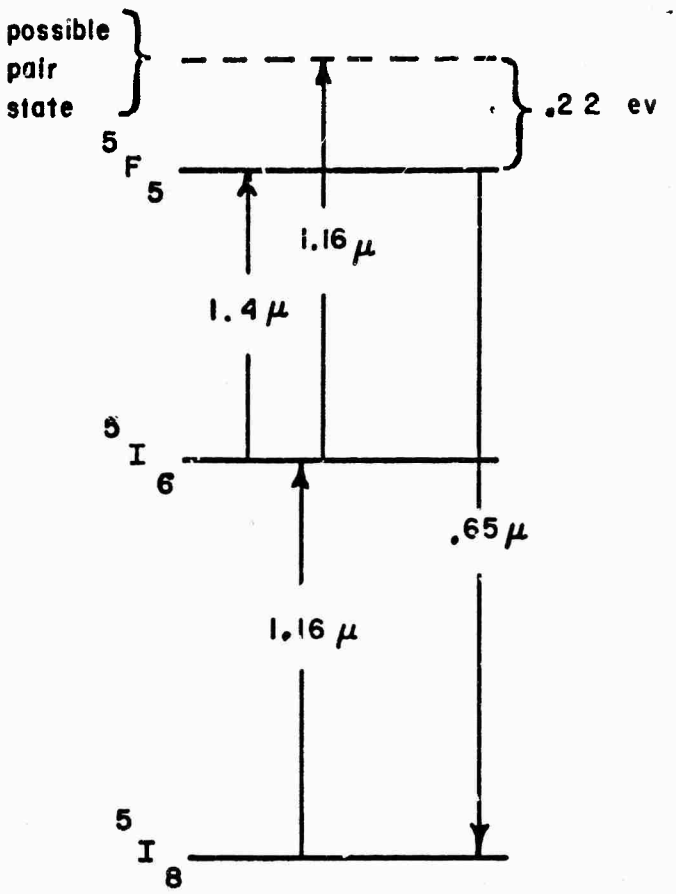

FIGURE 11. PARTIAL ENERGY LEVEL DIAGRAM OF Ho^{3+} IN CaF_2

As the temperature is decreased, n will decrease leading to a corresponding decrease in the rate of decay from the pair state and a consequent decrease in fluorescent output from the $^5F_5$ state. With this in mind the infrared-excited red fluorescence output was measured at room temperature and at 77 K. Within experimental error (~ 10%), the output did not change, providing no information with respect to the role of phonons in the decay process. If phonons are involved one can only conclude that $n \ll 1$ at both temperatures and hence the output does not reflect the change in phonon density in the crystal.

A straightforward method for observing the pair state would be by direct optical absorption measurements. One would expect to observe a relatively weak absorption about 0.22 eV away from a stronger absorption to the $^5F_5$ single ion state at 0.65 μm. A perturbation calculation was performed to determine the ratio of the absorption coefficients for these two absorptions. The results indicate that this ratio is on the order of 10^{-8}. This would make such an experiment prohibitively difficult and it was not attempted.

This completes the proposed work on non-radiative energy transfer. While we were not able to prove absolutely the existence of a pair state, we have shown rather conclusively through dynamic studies of the infrared-excited red fluorescence of Ho^{3+} in CaF_2 that one can differentiate between successive and cooperative excitation of fluorescence. For Ho^{3+} concentration greater than 0.5 to 1 atomic percent, this cooperative process is dominant. Since the cooperative process depends on the square of the concentration while the successive process involving a single ion ($^5I_8 \rightarrow {}^5I_6 \rightarrow {}^5F_5$) is linear, the successive process becomes dominant at lower concentrations. The results on Ho^{3+} in LaF_3 lead us to postulate the emission of phonons to conserve energy in the cooperative process.

VI. REFERENCES

1. T. F. O'Dell, The Electrodynamics of Magnetoelectric Media (North Holland, 1970).

2. L. N. Bulaevskii and V. M. Fain, JETP Letters 8, 165 (1968).

3. E. Ascher, J. Phys. Soc. Japan 28 (Supplement), 7 (1970) (Particularly discussion).

4. A. I. Akhiezer and I. A. Akhiezer, Sov. Phys.-JETP 32, 552 (1971).

5. E. F. Bertaut, F. Forrat, and P. Fang, Comptes Rendus 256, 1958 (1963).

6. R. Pauthenet and C. Veyret, J. de Physique 31, 65 (1970).

7. A. Waintal and J. Chenavas, Mat. Res. Bull. 2, 819 (1967); Comptes Rendus 264, 168 (1967).

8. G. V. Subba Rao et al, J. Phys. Chem. Solids 32, 345 (1971); P. Coeure, Solid State Comms. 6, 129 (1968); J. P. Van der Ziel and L. G. ran Uitert, Phys. Rev. 179, 343 (1969).

9. H. L. Yakel et al, Acta Cryst. 16, 957 (1963), and present work.

10. H. Brusset et al, Bull, Soc. Chim. France 8, 2886 (1967).

11. A. P. Young, P. B. Robbins, and C. M. Schwartz, p. 262, and P. N. LaMori, p. 321, in High Pressure Measurements (A. A. Giardini and E. C. Lloyd, eds.) (Butterworths, Washington, 1963).

12. J. E. Mee et al, IEEE Trans. Mag. 5, 717 (1969).

13. F. H. Wehmeier, J. Crystal Growth 6, 341 (1970).

14. K. Dwight and N. Menyuk, Phys. Rev. 119, 1470 (1960).

15. R. Buhl, J. Phys. Chem. Solids 30, 805 (1969).

16. N. Menyuk, A. Wold, et al., J. Appl. Phys. 33, 1144 (1962).

17. G. Gorodetsky and D. Treves, Proc. Internat. Conf. Magnetism (Nottingham, 1964); K. P. Belov et al., Izv. Akad. Nauk SSSR, Ser. Fiz., 34, 951 (1970).

18. E. F. Bertaut et al, IEEE Trans. Mag. 2, 453 (1966).

19. L. J. van der Pauw, Philips Res. Repts. 13, 1 (1958).

20. A. S. Viskov et al, Inorg. Mater. 4, 71 (1968).

21. H. S. Borchardt and P. E. Bierstedt, J. Appl. Phys. 38, 2057 (1967).

22. M. K. Wilkinson et al., Phys. Rev. 121, 74 (1961).

23. A. W. Smith and G. Burns, Phys. Letters 28A, 501 (1969).

24. S. E. Cummins, Ferroelectrics 1, 11 (1970).

25. E. T. Keve et al., Solid State Communs. 8, 1517 (1970).

26. A. Jayaraman et al., Phys. Rev. Letters 25, 368, 1430 (1970).

27. A. Menth et al., Phys. Rev. Letters 22, 295 (1969).

28. R. L. Cohen et al., Phys. Rev. Letters 24, 383 (1970); J. Appl. Phys. 41, 898 (1970).

29. J. C. Nickerson et al., Phys. Rev. B 3, 2030 (1971).

30. G. V. Samsonov et al, Soviet Phys. - Crystallography 4, 109 (1960).

31. J. F. Miller et al, Air Force Avionics Laboratory Report AL TDR 64-239, Contract AF 33(657)-10687 (Battelle)(1964).

32. M. Kuznietz, J. Appl. Phys. 42, 1470 (1971); R. J. Gambino et al, J. Appl. Phys. 42, 1468 (1971).

33. E. D. Jones, Phys. Rev. 180, 455 (1969).

34. H. T. Davis (private communication).

35. N. Sclar, J. Appl. Phys. 35, 1554 (1964).

36. F. Anselin, Comptes Rendus 256, 2616 (1963).

37. R. G. Shulman and B. J. Wyluda, J. Phys. Chem. Solids 23, 166 (1962).

38. R. J. Gambino et al, J. Appl. Phys. 41,933 (1970).

39. M. K. Wilkinson et al, J. Appl. Phys. 31, 358S (1960); R. Didchenko. and F. P. Gortsema, J. Phys. Chem. Solids 24, 863 (1963).

40. J. P. Dismukes and W. M. Yim, Tech. Report ECOM 0155-1, Contract DAAB07-70-C-0155 (RCA) (1970).

41. J. F. Miller et al., J. Amer. Chem. Soc. 81, 4449 (1959).

42. J. F. Miller and A. E. Austin, J. Less Common Metals (to be published).

APPENDIX A

MAGNETOELECTRIC PHENOMENA

In this Appendix, we present a brief description of those properties of solids which may be classified under the general term "magnetoelectric", in order to provide some general background for the specific discussion in Section II. We begin by defining a couple of terms relating to magnetic ordering which are used frequently in the main text and these appendices.

Weak ferromagnetism occurs when there exist two or more magnetic sublattices lined up nearly antiferromagnetically, but tilted slightly away from the direction of complete opposition, yielding a small net magnetic moment in a direction perpendicular to the principal component of sublattice magnetization. This may be illustrated schematically in a two-dimensional case as follows:

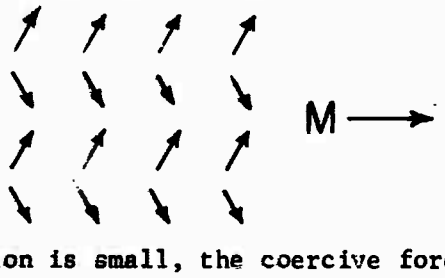

Since the net magnetization is small, the coercive force is also small, leading to the easy movement of domains which is exploited in the orthoferrites. This phenomenon is sometimes called pyromagnetism, "parasitic" ferromagnetism, Dzialoshinskii-Moriya magnetism, or canted antiferromagnetism. None of the terms is really entirely satisfactory.

In metamagnetic materials, discussed further in Appendix C, the ordering is antiferromagnetic when there is no applied field, but a net moment appears in a moderate external magnetic field, either through reversal of whole planes of spins or through some more complicated process.

Both of these phenomena may be considered as examples of ferrimagnetism which in its most general definition is the term given to any incomplete overall cancellation of magnetization among more or less opposing magnetic sublattices.

Now to magnetoelectric effects. We wish to define three terms:

1) "The" magnetoelectric effect is an induced effect in which an applied magnetic field produces an electric polarization, while an applied electric field produces a magnetization. The constitutive relations are most simply written in terms of the electric and magnetic flux densities

$$D = \epsilon E + \alpha H \quad ,$$

$$B = \mu H + \alpha_t E \quad .$$

Here α_t is the transpose of the magnetoelectric tensor α, which is not symmetric. This effect can occur in materials with certain types of magnetic ordering (which may be ferro-, antiferro- or ferri-); time-reversal symmetry requirements preclude its existence in para- or dia-magnetic regimes.

2) Magnetoferroelectric materials are ferroelectrics with some sort of magnetic ordering (again, ferro-, antiferro-, or ferri-) in some part of the temperature range in which ferroelectricity exists. They may or may not also show magnetoelectricity in the sense of the previous definition.

3) Ferromagnetoferroelectric materials are those magnetoferroelectrics in which there is a net magnetic moment - that is, all except the strictly antiferromagnetic ones. All the known cases, as it happens, are weak ferromagnets.

All these phenomena have been included in the catchall, and possibly somewhat misleading, term "magnetoelectric effects". There is no uniformity in the literature on the use of this or the other terms, and one should determine in any case just what kind of order is being considered. The logical relations among these phenomena may be made clearer by the accompanying diagram (Fig. A1).

Some examples of materials in each of these categories are given in Table A1. Some of the entries are slightly conjectural; for instance, the ferroelectricity of the manganites does not seem to have been actually demonstrated below the magnetic transition temperatures, though there seems to be little reason to doubt that it is there. The materials displaying these phenomena generally seem to be rather complex oxides of transition metals and other constituents. Questions concerning the homogeneity of some of the solid-solution materials appear to have been settled in a few cases by the preparation of single crystals. In the materials discovered so far, the phenomena of interest tend to occur at rather low temperatures, but there does not seem to be any fundamental reason why this should always be the case. The magnetoelectric effect (1) seems to be somewhat small in known materials and is estimated to require an order of magnitude increase to be useful. It may in principle be larger in magnetoferroelectrics than in paraelectrics.

The magnetic symmetry of a material may be described in terms of its magnetic space group. In the modification of the notation for ordinary space groups used in this report, a prime on a spatial symmetry element indicates that the element followed by time reversal is an element of the magnetic group. Thus m' indicates a reflection in some mirror plane followed by turning over all the spins. (It is important to remember that the spatial reflection involves reversing all spin components parallel to the reflection plane too.) Knowledge of the magnetic space group lets one determine whether a compound may be ferromagnetic,

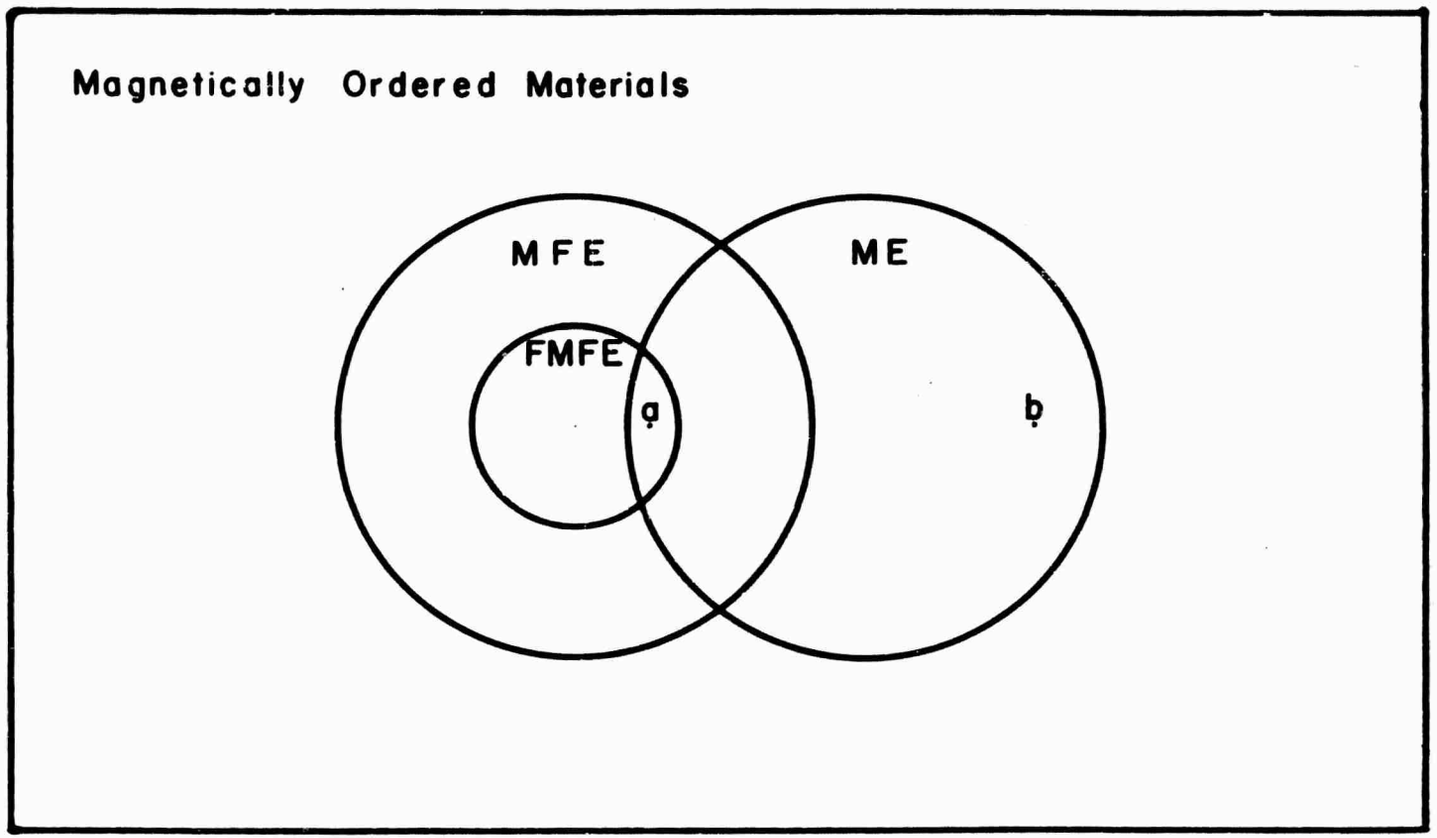

FIGURE A1. LOGICAL INTERRELATION AMONG MAGNETIC, MAGNETOELECTRIC, MAGNETOFERROELECTRIC, AND FERROMAGNETOFERROELECTRIC MATERIALS. OVERLAP DENOTES INTERSECTION OF SETS; INCLUSION DENOTES BEING A SUBSET. AS EXAMPLES, "a" DENOTES THE LOW-TEMPERATURE PHASE OF $Ni_3B_7O_{13}I$, WHICH IS WEAKLY FERROMAGNETIC, FERROELECTRIC, AND MAGNETOELECTRIC, WHILE "b" DENOTES Cr_2O_3, WHICH BELOW ROOM TEMPERATURE IS ANTIFERROMAGNETIC, PARAELECTRIC, AND MAGNETOELECTRIC.

TABLE A1. Examples of "magnetoelectric" materials. $T(\alpha_{max})$ = temperature at which maximum effect is observed. T_{cmin} = lower of magnetic and electric ordering temperatures.

Magnetoelectric	$10^4 \alpha_{max}$	$T(\alpha_{max})$(K)
Cr_2O_3	5	250
$Ga_{.9}Fe_{1.1}O$	5	200
$DyPO_4$	12	1.7
$TbAlO_3$	350	2

Magnetoferroelectric	$T_{c\ min}$(K)	Magnetic Order
$PbFe_{.5}Nb_{.5}O_3$	143	AFM
$YMnO_3$	80	AFM
Ferromagnetoferroelectric		
$PbCo_{.5}W_{.5}O_3$	9	WFM
$Ni_3B_7O_{13}I$	64	WFM
$ErMnO_3$	9	WFM

antiferromagnetic, magnetoelectric, and so forth, but does not necessarily specify any one particular spin arrangement, just as the ordinary space group does not determine a unique structure type.

Rather than references keyed to the text, it seems more appropriate in this appendix just to list some of the more helpful general references.

A1. R. R. Birss, Symmetry and Magnetism (North Holland, 1964). (Weak ferromagnetism, magnetoelectricity, magnetic point groups.)

A2. A. R. Billings, Tensor Properties of Materials (Wiley-Interscience, 1970) (Magnetic symmetry, magnetoelectricity).

A3. N. N. Neronova and N. V. Belov, Soviet Phys.-Crystallog. 4, 769 (1960). (Ferroelectric and ferromagnetic symmetries)

A4. R. M. Hornreich, Solid State Communs. 7. 1081 (1969). (Magnetoelectric materials, known and conjectured - good list of references).

A5. G. A. Smolenskii and N. N. Krainik, Sov. Phys.-Uspekhi 12, 271 (1969). (Review progress in ferroelectricity - section IX-2 on FMFE's.)

A6. S. M. Skinner, IEEE Trans. PMP-6 68 (1970). (Review MFE's).

APPENDIX B

MAGNETIC SUSCEPTIBILITY OF ORTHORHOMBIC $YMnO_3$

The magnetic susceptibility of two samples of orthorhombic $YMnO_3$ was measured over the temperature range of 4.2 K to 559 K. As discussed below the first sample (ortho-$YMnO_3$-I) is believed to contain a few percent of a ferrimagnetic contaminant while the second specimen (ortho-$YMnO_3$-II), obtained using higher purity starting materials and a more careful synthesis, showed no trace of such a contaminant. We treat this example in detail in order to demonstrate the correction procedures discussed in Section IIB2 of the text.

The magnetic susceptibility of ortho-$YMnO_3$-I is shown as a function of temperature in Figs. B1 and B2. There are two interesting temperature regimes: i) over the range 78 K to 559 K, the susceptibility is independent of the applied magnetic field and obeys a Curie-Weiss law, $\chi = C/(T - \theta)$, with a negative θ value, ii) below about 40 K there is an onset of weak ferromagnetism evidenced by the discrepancy between measured χ's at two different field strengths, 9.88 and 5.82 kOe. Since this change in behavior occurs very near the known Curie temperature[B1] of Mn_3O_4 and since magnetic studies of hexagonal $YMnO_3$ often reveal[B2] small amounts of this contaminant, we attribute the onset of weak ferromagnetism to ferrimagnetic Mn_3O_4. Using published data[B3] on the magnetic properties of Mn_3O_4 in the ferrimagnetic state, we now calculate the fraction of this impurity which is present in the specimen.

Below the Curie temperature of the ferrimagnetic contaminant the total susceptibility of the sample may be expressed approximately as

$$\chi_{obs} = \frac{c\sigma_o}{H} + \chi_\infty \quad , \tag{B1}$$

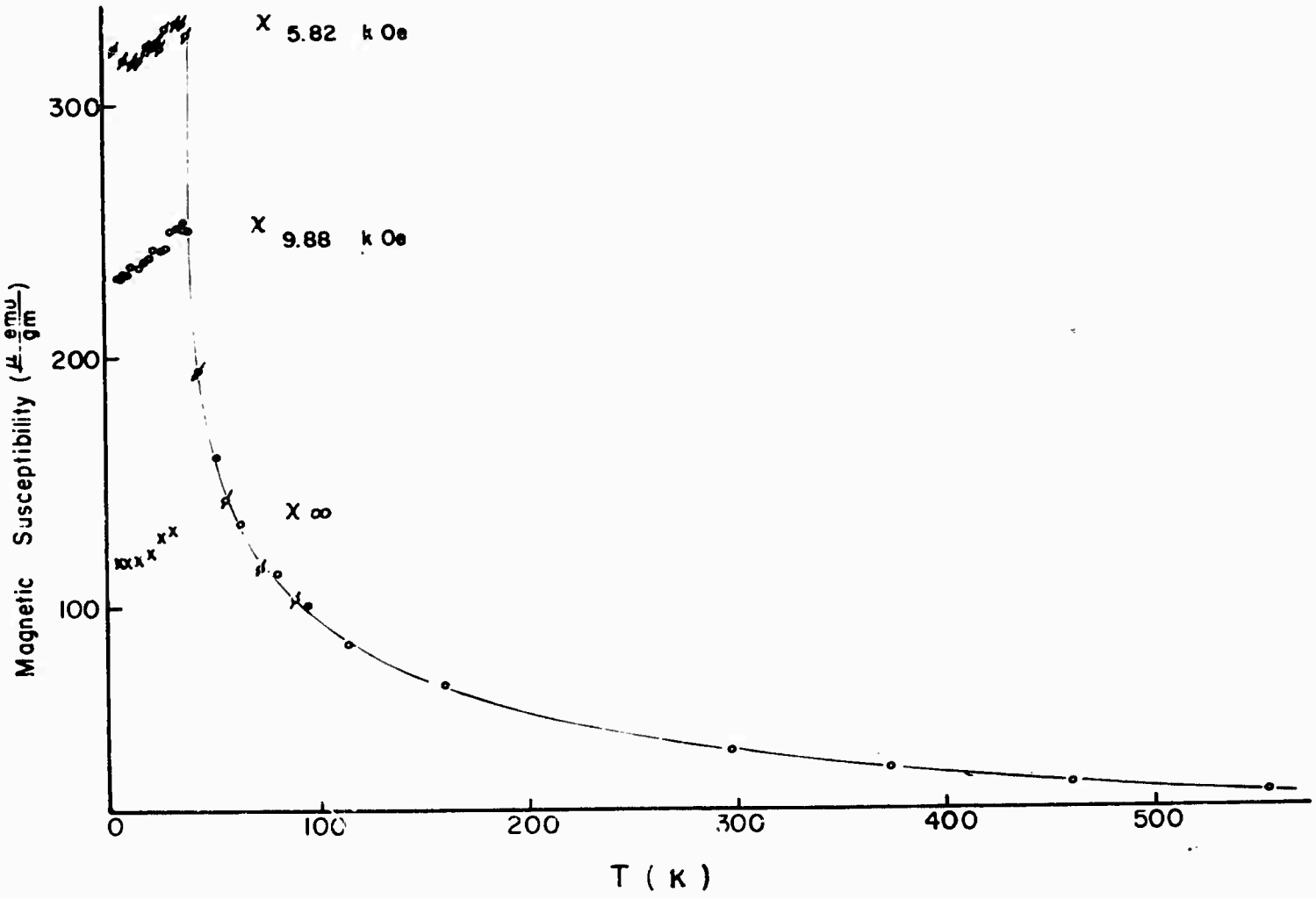

FIGURE B1. TEMPERATURE AND FIELD DEPENDENCE OF THE MAGNETIC SUSCEPTIBILITY OF AN ORTHORHOMBIC $YMnO_3$ SPECIMEN CONTAINING ABOUT 2.6 WEIGHT PERCENT Mn_3O_4. χ_∞ IS OBTAINED FROM THE MEASURED SUSCEPTIBILITIES BY EXTRAPOLATION TO INFINITE FIELD (SEE EQUATION B1)

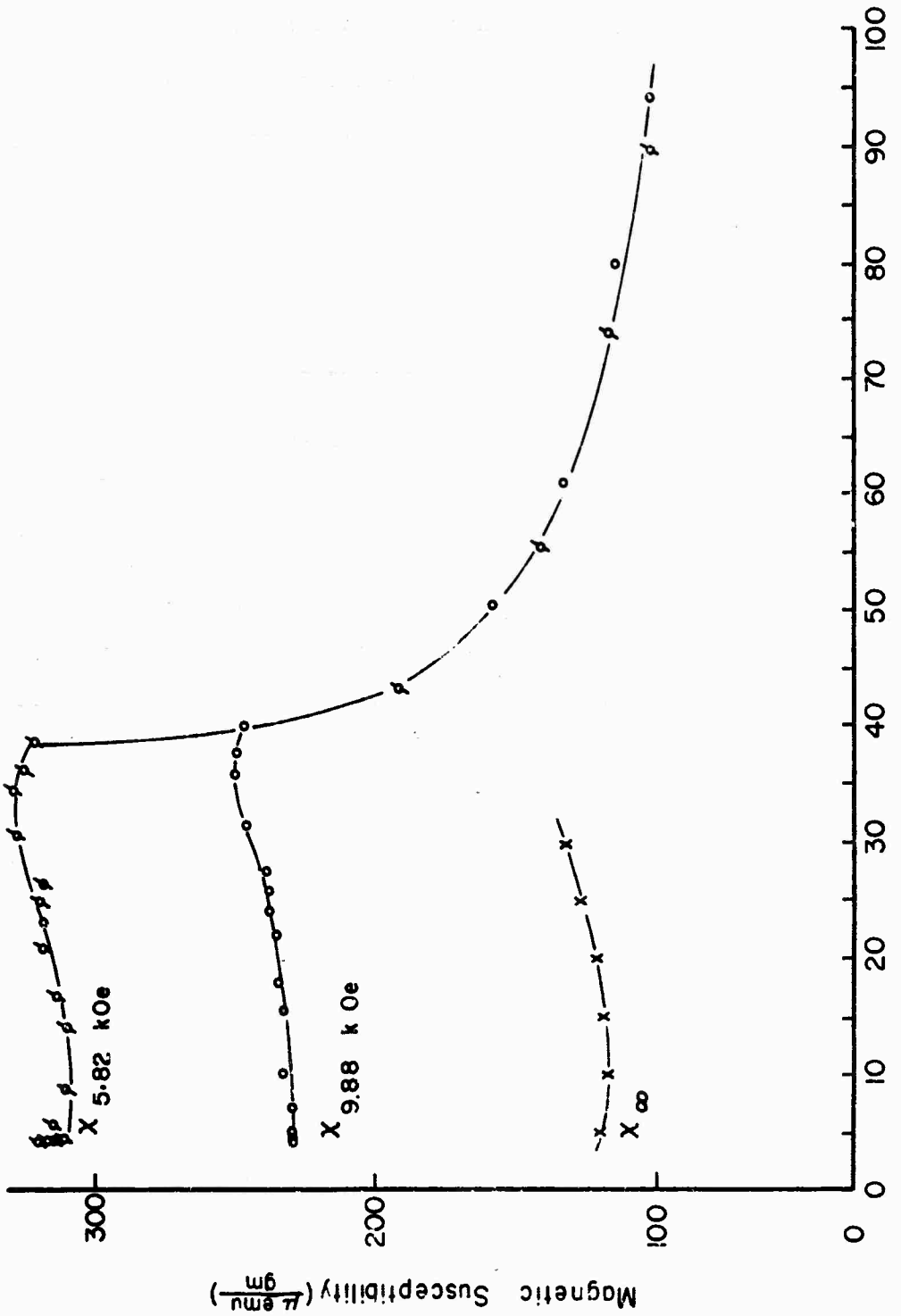

FIGURE B2. LOW-TEMPERATURE DATA OF FIGURE B1 PLOTTED ON AN EXPANDED SCALE

ere χ_{obs} = measured susceptibility at the applied field H,

χ_{∞} = measured susceptibility extrapolated to infinite field,

σ_o = saturation magnetization, 1.7 Bohr magnetons per molecule of Mn_3O_4, of the ferrimagnetic contaminant of concentration.

Eq. B1 has been fitted to the data of Fig. B2 at seven different temperatures below 40 K. The extrapolated susceptibilities are listed in column 2 of Table B1. The average value obtained for the concentration of ferrimagnetic contaminant is c = 2.6 wt percent. This value of c is used to determine the susceptibility of orthorhombic $YMnO_3$ from the relation $\chi_{ortho\text{-}YMnO_3} = \chi_{\infty}/(1\text{-}c)$, at the above seven temperatures. The results are listed in column 4 of Table B1 for temperatures below 40 K.

Above the Curie temperature of Mn_3O_4 the observed susceptibility of the specimen must be corrected for the paramagnetism of the contaminant, and unlike the low temperature case this correction cannot be accomplished by infinite-field extrapolations. Furthermore, a detailed description of the spin configuration in the ordered state of Mn_3O_4 is not available so that the individual Mn ion moments cannot be determined from the saturation magnetization per molecule. Thus we cannot obtain corrections for the paramagnetism of the contaminant by simply scaling the measured quantity $c\sigma_o$ by a known factor and introducing a Curie-Weiss θ value. Instead we use the reported susceptibility[B4] of Mn_3O_4 above the Curie temperature and our measured value of the concentration to obtain the paramagnetic corrections listed in column 3 of Table B1. The corrected susceptibilities for this temperature regime are listed in column 4 along with those obtained at the lower temperatures. In Fig. B3 we plot the corrected susceptibility over the temperature range 4.2 K to 100 K and compare it with the observed susceptibility of the pure orthorhombic $YMnO_3$ sample. It is to be noted

TABLE B1

Susceptibility of Impure Orthorhombic $YMnO_3$

(units of μemu/gm)

Temperature K	χ_∞*	$c\chi_{Mn_3O_4}$	χ_{YMnO_3}**
5	120		123
10	117		120
15	120		123
20	122		125
25	128		131
30	132		136
37	139		143
45	182	15.2	171
50	159	8.1	155
60	135	4.8	134
70	122	3.7	121
80	112	3.0	112
90	104	2.6	104
100	98	2.2	98
116	84.6	1.89	84.9
160	68.1	1.44	68.4
298	40.9	1.06	40.9
376	33.5	.97	33.4
460	28.3	.89	28.1
559	23.9	.82	23.7

* Extrapolated susceptibilities below 40 K; measured susceptibilities above 40 K.

** $\chi_{YMnO_3} = \chi_\infty/(1-c)$, $T < 40$ K; $\chi_{YMnO_3} = (\chi_\infty - c\chi_{Mn_3O_4})/(1-c)$, $T > 40$K.

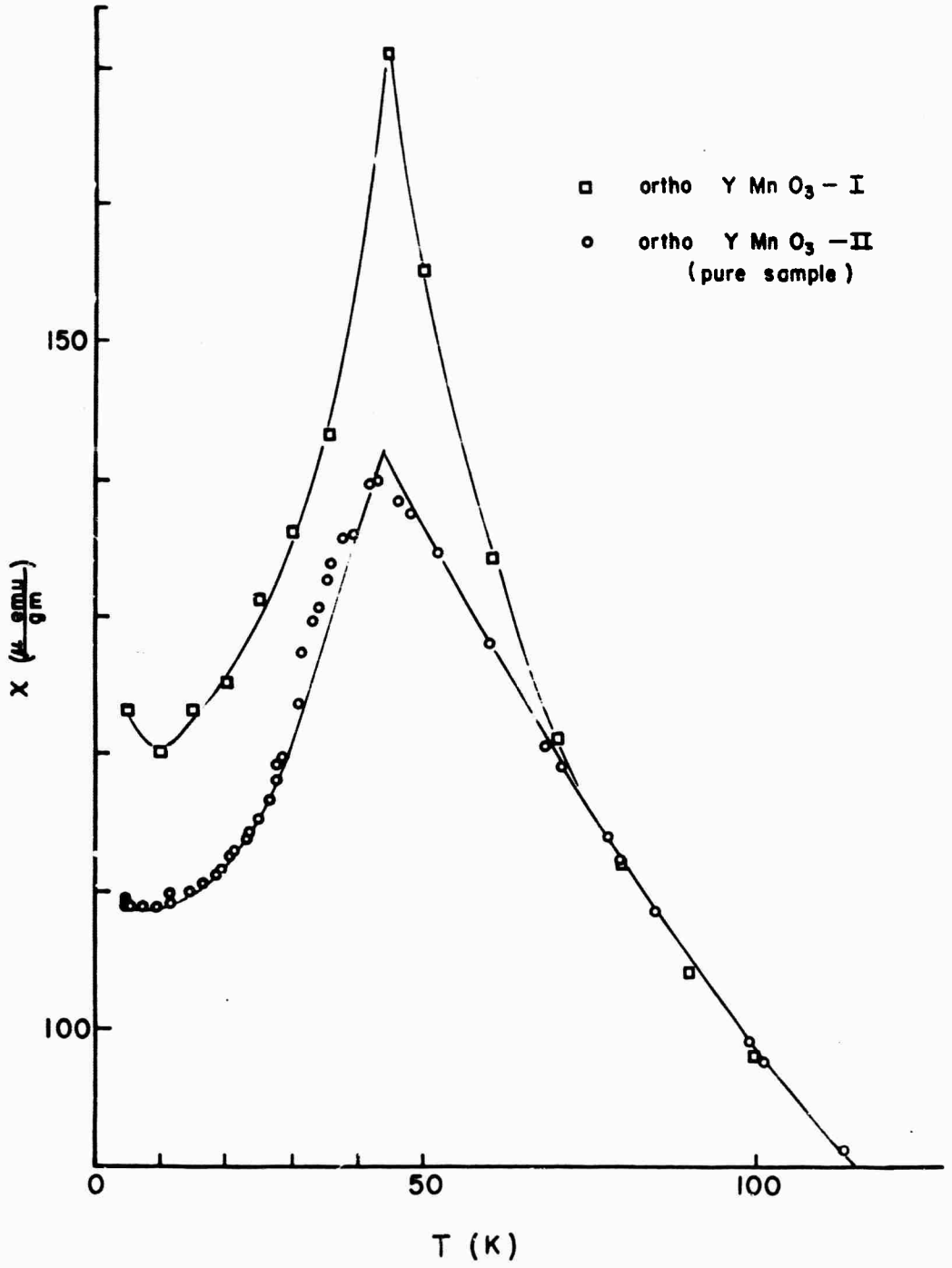

FIGURE B3. TEMPERATURE DEPENDENCE OF THE MAGNETIC SUSCEPTIBILITY OF ORTHORHOMBIC $YMnO_3$. THE LOWER CURVE IS OBTAINED FROM A PURE SAMPLE WHILE THE UPPER CURVE RESULTS FROM MAKING CORRECTIONS (SEE TEXT) FOR MAGNETIC CONTAMINANTS

that despite a relatively low accuracy in the region near 40 K the lambda-type anomaly of the pure sample is obtained for the contaminated specimen when these correction procedures are used.

In the high temperature regime (150 K - 560 K) we have fitted the susceptibility to a Curie-Weiss law, $\chi = C/(T - \theta)$. The data for the pure sample give a Curie constant of C = 3.10 emu deg/mole, an effective moment μ_{eff} = 4.98 Bohr magnetons and a θ value of - 67 K while the corrected data for the impure sample yield C = 2.82 emu deg/mole, μ_{eff} = 4.75 Bohr magnetons and θ = - 63 K. For comparison, the uncorrected high temperature data of the impure sample give C = 2.88 emu deg/mole, μ_{eff} = 4.79 Bohr magnetons and θ = - 71 K. Results of new susceptibility measurements on Mn_3O_4 single crystals have just been published.[B5] While there are some differences between these measurements and the older ones used in the foregoing analysis, changes resulting from using the new data are relatively insignificant.

B1. R. Buhl, J Phys. Chem. Solids 30, 805 (1969).

B2. R. Pauthenet and C. Veyret, J. de Physique 31, 65 (1970).

B3. K. Dwight and N. Menyuk, Phys. Rev. 119, 1470 (1960).

B4. A. S. Borovik-Romanov, and M. P. Orlova, Sov. Phys. JETP 5, 1023 (1957).

B5. O. V. Nielsen, J. de Physique 32, C1-51 (1971).

APPENDIX C

ANALYSIS OF LOW-TEMPERATURE MAGNETIC SUSCEPTIBILITY OF ORTHORHOMBIC $HoMnO_3$

Because of the large effective moment of the Ho^{3+} ion (about 10.6 Bohr magnetons), the use of an extremely sensitive electrobalance to measure the susceptibility of holmium compounds necessitates using very small samples. Difficulties in determining the mass ($\sim 10^{-4}$g in apparatus such as ours) then lead to some inaccuracy in the experimentally determined values of the susceptibility, since the susceptibility is an extensive variable. This inaccuracy only corresponds to a change of vertical scale, though, and the relative accuracy of the data to be discussed is quite high. The low-temperature data on ortho-$HoMnO_3$ given in the semiannual report was for a relatively large sample (4 mg), and thus it was difficult to determine the field dependence at low temperatures or even to make measurements at the highest fields. In addition, the measured susceptibility had to be corrected for the presence of a small amount of Mn_3O_4. More recently, we remeasured the low-temperature susceptibility using a much smaller sample taken from the same lot. Fortuitously, this sample contained much less Mn_3O_4; so no correction of the data was necessary. To avoid unnecessary complication, only this new low-temperature (4.2 - 53K) data is discussed in this appendix. The high-temperature data (on the larger sample containing a small amount of Mn_3O_4) was analyzed in the semiannual report along the lines discussed in the previous appendix, and the results are given in the main text of the present report.

The usual method of accurately determining the mass of a small paramagnetic sample is by comparing its susceptibility at room temperature with that of a larger mass of the same material. For the sample studied in these experiments the mass found in this way is 0.124 mg. Using this mass in analysis of the data leads, as we shall see, to considerably higher susceptibilities at low temperatures than with the larger sample. While this discrepancy may be due largely to error in the mass, particularly since these materials are somewhat hygroscopic, comparison of the results in the two cases shows that the enhanced susceptibility cannot be ascribed entirely to this cause; we believe it simply reflects the difficulty inherent in making accurate low temperature measurements on heavy samples.

The overall low-temperature susceptibility data is shown in Fig. C1, for applied fields of 5.674 kOe (circles) and 10.120 kOe (squares). The high-field data tends to lie above the low-field data at all temperatures, beginning to depart significantly only below about 10 K. This low-temperature data is shown in more detail in Fig. C2. The low-field data indicate an antiferromagnetic transition similar to that found at higher temperature in ortho-$YMnO_3$, while the high-field data scarcely show any break. In contrast to the cases of minor-second-phase ferrimagnetism discussed in the Appendix B or of weak ferromagnetism exemplified in the case discussed in the Appendix D, the susceptibility <u>increases</u> with increasing field. This indicates that below about 10 K the material is <u>metamagnetic</u> -- that is, it is antiferromagnetic in zero field, but tends to have its spins aligned readily by an external magnetic field. To determine the Néel temperature accurately, one should extrapolate the susceptibilities to zero field. (Ideally, one should have measurements on

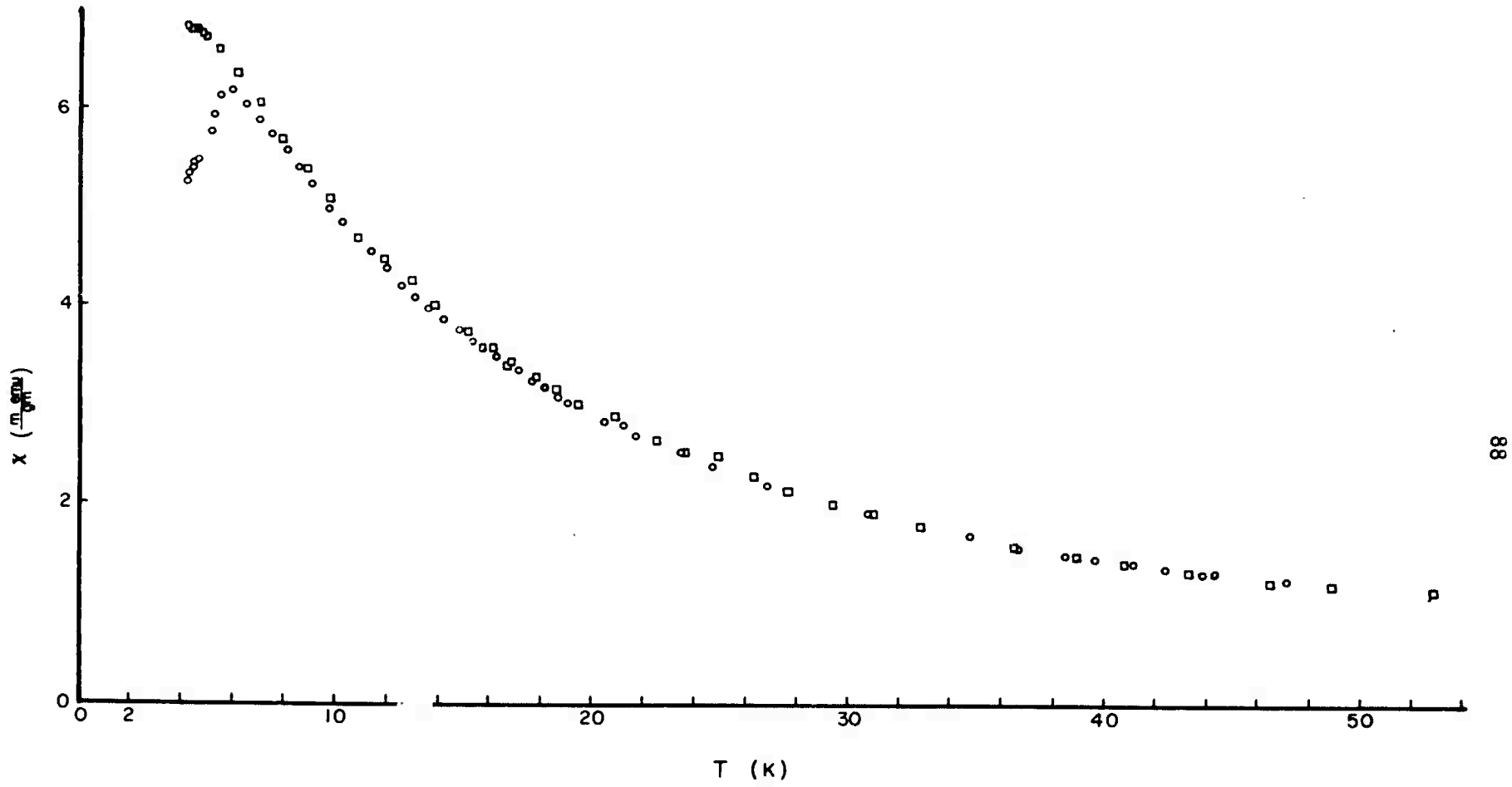

FIGURE C1. LOW-TEMPERATURE SUSCEPTIBILITY OF ORTHORHOMBIC $HoMnO_3$. CIRCLES: 5.674 kOe; SQUARES: 10.120 kOe

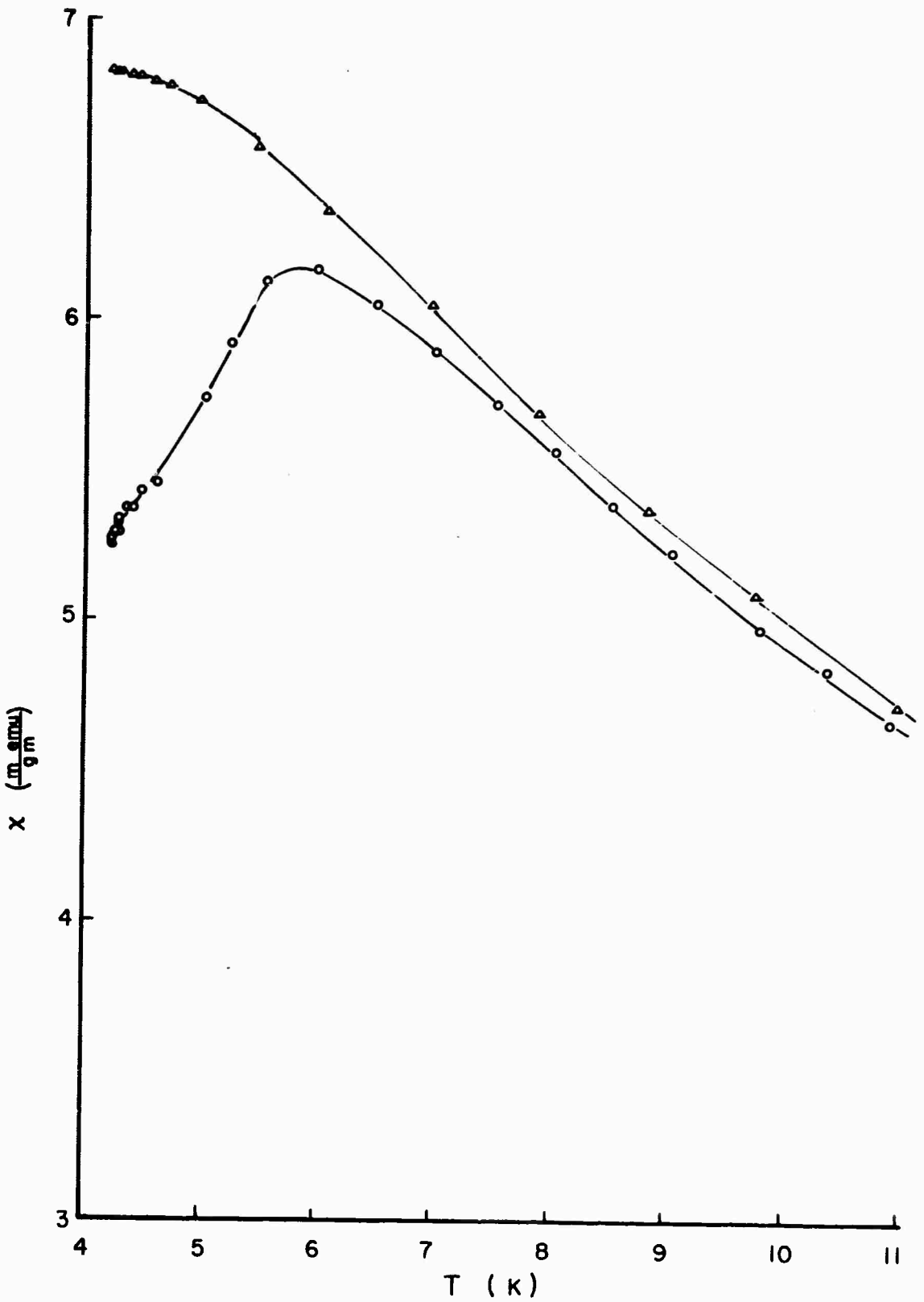

FIGURE C2. LOW-TEMPERATURE SUSCEPTIBILITY OF ORTHO-$HoMnO_3$
CIRCLES: 5.679 kOe; TRIANGLES: 10.120 kOe

single crystals as well, but this of course seems out of the question here.) To determine the field dependence of the susceptibility, a large number of measurements were made, in two separate runs, at 4.2 K, where the temperature can be controlled most accurately, and at various fields. The results of these measurements are plotted in Fig. C3. The error bars represent standard deviations of the mean values plotted. Although the slight upturn in the curve at low fields may not be statistically significant, in view of the difficulty of making force measurements at such small fields, but an examination of the original data suggests that it represents a real hysteresis effect in the sample. In principle, initial magnetization curve measurements could be made, but since the effect is small, we have decided this would not be worth while. Symmetry requires that the metamagnetic susceptibility change be an even function of H; thus the curve should have zero slope at H = 0. Also shown is the magnetization ($M = \chi H$) as a function of applied field. This is similar, for instance, to the low-temperature magnetization curve[C1] of the metamagnet $FeCl_2$. About the simplest sort of expression that might be expected to fit the magnetization data reasonably well is[C2]

$$M = \frac{N_o \mu}{W} \frac{\sinh y}{1/2 \exp (T_1/T) + \cosh y}, \quad y = \frac{\mu}{kT} (H+\Delta M), \qquad (C1)$$

where H is the applied field, N_o is Avogadro's number, W is the molecular weight, and μ, Δ, and T_1 may be considered as parameters. This is a transcendental equation which must be solved numerically or graphically to determine M for a given field and temperature. Solutions of this equation do fit the 4.2 K data quite well -- the magnetization curve drawn in Fig. C3 represents the locus

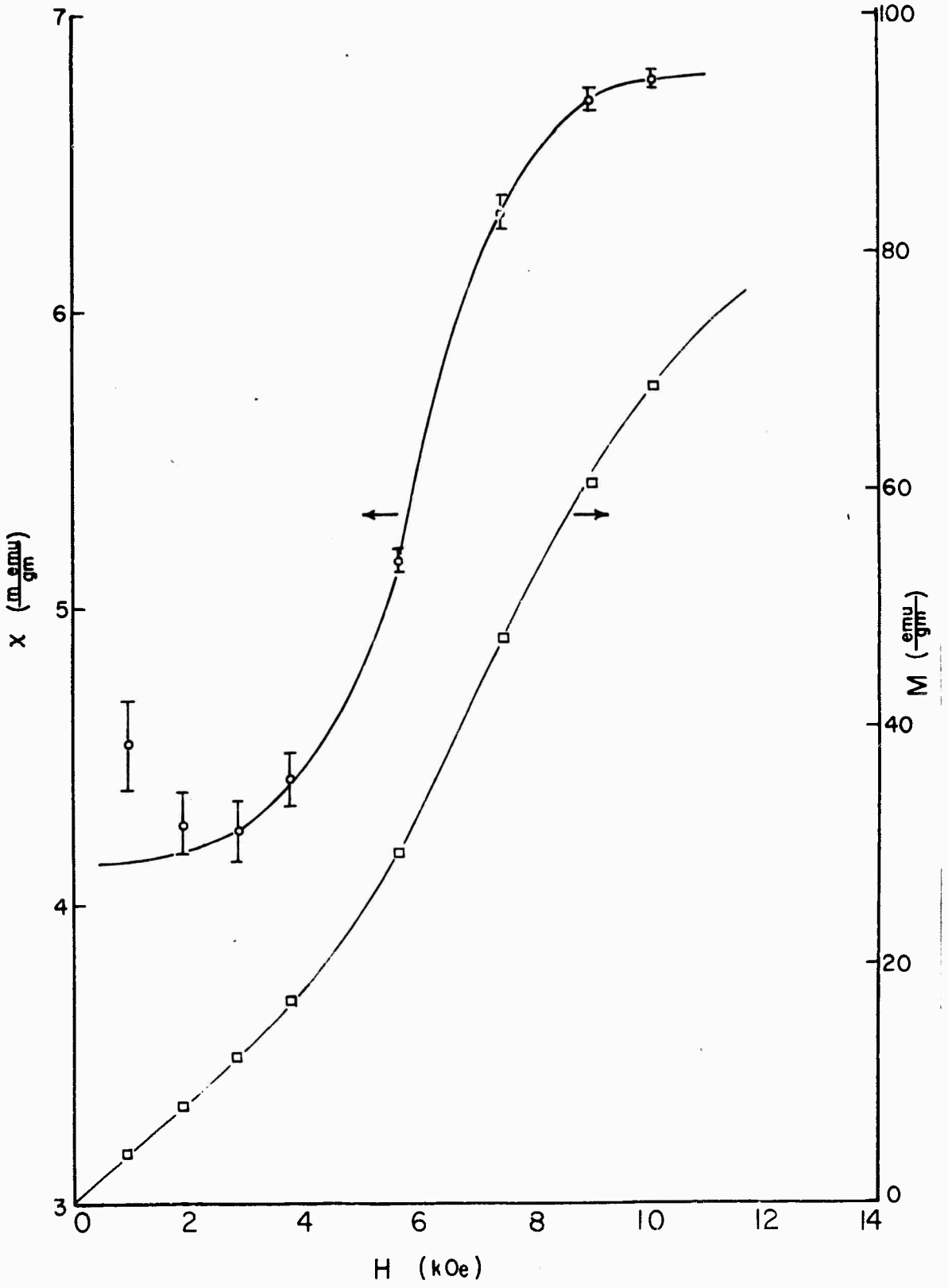

FIGURE C3. SUSCEPTIBILITY (LEFT SCALE) AND MAGNETIZATION (RIGHT SCALE) OF ORTHO-$HoMnO_3$ AT 4.2K AS A FUNCTION OF APPLIED MAGNETIC FIELD. CURVE THROUGH MAGNETIZATION DATA IS A FIT OF EQUATION C1.

of solutions of Eq. C1 for parameters μ = 4.856 Bohr magnetons, Δ = 384.9 (where M is in emu/gm and H is in Oe) and T_1 = 8.720 K. Such an expression does not provide such a good fit to the higher temperature magnetization data, perhaps because the parameters are temperature-dependent or because the simplified molecular field theory on which Eq. C1 is based is not really adequate in the present situation. Moreover, Eq. C1 is not particularly good for determining the Néel point, since it does not have the cusp-like behavior characteristic of a second-order transition but rather has a smooth maximum at T = 0.6835 T_1 when H = 0, or, in the present case, at about 6 K. (A better molecular field approximation with more adjustable parameters would lead to a second-order transition, but still would not necessarily be reliable for predicting the transition temperature.[C2] It should be pointed out that the Néel temperature is sometimes defined in theoretical studies as the temperature at which the sublattice magnetization vanishes; this can be slightly different from the temperature at which the low-field susceptibility peaks.) Since the maximum in the 5.674 kOe data occurs near this temperature, the actual Néel temperature must be higher, and in fact should be above 8 K, where the low-field and high-field curves become substantially parallel. About the best one can say is that $T_N = 9 \pm 1$ K. It seems likely that this transition is associated with the ordering of the Ho^{3+} ions, which order at similar temperatures (5 K, 12 K) in the hexagonal manganite and the orthochromite.[C3] It is quite possible that the Mn spins order at around 40 K, since the Mn ordering temperature varies very little when Ho replaces Y in related compounds.[C3] The large paramagnetic susceptibility due to the Ho^{3+} spin tends to mask effects of any such ordering.

The data of Fig. C1 lead one to suspect that there may be small metamagnetic effects associated with the Mn ions too, since, as previously mentioned, there appears to be a slight tendency (possibly not statistically significant) for the high-field data to lie above the low-field data below about 40 K. This would further complicate interpretation of the low-temperature ordering.

Metamagnetism at very low temperatures (around 2 K) appears to occur in the neighboring normally orthorhombic compounds $TbMnO_3$ and $DyMnO_3$, but the effect is not as pronounced as in the present case and requires stronger fields for its observation.[C3] Low-temperature metamagnetism in the closely related compound $ErCrO_3$ has also been reported recently.[C4] Metamagnetism at temperatures in the range 1-4 K has also been observed in several orthoferrites[C5] and in $Dy\ Fe_x\ Cr_{1-x}\ O_3$ solid solutions.[C6] Ortho-$HoMnO_3$ appears to have considerably higher rare-earth ordering temperature than any of these other compounds.

C1. C. Starr, F. Bitter, and A. R. Kaufmann, Phys. Rev. 58, 977 (1940).

C2. P. Carrara, Rapport CEA-R-3535, C.E.N. Saclay (France), (1968).

C3. E. F. Bertaut et al., IEEE Trans. Mag. 3, 453 (1966); R. Pauthenet and C. Veyret, J. de Phys. 31, 65 (1970) and private communication.

C4. C. Veyret et al, J. de Phys. 31, 607 (1970).

C5. A. Apostolov and J. Sivardière, Comptes Rendus B 267, 1315 (1968).

C6. A. Apostolov, Comptes Rendus Acad. Bulg. Sci. 22, 375 (1969).

APPENDIX D

DETAILED ANALYSIS OF THE MAGNETIC SUSCEPTIBILITY OF ORTHO-$YbCrO_3$

The magnetic susceptibility of orthorhombic $YbCrO_3$ was measured over the temperature range 4.2 K - 560 K. The results are shown in Fig. D1. Above 115 K the data is seen to be independent of the applied magnetic field while below this temperature the observed susceptibility has a pronounced field dependence. There are three gross features of this curve which are noteworthy. First is the onset of weak ferromagnetism at about 114 K, near the reported Curie temperature of $YbCrO_3$.[D1] Second is the change in slope of χ_{obs} vs T near 45 K, the same change for both field values. Third is the disappearance of the field dependence of χ_{obs} over a very narrow temperature range near 18 K. The latter effect, which could stand further verification, is also evidence that one is observing a bulk effect. As discussed in the main text, no likely ferrimagnetic contaminants exhibit such behavior. In what follows a detailed analysis of susceptibility data is given for both the paramagnetic region and the "weak ferromagnetic" region.

Above the transition temperature both the Cr spins and the Yb spins are disordered and thus should obey Curie-Weiss laws. As a first approximation it is assumed that a single Curie-Weiss law, $\chi_{obs} = C/(T-\theta)$, may be used to describe the data. This assumption is justified later. In Fig. D2 the values of $1/\chi_{obs}$ are plotted as a function of temperature for temperatures above 115 K (for temperatures below 115 K the data shown refer to χ_∞ which is defined later). Using data from well above the Curie point (150 K to 560 K) a least-square fit to the Curie-Weiss law yields $C = 0.0158 \frac{\text{emu deg}}{\text{gm}}$ and $\theta = -102$ K. Despite the closeness of their values it is not possible to make a meaningful comparison between

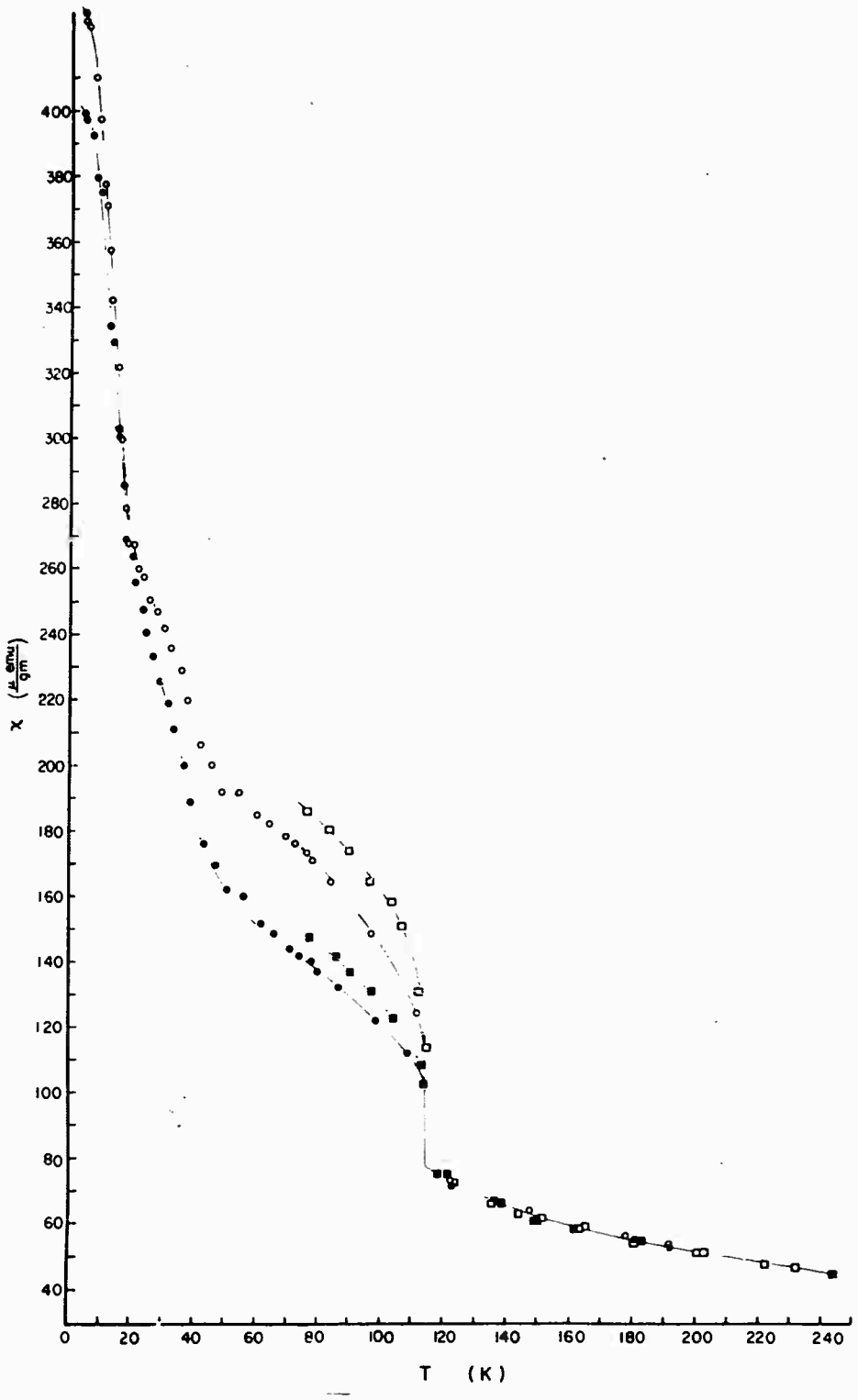

FIGURE D1. TEMPERATURE DEPENDENCE OF THE MAGNETIC SUSCEPTIBILITY OF ORTHORHOMBIC $YbCrO_3$. SOLID POINTS: 10.120 kOe; OPEN POINTS: 5.674 kOe. CIRCLES REPRESENT DATA FOR A SAMPLE RUN FROM 4.2 TO 300 K. SQUARES ARE DATA FOR A LIQUID NITROGEN RUN ON A SPECIMEN HAVING A SIGNIFICANTLY LARGER MASS WHICH WAS DETERMINED BY NORMALIZATION TO THE OTHER DATA AT ROOM TEMPERATURE. THE DISCREPANCIES AT LOW TEMPERATURE ARE BELIEVED TO BE DUE TO THIS NORMALIZATION PROCEDURE.

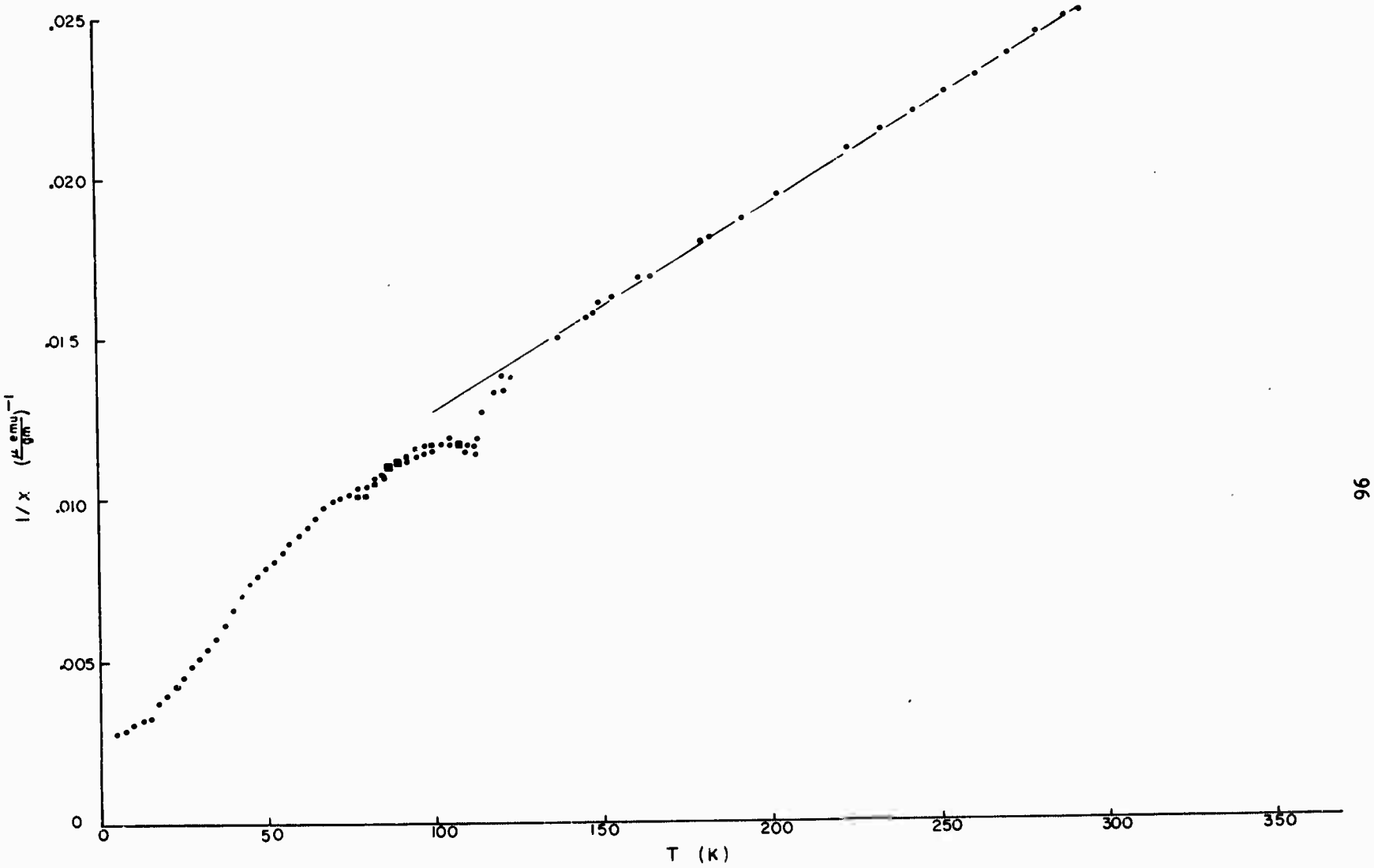

FIGURE D2. TEMPERATURE DEPENDENCE OF THE INVERSE SUSCEPTIBILITY (DEFINED IN THE TEXT) FOR ORTHORHOMBIC $YbCrO_3$. THE HIGH-TEMPERATURE STRAIGHT LINE REPRESENTS A LEAST SQUARE FIT OF THE DATA TO A CURIE-WEISS LAW WITH AN EFFECTIVE MOMENT OF 5.87 BOHR MAGNETONS AND A θ VALUE OF -102 K. DATA POINTS REPRESENTED BY SQUARES WERE OBTAINED ON A SEPARATE SPECIMEN

the θ value and the observed transition temperature. As seen in Fig. D2, the single Curie-Weiss law with these parameters provides an extremely good fit to the observed data above 150 K. The molecular weight is 273.03 gm/mole, so the Curie constant becomes $\frac{4.31 \text{ emu deg}}{\text{mole}}$; equating this to $N_o p_{eff}^2 \beta^2/3k$ where N_o is Avogadro's number, β is the Bohr magneton and k is Boltzmann's constant, an effective moment of $p_{eff} = 5.87$ Bohr magnetons is obtained. For comparison a theoretical value of p_{eff} has been calculated assuming a single Curie-Weiss law. This means that the total moment is given by

$$p_{eff} = \sqrt{p_{Yb}^2 + p_{Cr}^2} \quad .$$

In $YbCrO_3$ both the Yb and Cr ions are trivalent. For Yb^{3+}, the ground state electron configuration is $4f^{13}$ which according to Hund's rule gives S = 1/2, L = 3 and J = L + S = 7/2. Now $p_{Yb} = g_J\sqrt{J(J+1)}$ where g_J is the Landé g factor given by

$$g_J = 1 + \frac{J(J+1) - L(L+1) + S(S+1)}{2\,J(J+1)} \quad .$$

From this we find $p_{Yb} = 4.54$ Bohr magnetons. For Cr^{3+} it is assumed, as is usually the case for transition metal ions, that the orbital angular momentum is quenched by the crystalline electric fields. Thus p_{Cr} is just $g_s\sqrt{S(S+1)}$, which is 3.87 Bohr magnetons. The theoretical effective moment is 5.96 Bohr magnetons, in very good agreement with the observed value. This agreement, along with the fact that the onset of weak ferromagnetism occurs close to the previously reported Curie temperature of ortho-$YbCrO_3$, provides a good test of the purity of our sample. (The slightly higher moment and Curie temperature reported by Bertaut et al. probably indicate that their samples contained a small amount of some lighter high-moment rare earth such as erbium.) The next step in analyzing

the high-temperature data is to remove the restriction of a single Curie-Weiss law. That this procedure yields only small corrections to the previous approximation may be seen as follows: Again it is assumed that both spin systems are disordered, and furthermore it is assumed that the spin systems are not coupled. In this case the total susceptibility is given by

$$\chi_{tot} = \frac{C_1}{T + \theta_1} + \frac{C_2}{T + \theta_2} = \frac{C_1 + C_2}{T + \theta_1}\left[1 + \frac{C_2\,(\theta_1 - \theta_2)}{(T + \theta_2)(T + \theta_1)}\right]$$

$$\chi_{tot} = \frac{N_o\beta^2(p_{Yb}^2 + p_{Cr}^2)}{3k(T + \theta_1)}\left[1 + \frac{p_{Yb}^2}{p_{Cr}^2 + p_{Yb}^2}\,\frac{\theta_1 - \theta_2}{(T + \theta_1)(T + \theta_2)}\right] \qquad \text{(D1)}$$

The first term in this equation is entirely equivalent to the previous assumption of a single Curie-Weiss law. The validity of its use can be demonstrated by showing that the second term is such a minor correction that meaningful values for θ_1 and θ_2 cannot be obtained from a fit of Eq. D1 to the data. Using the theoretical values for p_{Yb} and p_{Cr}, the observed Curie point for θ_1 and zero for θ_2 (Bertaut et al. have shown that the Yb spins do not order down to 4.2 K), the total susceptibility can be approximated as

$$\chi_{tot} = \frac{N_o\,\beta^2}{3k(T + \theta_1)}\,(p_{Yb}^2 + p_{Cr}^2)\left[1 + \frac{66.98}{(T + 114)\,T}\right] \quad . \qquad \text{(D2)}$$

At 150 K the correction term is 0.2% while at the high temperature limit of 560 K it has a value of 0.02%. Although such small corrections, which are equivalent to curvature in the high temperature data, may change the calculated θ value by several percent they make less than 0.1% change in the effective moment.

As previously noted, the data of Fig. D1 show a pronounced field dependence of the susceptibility below 115 K. Although only two field values

are shown for each temperature it has been demonstrated that in the range of 2 - 10 kOe the observed magnetization at fixed temperature points throughout this region is a linear function of the applied field. Thus below the transition temperature the observed magnetization may be expressed as

$$M_{obs} = M_o + \chi_\infty H \quad , \tag{D3}$$

where χ_∞ is a function of temperature only and the subscript denotes the fact that D3 is not necessarily valid at very low fields.

Since $YbCrO_3$ is known to be weakly ferromagnetic, it is quite reasonable to assume that its magnetization would obey an equation of the form given above. M_o would correspond to the spontaneous magnetization, extrapolated to zero field, resulting from incomplete cancellation of the Cr sublattice magnetizations and χ_∞ would represent the sum of the Yb paramagnetism and the field-induced magnetism of the Cr spins. In general, the latter quantity might be expected to make a field-dependent contribution to χ_∞, but the data suggest that this is not the case. Eq. D3 may be rewritten in terms of susceptibility as

$$\chi_{obs} = \frac{M_o}{H} + \chi_\infty \quad . \tag{D4}$$

Using the smoothed curves drawn through the data shown in Fig. D1, χ_∞ and M_o have been calculated from Eq. D4 at temperature intervals of 2.5 K between 5 K and 115 K. It is necessary to use a smoothing procedure because the observed values at the two different fields do not correspond to exactly the same temperature. For this temperature range the values of $1/\chi_\infty$ are plotted in Fig. D2 as an extension of the $1/\chi_{obs}$ data. It is now seen that $1/\chi$ shows a dip at the Curie temperature, as might be expected, and also exhibits a low-temperature slope which is larger than that observed above the Curie point. The increase

in slope at low temperature corresponds to a substantial decrease in the paramagnetic moment of the sample, leading to the conclusion that the field-independent χ no longer results from the paramagnetism of both the Cr and Yb spins. This indicates that most, if not all, of the Cr spins have ordered magnetically and thereby provides further evidence that the observed weak ferromagnetism does not result from a small amount of second phase.

In Fig. D3 we show the temperature dependence of the field-independent magnetization M_o. Apart from the obvious transition at the Curie temperature the most striking feature is the abrupt drop in M_o at 17 ± 2 K. Such behavior, which has not been observed previously in this material, may be indicative of a compensation point where the Cr sublattice magnetization is cancelled by the polarization it induces on the rare earth sublattice.[D2] Alternatively, it may represent a reorientation of the Cr sublattice; a similar reorientation takes place[D3] at around 10 K in $YbFeO_3$. No change in spin configuration between 4.2 and 77 K was observed by Bertaut, et al.,[D1] so the former possibility seems more plausible.

Since the calculated magnetizations are obtained after smoothing and extrapolation of the original data and also are derived from relatively small differences between large, rapidly changing quantities, one may question the detailed accuracy of the magnetization-temperature curve. But the smoothness of the $1/\chi_\infty$ plot and an examination of the original data lead us to believe that the general trend of the data is represented correctly. Nonetheless, we have observed cases in which spurious, though much less pronounced, "reorientation points" occur, and confirmatory evidence would be helpful in understanding the more complicated effects in alloys discussed in the main text.

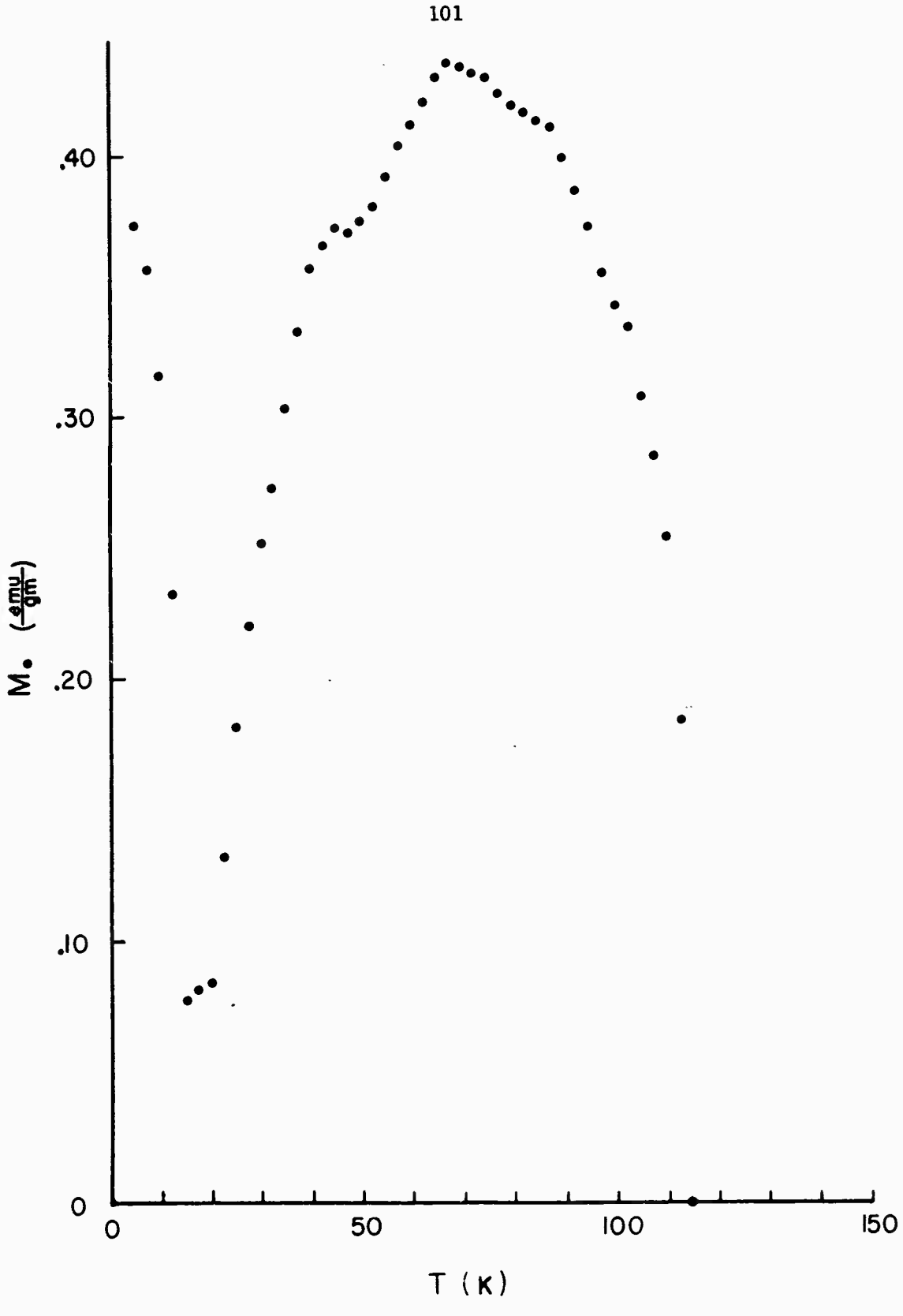

FIGURE D3. FIELD-INDEPENDENT MAGNETIZATION (EQUATIONS D3 AND D4) AS A FUNCTION OF TEMPERATURE IN THE ORDERED STATE OF ORTHORHOMBIC $YbCrO_3$. POINTS OBTAINED FROM DATA REPRESENTED BY CIRCLES IN FIGURE D1.

D1. E. F. Bertaut, et al., IEEE Trans. Mag. 2, 453 (1966).

D2. J. Mareschal and J. Sivardière, J. de Phys. 30, 967 (1969).

D3. K. P. Belov, et al., Izv. A. N. SSSR, Ser. Fiz. 34, 951 (1970).

APPENDIX E

PIEZOELECTRIC RESONANCES

The complete characterization of new ferroelectric materials generally requires the availability of bulk single crystals or, at least, bulk specimens having reasonably good homogeneity. The synthesis of such specimens often involves laborious preparation procedures so that it is extremely important to reject from consideration those materials which because of crystal symmetry cannot exhibit ferroelectricity. What is needed is a reliable test which when applied to small quantities of polycrystalline powder will detect the presence, or with some degree of confidence the absence, of acentricity, i.e., a lack of a center of inversion symmetry. X-ray powder patterns are quite suitable for this purpose except in those cases where the crystal space group is a Buerger group. Unfortunately, this situation is often found. Another simple method for detecting acentricity is the Wooster test for pyroelectricity; however, this method is not reliable when applied to powders. Observation of second harmonic generation is a sensitive method for materials which are sufficiently transparent. The most popular method for determining acentricity in powdered specimens has been to detect piezoelectricity at RF frequencies using an RF oscillator-detector and a loudspeaker. In this program, a very sensitive piezoelectric resonance spectrometer has been developed primarily for the purpose of detecting acentricity in minute quantities of piezoelectric materials. With some modification the spectrometer system may also be used to investigate individual components of the piezoelectric-coupling tensor and polarization relaxation times. Here we describe the spectrometer system in detail and discuss separately these applications.

The piezoelectric resonance technique involves placing the sample of interest in a capacitor which forms part of the tank circuit of an RF oscillator. If the specimen is piezoelectric, the oscillating electric field of the specimen capacitor will induce acoustic vibrations by means of the piezoelectric coupling. At mechanical resonance frequencies of the sample (for powders many such frequencies exist), energy will be resonantly absorbed and large changes in the level of oscillation will be observed. With suitable detection apparatus these resonances may be displayed by frequency-modulating the RF oscillator and slowly sweeping the center frequency over the range of several tens of MHz. Fig. E1 is a block diagram of the spectrometer system. Depending upon the required sensitivity and/or the desire to study relaxation times, one of two types of oscillators is used (this will be discussed later). The RF oscillator is frequency-modulated with an audio oscillator by means of a variable capacitor in the tank circuit. This audio oscillator also drives the horizontal axis of the scope and the reference channel of the lock-in amplifier. After diode detection of the RF level, which at resonance varies with the modulation frequency, the signal is passed thru a narrow-band amplifier. As noted in the figure the narrow-band amplifier should include both a low-frequency and a high-frequency cut-off filter to suppress unwanted noise. When large modulation is employed (i.e., large compared to the resonance width) a notch filter at the modulation frequency can be used to reduce d rect modulation pick-up in the tank circuit. Of course this filter also removes the signal component at the modulation frequency, but under these conditions there is a sufficient amount of harmonic content in the signal to display the resonance. For small modulation, it is often desirable to use a 60 Hz notch filter to remove line pickup. The output of the broad-band amplifier is displayed on the vertical axis of the oscilloscope and, in the case of weak

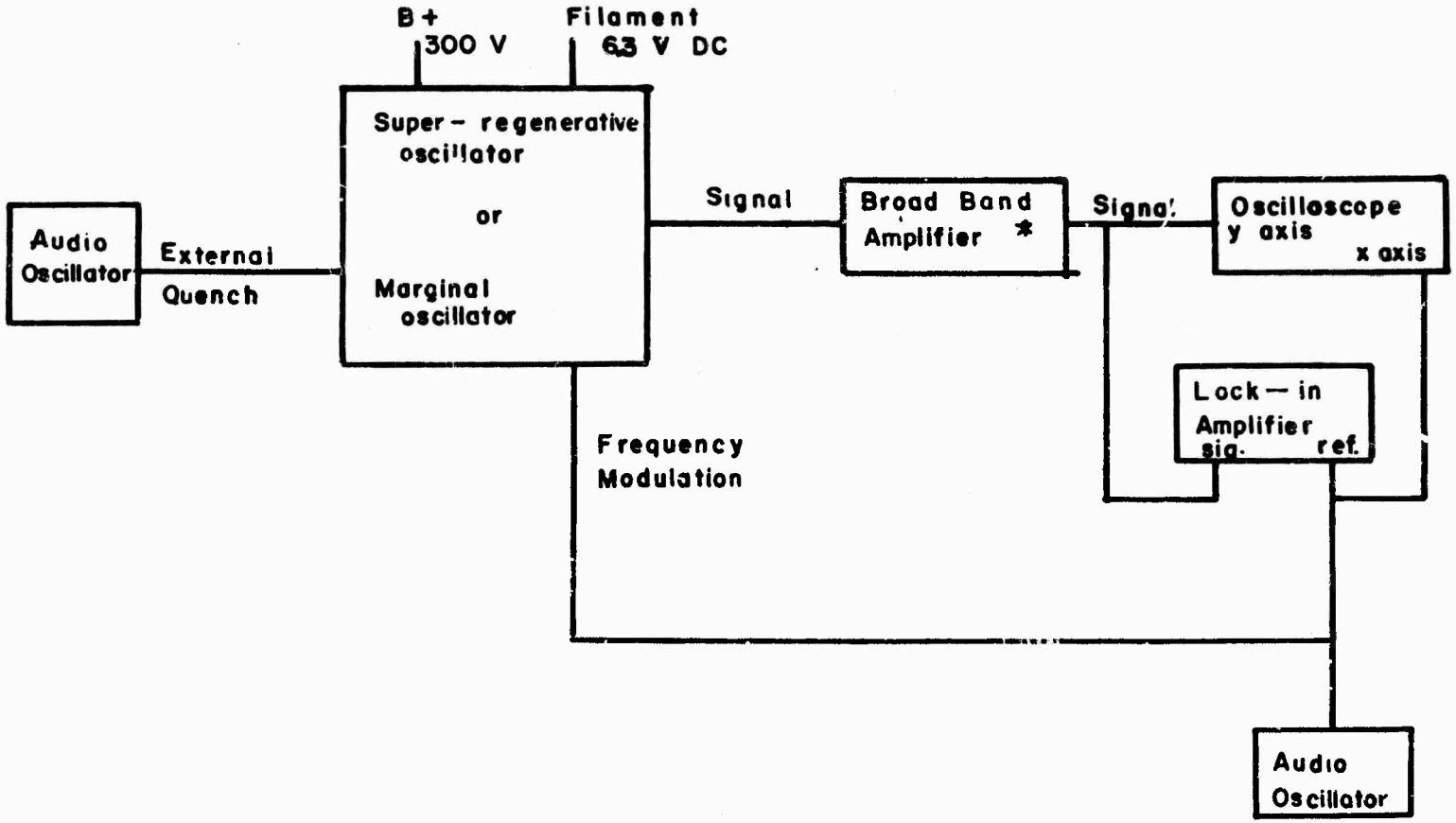

* Should include

a.) Low frequency cut off (below 10 Hz)

b.) High frequency cut off (above a few k Hz)

c.) Notch filter at the modulation frequency (optional)

FIGURE E1. BLOCK DIAGRAM OF THE PIEZOLELECTRIC RESONANCE SPECTROMETER SYSTEM

signals, is also fed to the signal channel of a lock-in amplifier which serves to enhance the signal-to-noise ratio by a factor of 1000 or more. The output of the lock-in is directed to a suitable recorder (not shown). The center frequency of the RF oscillator is slowly varied using a motor-drivenvariable capacitor in the tank circuit.

As previously mentioned, two types of RF oscillators have been employed. For maximum sensitivity a superregenerative oscillator (quenched CW oscillator) is used. The periodic quenching of the RF level (quench frequencies of about 30 100 kHz are most effective) is provided by the audio oscillator labeled "external quench" in Fig. E1. In Fig. E2 a circuit diagram of the superregenerative oscillator is shown. The tank circuit of the 6C4 contains: the sample capacitor, the motor-driven sweep capacitor (VU 45), the varicaps (H IN 750) to provide frequency modulation, and the center tap coil which is custom-wound to resonate at the desired frequency. With suitable tank coils the oscillator may be operated over the range of a few MHz to about 100 MHz.

The sensitivity of the apparatus is demonstrated in Fig. E3 which was obtained by photographing the oscilloscope display of signals from a polycrystalline $Gd_2(MoO_4)_3$ sample about the size of a pin head. In this experiment the superregenerative oscillator was operated at a center frequency of about 20.4 MHz and was frequency-modulated at a 60 Hz rate with an amplitude of about 80 kHz. The horizontal sweep of the oscilloscope was triggered by the modulation signal and the full range of the horizontal display was set at 20 msec. It is seen that the first and third signals are separated in time by exactly the modulation period (17 msec). Thus these signals correspond to passage through resonance in the same direction. The middle signal results from passage through resonance in the opposite direction as the modulation completes its cycle. The fact that this resonance does not occur midway between the other two simply means that the center

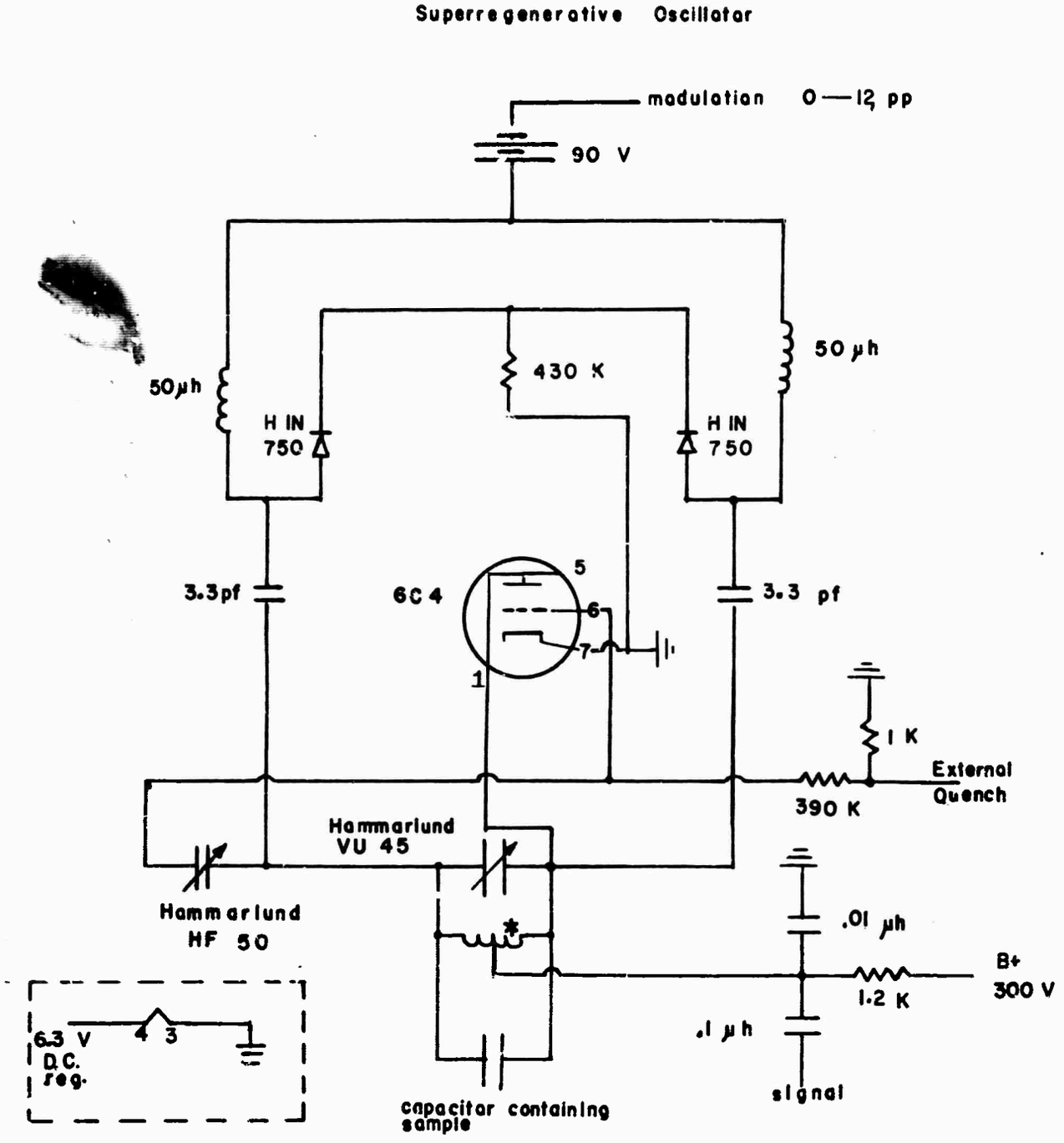

FIGURE E2. SCHEMATIC DIAGRAM OF THE SUPERREGENERATIVE OSCILLATOR

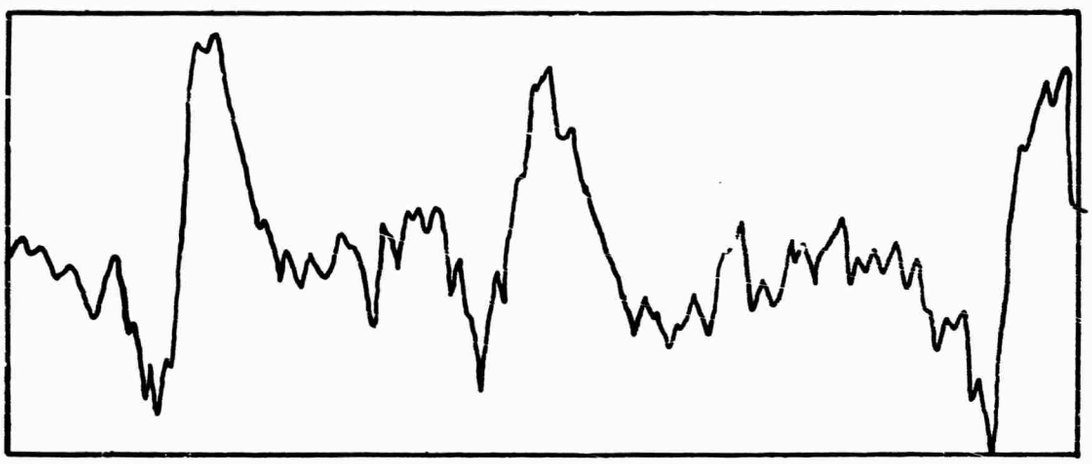

FIGURE E3. PIEZOELECTRIC RESONANCES FROM A SMALL QUANTITY (ABOUT THE SIZE OF A PIN HEAD) OF POLYCRYSTALLINE $Gd_2(MoO_4)_3$ OBTAINED WITH THE SUPERREGENERATIVE OSCILLATOR DESCRIBED IN THE TEXT

frequency of the oscillator was slightly off resonance. It is important to emphasize that these signals were obtained without using the lock-in amplifier which would greatly enhance the signal-to-noise ratio.

The reliability of the apparatus for detecting acentricity has been tested by a systematic study of several known piezoelectric materials. The results are shown in Table E1. The somewhat indefinite terms "high" and "low" conductivity are used since detailed measurements of the electrical properties were not made. In all cases the high-conductivity materials are nearly metallic. These results demonstrate one shortcoming of the spectrometer system, i.e. if the electrical conductivity of the specimen is sufficiently high that the free carriers can screen out the piezoelectrically-induced polarizations of the lattice, no effect will be seen. As mentioned in the text this condition may be quantitatively stated as follows: In order to observe piezoelectricity in materials containing free carriers, the detection frequency must be much higher than the conductivity relaxation frequency, $f_c = \sigma/2\pi\epsilon$, where σ is the electrical conductivity and ϵ is the dielectric constant. Finally, it should be noted that several known centrosymmetric materials were tested and in no case were signals observed even using the lock-in amplifier for signal enhancement.

The feasibility of using piezoelectric resonance experiments to study both piezoelectric coupling coefficients and polarization relaxation times has been demonstrated with a single crystal of $Gd_2(MoO_4)_3$ obtained from Isomet, Inc. For this purpose the superregenerative oscillator was replaced by a continuous-wave marginal oscillator.[E1] Fig. E4 shows a typical resonance observed at about 15 MHz. The decaying oscillations, seen after passage through the resonance (large peak), result from beats between the decaying polarization and the oscillating electric field of the sample capacitor. This pattern is entirely analogous

TABLE E1. Observation of piezoelectric resonance in various acentric materials.

Materials	Conductivity	Piezoelectric Resonance Observed
$Gd_2(MoO_4)_3$	Insulating	yes - very large
$Tb_2(MoO_4)_3$	"	"
$Eu_2(MoO_4)_3$	"	"
$NaClO_3$	"	"
$NaNO_2$	"	"
KIO_3	"	"
$KBrO_3$	"	"
Tartaric Acid	"	"
GaAs	low	yes
GaAs	high	no
CdS	low	yes
CdS	high	no
ZnO	low	yes
CdTe	low	yes
InSb	very high	no
InAs	"	no

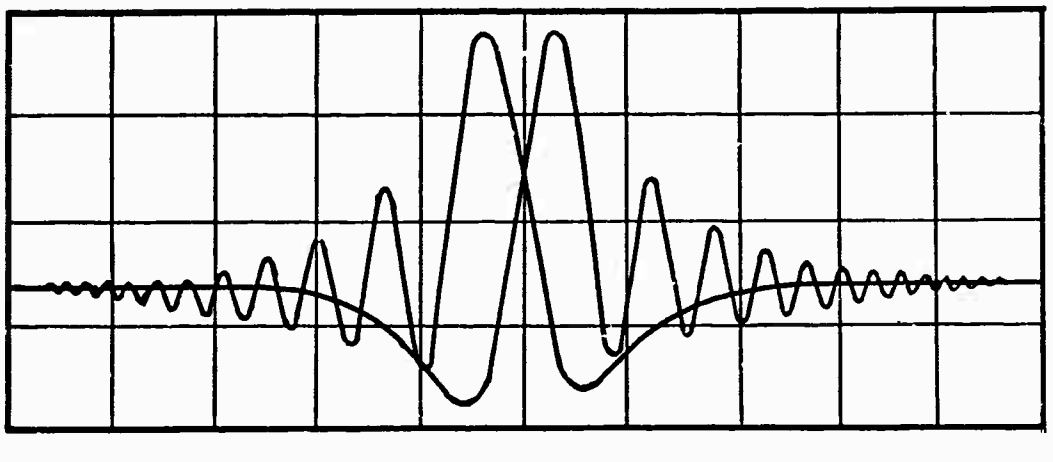

FIGURE E4. OSCILLOSCOPE DISPLAY OF A PIEZOELECTRIC-RESONANCE SIGNAL OBSERVED IN A SINGLE CRYSTAL OF $Gd_2(MoO_4)_3$ AT 15 MHZ. THE X AXIS DEFLECTION IS PROPORTIONAL TO THE OSCILLATOR FREQUENCY WHICH IS MODULATED AT 60 HZ WITH AN AMPLITUDE OF ABOUT 10 kHZ. THE PATTERN IS A DUAL DISPLAY CORRESPONDING TO PASSAGE THROUGH RESONANCE (LARGE PEAK) FROM BOTH DIRECTIONS.

to the familiar "wiggles" observed in nuclear magnetic resonance experiments.[E2] The envelope of these oscillations provides a measure of the decay rate. In order to measure the tensor components of the coupling coefficient and corresponding relaxation times in this way, it is necessary to study several single crystals cut in various orientations. In the case discussed here it is assumed that only the shear mode about the c-axis is excited since all other coupling coefficients are small in $Gd_2(MoO_4)_3$.

E1. R. V. Pound and W. D. Knight, Rev. Sci. Instr. 21, 219 (1950).

E2. A. Abragam, Principles of Nuclear Magnetism, p. 86 (Oxford Univ. Press, 1961).